AD NUMBER

AD814838

LIMITATION CHANGES

TO:

Approved for public release; distribution is unlimited.

FROM:

Distribution authorized to U.S. Gov't. agencies and their contractors; Critical Technology; FEB 1967. Other requests shall be referred to Air Force Flight Dynamics Laboratory, Attn: RTD, AFSC, Wright-Patterson AFB, Ohio 45433. This document contains export-controlled technical data.

AUTHORITY

AFFDL per ltr, 8 Jun 1972

AFFDL-TR-66-162 FA REPORT R-1817

DEVELOPMENT OF THE XM15 ESCAPE ROCKET

HUGH D. MacDONALD, JR.

Frankford Arsenal
Philadelphia, Pa.

TECHNICAL REPORT AFFDL-TR-66-162

February 1967

Air Force Flight Dynamics Laboratory
Research and Technology Division
Air Force Systems Command
Wright-Patterson Air Force Base, Ohio

NOTICES

When Government drawings, specifications, or other data are used for any purpose other than in connection with a definitely related Government procurement operation, the United States Government thereby incurs no responsibility nor any obligation whatsoever; and the fact that the Government may have formulated, furnished, or in any way supplied the said drawings, specifications, or other data, is not to be regarded by implication or otherwise as in any manner licensing the holder or any other person or corporation, or conveying any rights or permission to manufacture, use, or sell any patented invention that may in any way be related thereto.

Copies of this report should not be returned to the Research and Technology Division unless return is required by security considerations, contractual obligations, or notice on a specific document.

AFLC—WPAFB—MAR 56 1500

AFFDL-TR-66-162 FA Report R-1817

DEVELOPMENT OF THE XM15 ESCAPE ROCKET

HUGH D. MacDONALD, Jr.

Components Engineering Directorate
Frankford Arsenal
Department of the Army

for

Air Force Flight Dynamics Laboratory
Research and Technology Division
Air Force Systems Command
Wright-Patterson Air Force Base, Ohio

February 1967

FOREWORD

The program upon which this report is based was accomplished by Frankford and Picatinny Arsenals of the U.S. Army Munitions Command, authorized by U.S. Air Force MIPRs Nos. 33(616)60-15, 33(616)60-8, and AS-3-238, for the Air Force Flight Dynamics Laboratory (AFFDL), Wright-Patterson Air Force Base, Ohio. The program was performed under Project 1362, "Crew Escape for Flight Vehicles," and Task 136205, "Propellant Actuated Devices Research," from January 1960 through March 1963.

Captain D. R. Barron of the AFFDL was the Project Engineer. Mr. H. D. MacDonald, of Frankford Arsenal, was the Army Munitions Command Project Engineer. The stress analysis was performed by Mr. C. W. Larsen and the static testing was performed by Messrs. F. C. Femia and H. A. Pontious of Picatinny Arsenal. The Frankford Arsenal report number is FA Report R-1817.

Acknowledgement is made of the assistance and contributions provided by Mr. B. J. White, of AFFDL; Mr. D. L. Robertson, of Frankford Arsenal; Messrs. S. Newman, S. Harnett, J. Guerrera, R. Vecchio, and Dr. F. Soechting, of Picatinny Arsenal; and Captain V. W. Hodges and Mr. R. Christopherson, of Edwards Air Force Base, Calif.

This report was submitted by the author in November 1966.

This technical report has been reviewed and is approved.

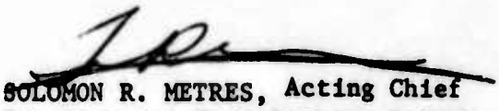

SOLOMON R. METRES, Acting Chief
Recovery and Crew Station Branch
Vehicle Equipment Division
AF Flight Dynamics Laboratory

ABSTRACT

This report summarizes the design study and testing of the XM15 Escape Rocket, a device designed to satisfy the ejection propulsion needs for a single place separable nose emergency crew escape capsule. The XM15 was used in the feasibility testing of the separable nose escape concept, the test capsule being based on the F104 aircraft configuration.

The XM15 Escape Rocket is designed to deliver a maximum thrust of 45,000 pounds, decreasing to 27,000 pounds at rocket burnout. The rocket's burn time is 0.50 second. The XM15 utilizes 12 singly perforated uninhibited grains of HE-N12 propellant and was validated to operate over a temperature range of 70° ± 20° F.

The over-all performance of the XM15 rocket was satisfactory throughout both static testing of the motor and feasibility testing of the capsule. Performance was demonstrated to be consistent and reproducible.

TABLE OF CONTENTS

TABLE OF CONTENTS (Cont'd)

List of Tables

List of Tables (Cont'd)

List of Illustrations

List of Illustrations (Cont'd)

List of Illustrations (Cont'd)

List of Illustrations (Cont'd)

List of Illustrations (Cont'd)

SECTION I

INTRODUCTION

The anticipated development of high performance advanced flight vehicles, operating in the supersonic range, generated a requirement for the U. S. Air Force to conduct feasibility studies and establish design criteria for escape systems whose performance envelopes would be compatible with those of the advanced vehicles. One of the systems selected for feasibility testing was the separable nose capsule, which has a design performance envelope of zero to 900 knots equivalent air speed (KEAS) or a Mach number of 4 (whichever is lower), and an altitude range from sea level to 100,000 feet.

This program was conducted to design, test, and fabricate an escape rocket capable of separating the 2400-lb capsule and providing a safe escape trajectory without exceeding the human tolerance to acceleration. This latter factor dictated the thrust requirement of the motor. The external dimensions and nozzle cant angle were dictated by the available space and the separation requirements of the capsule.

Other factors considered in the design of the rocket motor were high strength casing to minimize weight, reproducible performance from round to round, and placement of thrust alignment within 0.25 inch of the capsule center of gravity (c.g.).

Initial studies were aimed at acquiring an intimate working knowledge and understanding of the objectives of the study. Accordingly, Report WADC-TR-59-493[1]* was thoroughly studied and conferences were held with U. S. Air Force personnel. Coordination was accomplished with Lockheed California Company (a Division of Lockheed Aircraft Corp.) and with personnel at the Experimental Track Branch, Air Force Flight Test Center, Edwards Air Force Base, California.

The space available for the escape rocket measured approximately 10 in. deep by 17 in. wide by 34 in. high. The rocket projected for this

---

*See REFERENCES.

space (Ref 1, pp 44-47) was constructed of titanium and loaded with a polyurethane propellant. The scope of this study did not include work on titanium cases or polyurethane propellant, both of which were highly experimental. The main objective of the program was the acquisition of aerodynamic data under as many known and controlled conditions as possible.

SECTION II

DESIGN STUDY

Design Considerations

Informal inquiry was made of several government and industrial sources as to available case materials and fairly well characterized propellants. One single motor, designed in steel and not exceeding the 10 inch diameter limitation of the package and loaded with a semiexperimental propellant, looked promising because it met package requirements (Figure 1). However, the manufacturer could not supply sufficient data on the propellant nor guarantee any precision in thrust alignment.

A misalignment limit of 0.25 inch maximum at the center of gravity of the capsule (Ref 1, p 41) was selected. As a result of discussions with Lockheed personnel, the tail-off time of the thrust was to be held to a minimum. This means that, at web burn-out time (0.5 sec), the thrust was to be 27,000 lbf, rapidly falling to zero. In actual practice, the XM15 tail-off time was found to be 0.030 second. A review of commercially available escape motors showed tail-off times equal to the burn time and random from round to round; therefore, they were unacceptable.

In further seeking to satisfy the package, consideration was given to multiple rocket tubes taken from seat rockets and "ganged" together to form the escape rocket. The weight was about equal to the single

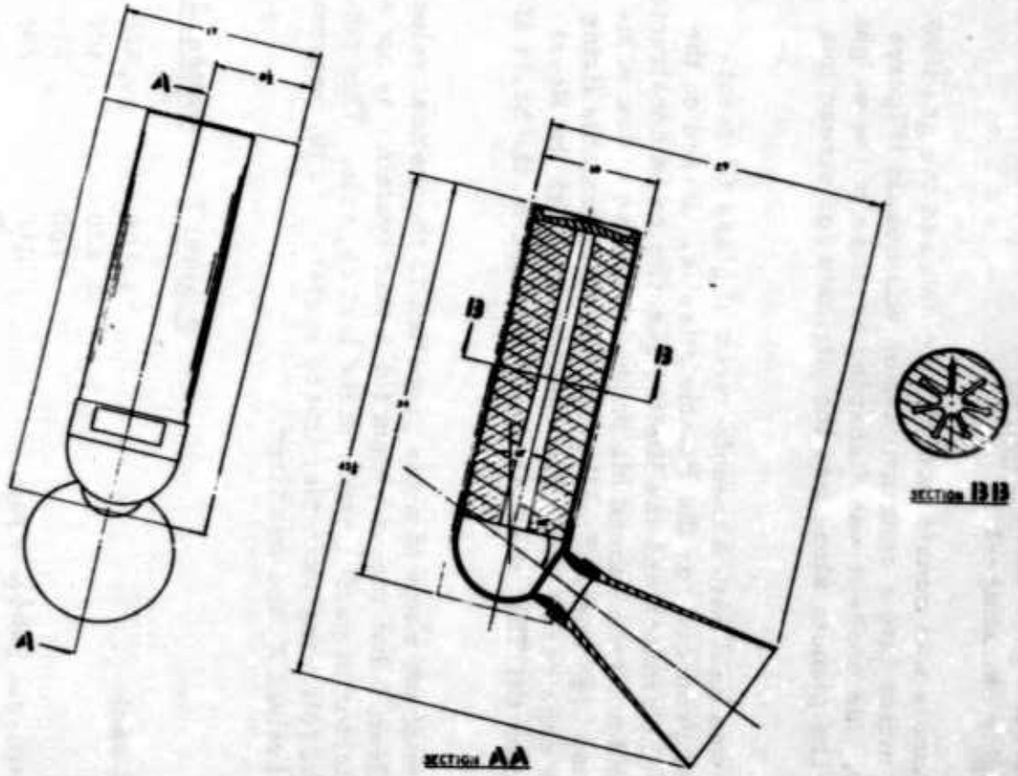

Figure 1. Proposed 10 inch diameter Single Chamber Motor

motor approach, but tolerance accumulation made determination of thrust alignment highly unmanageable.

A rocket assembly was considered which combined the gas flow from the multitube motor into a common plenum and nozzle (Figures 2 and 3). However, this concept was discarded because of the weight and size penalty. The plenum alone was too intricate for streamline gas flow.

Consultation was held with a manufacturer of glass filament-wound motor cases, produced for the Polaris missile. Based on the design of a 12.525-inch motor and the limited quantity to be constructed, the manufacturer did not recommend his product because of low volumetric efficiency and high cost. Small quantities of repeatable firing liquid motors were considered but, after consultation with the Naval Ordnance Test Station (NOTS), the idea was abandoned on the basis of high cost.

Consideration of the ratio of mass propelled to theoretical velocity at web burnout indicated that motor weight for a test system was not a highly significant factor in performance of the test capsule. This point is illustrated by the following example, where system 1 is the proposed flight system and system 2, the one fired.

	System 1	System 2
Total impulse (lbf-sec)	17,500	17,500
Propelled mass (lb)	2,270	2,400
Motor weight (lb)	100	218
Velocity at web burn-out (wbo), (fps)	248	235
% velocity change	0	-5.2

Thus, an increase in motor weight of 118 percent reduces the velocity about 5.2 percent. Hence, from this and other illustrations,[2, 3, 4, 5] it can be shown that available volume is a prime factor in the escape motor design for this capsule feasibility program, and that motor weight is of secondary importance in the performance of the capsule. However, while the importance of lightweight components in a weapons system and the effect of weight summation on the mission and pay load of an aircraft cannot be discounted, the flight weight reduction approach is properly the objective of a system development project.

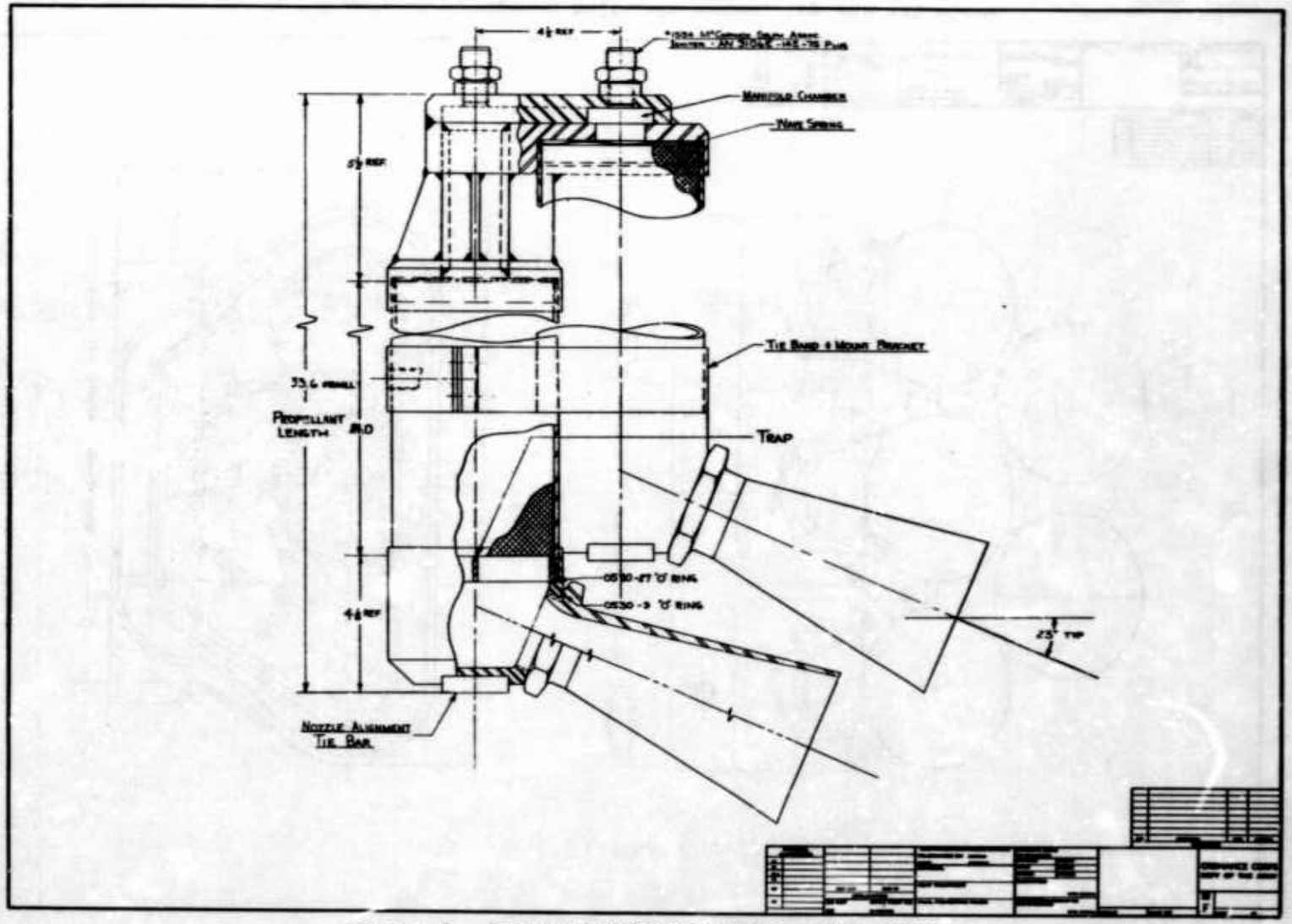

Figure 2. Proposed Multitube Motor, side view

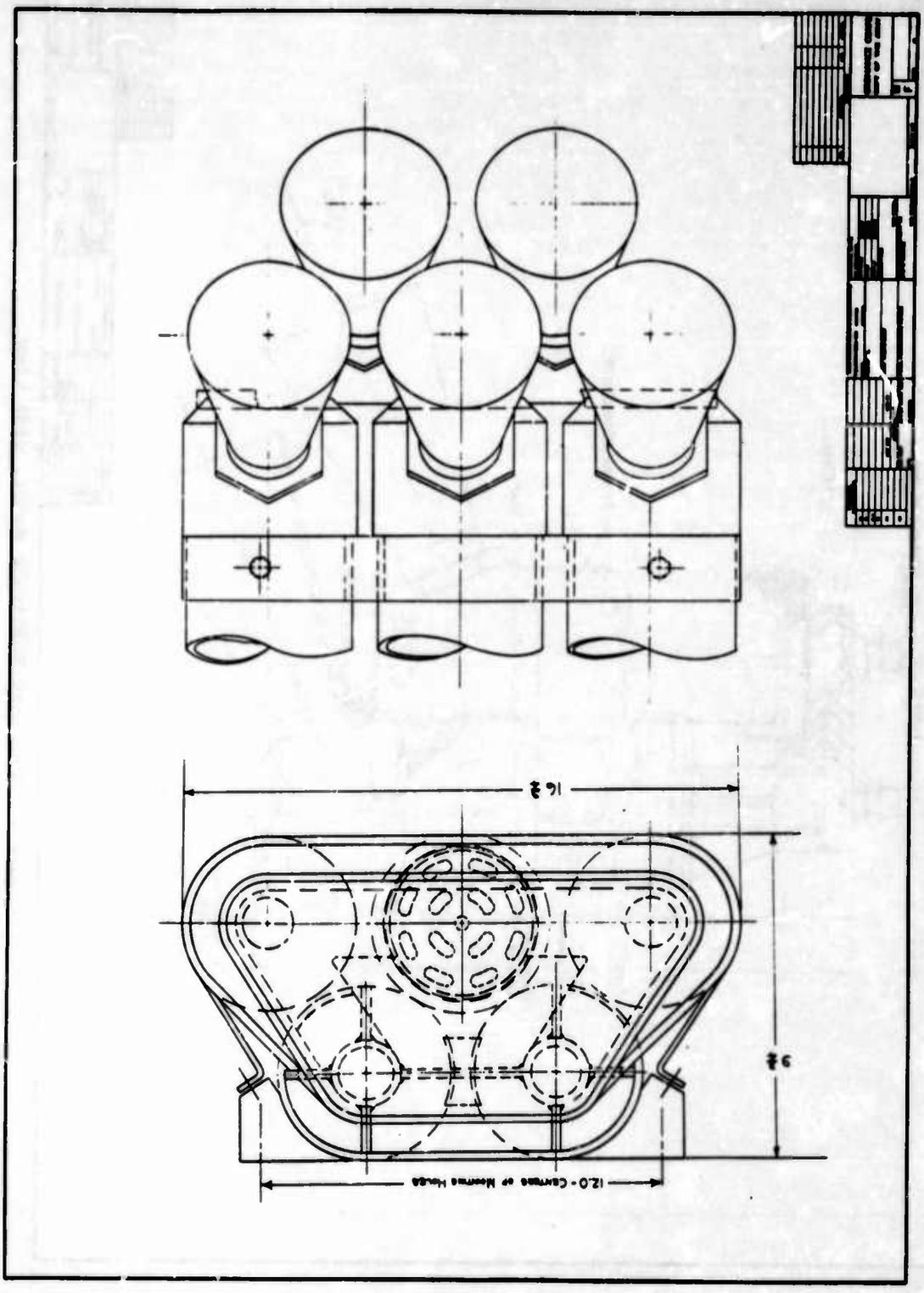

Figure 3. Proposed Multitube Motor, top and aft views

The effect of added motor weight on the capsule moment of inertia and the structure is greater than the effect on performance. The capsule project was therefore faced with resolving the problem of the uncertain development costs of a highly experimental motor in favor of a more easily estimated increase in the cost of construction of the capsule (Ref 6, p 50). To further limit the cost hazards of developing a charge in a "boiler plate" type motor and then redeveloping and refining the charge in a lightweight motor, a carefully calculated risk was taken in constructing an interim weight motor that would serve for development and track testing.

Initial Design Criteria

Following the informal assessment of various approaches and sources, Picatinny Arsenal was requested to prepare a formal proposal.[7] The general criteria established was a motor constructed of the lowest possible tensile aircraft-quality alloy steels to avoid fabrication difficulties in the small numbers to be fabricated. The detail criteria were:

1. A simple groove and lock wire key assembly for the head end for attachment of the motor body.

2. A generously sized plenum chamber, to reduce the velocity of gas to the lowest possible value in order to minimize erosion of the interior parts and provide uniform distribution of gas in the entry of the nozzle.

3. The use of replaceable nozzles.

4. Repeated use of a single case, based on the conclusions of work already accomplished.[8,9]

5. The inclusion of head and plenum pressure stations for monitoring pressures during all tests, to allow correlation of flight test performance with static tests in the thrust stand.

6. The use of a relatively simple weight-reduction technique from boiler plate motor to medium weight flight motor by machine-turning the outside diameter of the boiler plate motor.

7. The presentation of various alternatives (Figure 4) in regard to tensile value of alloy steel and propellants used (Figure 5), and their influence on weight and size.

8. The design of twin motors (Figure 6) as the assembly of the XM15 escape rocket, but with a capability of scaling up quickly to a single motor.

It was recognized that the ratio of surface area to weight of propellant consumed would be higher than that of other rockets because of the high mass rate of flow required by the thrust-time program. This would incur a penalty on volumetric loading density.

Placing of attachment points of rocket to capsule exactly in line between the target center of gravity and the center line of the nozzle throat was specified.

Design Selection

The heavy weight case was chosen for ease of welding and machining. HE-N12 propellant was selected on the basis of production characterization and batch-to-batch reliability. The penalties were lower density impulse and the restriction of case length, the latter causing the grains to extend deeper into the plenum chamber than is ideally desired. This extension meant that the grains would be subject to the stress of high mass rate transverse flow as the gases turned the corner.

Although Picatinny Arsenal was authorized to proceed with the design of twin motors, the U. S. Air Force requested the design of a single motor because the exhaust exit cones of the twin canted nozzles would interfere with some structural members of the capsule, entailing considerable redesign.

Description of Motor

Salient dimensions of the motor follow. The length from top of motor to bottom of plenum is 32.640 inches; from bottom of nozzle cone to top of ignition port is 39.530 inches; the motor diameter, exclusive of attachment points, is 12.400 ± 0.015 inches, except at the

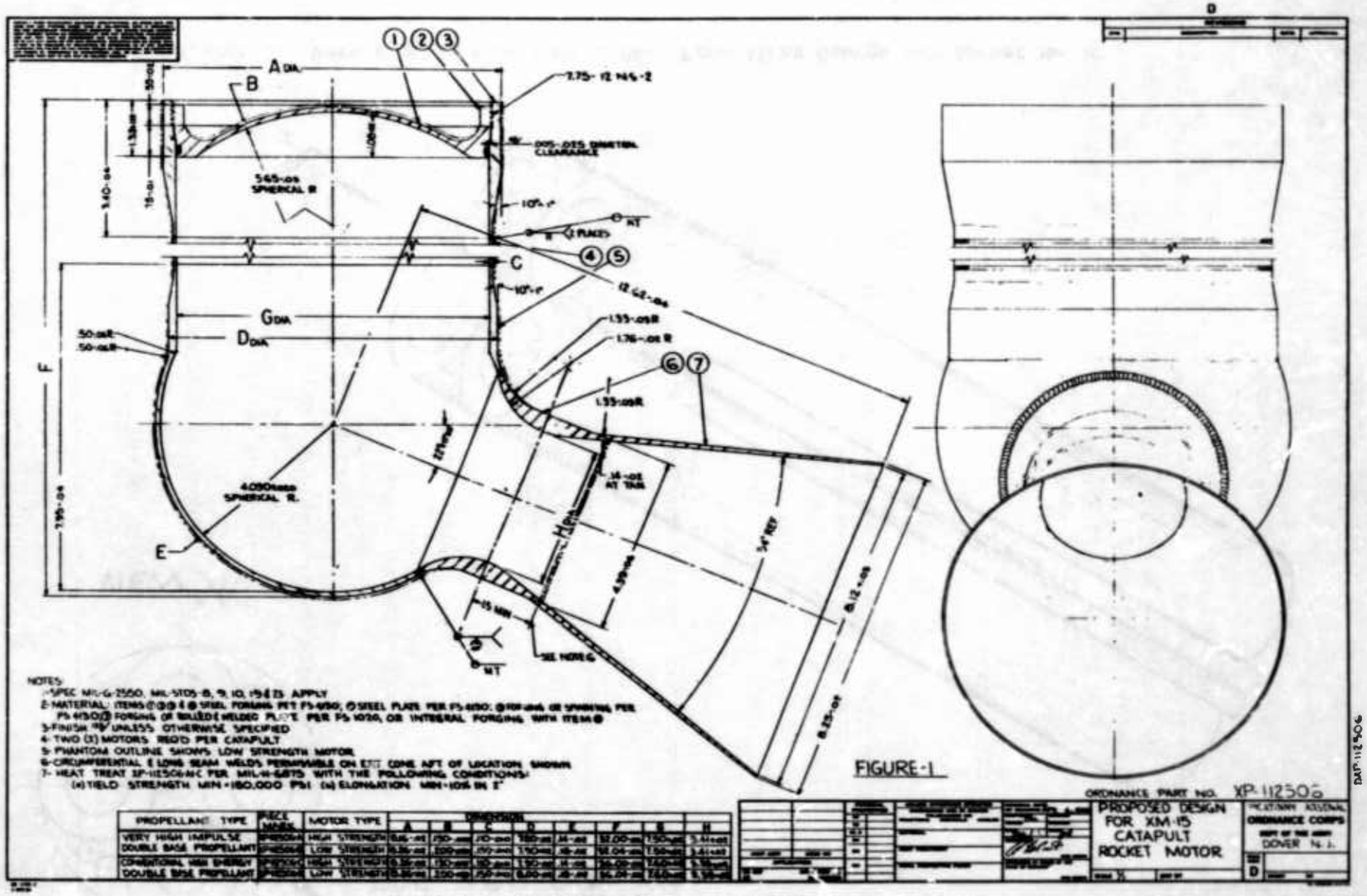

Figure 4. Proposed design for XM15 Escape Rocket

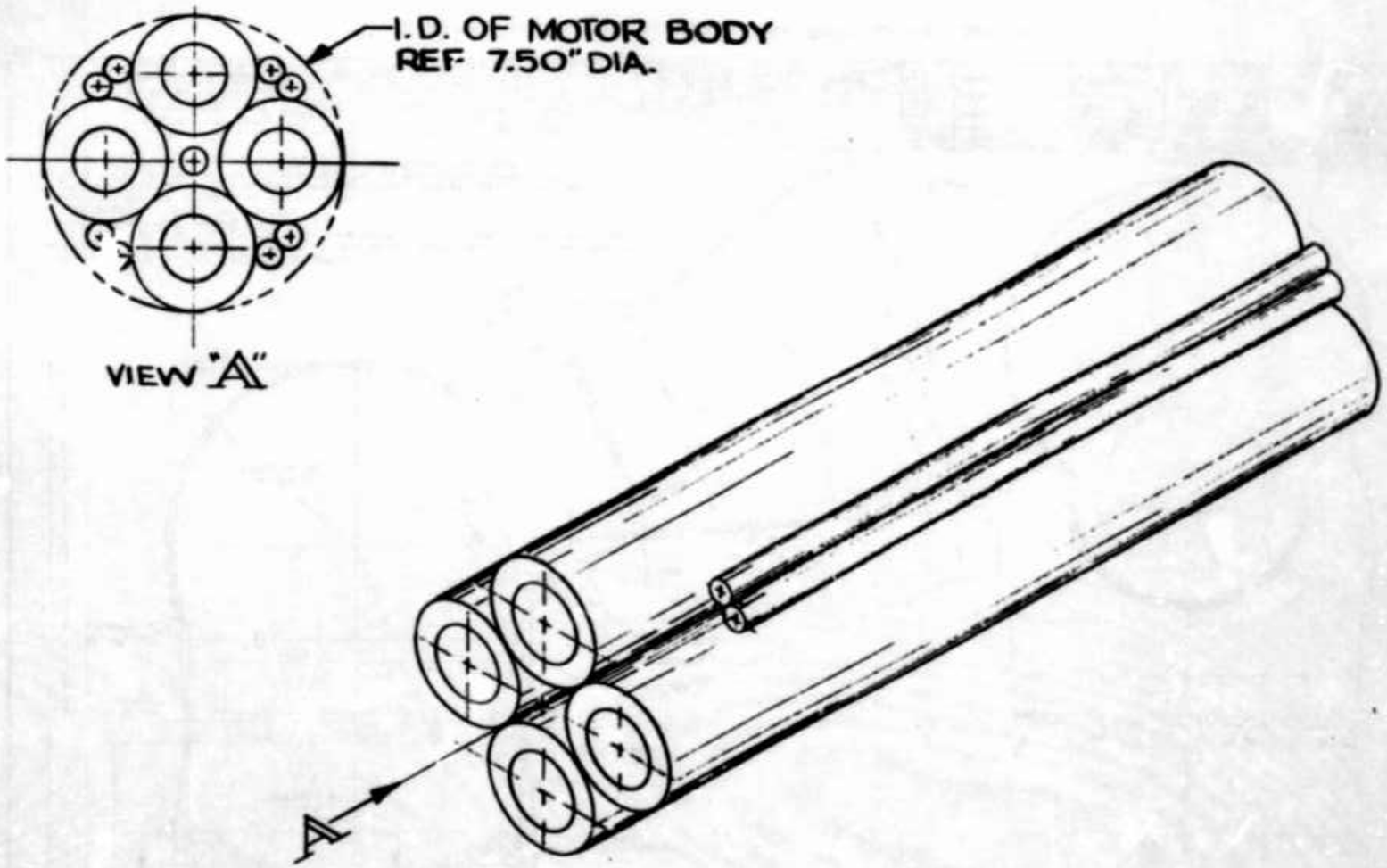

Figure 5. Very High Impulse Double Base Propellant Charge for Rocket Motor

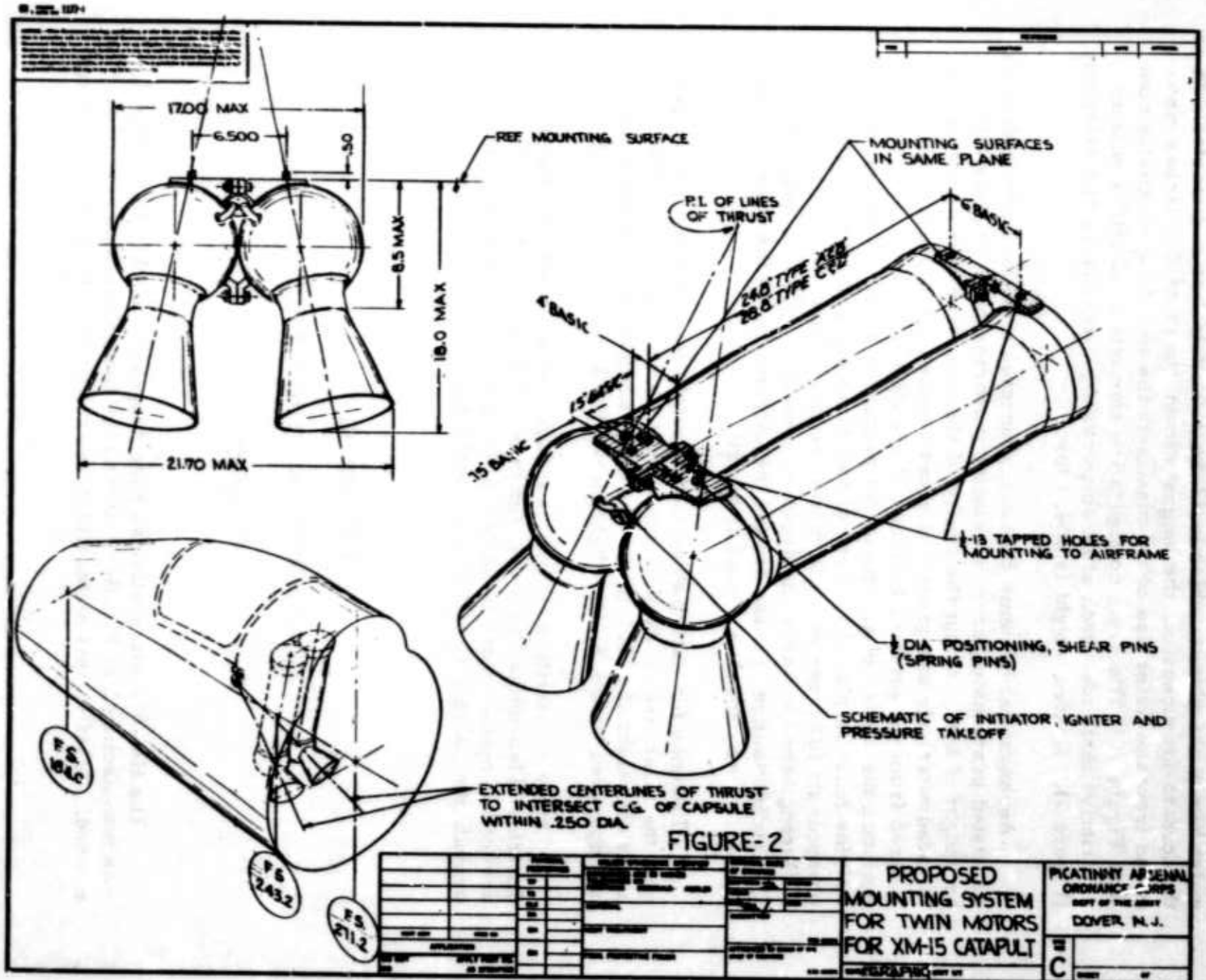

FIGURE-2

Figure 6. Proposed Mounting System for Twin Motors for XM15 Escape Rocket

waist line of the plenum which is 12.56 ± 0.06 inches in diameter. In the fore-to-aft direction, the longest dimension is 25.070 inches measured from the waist line of the plenum to the top of the expansion cone. (See Figure 7.) The grain configuration consists of 12 sticks with no restrictive inhibitor, each stick supported by a resonance rod assembly (Figure 7). Loaded weight is 244.2 lbw.

Aeronautical Systems Division requested a 26-lb weight reduction. As stated previously, capsule velocity performance is slightly affected by weight of the unit, but the design of the structure of the capsule and the sled afterbody are greatly affected because the capsule is cantilevered from the forward bulkhead of the sled afterbody. In order to maintain the center of gravity at the proper location, additional counter weights must be placed forward of and above the previous location to compensate for increments in motor weight. Thus, the vehicle must be strengthened to carry the greater moment load (Ref 6, page 50). The redistribution of mass toward the extremities of the capsule also increased the capsule moment of inertia.

Guidance for establishing motor weight was "the lightest weight with the least risk to the performance of its mission." Accordingly, a loaded weight of 217.1 lb was recommended by the Ordnance Corps and approved by the A. F. Flight Dynamics Laboratory (see Figure 7).

After competitive bidding, a contract was placed with Kaiser Industries (Fleetwings Division), for production of 15 motors. Two preproduction motors were to be delivered to Picatinny Arsenal for approval, the balance to follow after authorization to proceed.

SECTION III

COMPONENT MANUFACTURE[10]

Propellant

The HE-N12 nitrocellulose base propellant used in this catapult was manufactured at Picatinny Arsenal by the solventless extrusion method. Briefly, this method involves the manufacture of a propellant

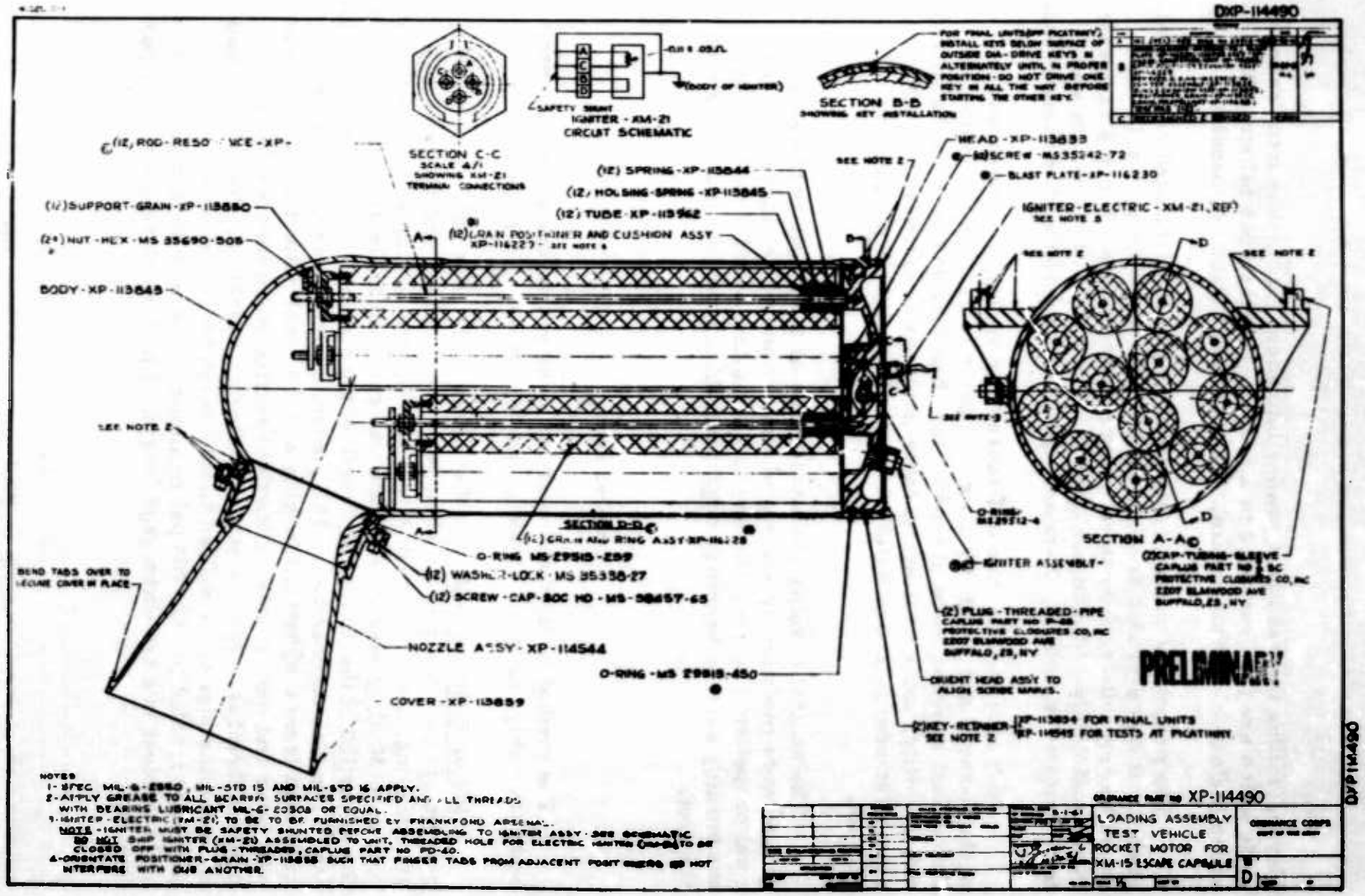

Figure 7. XM15 Escape Rocket Assembly used with Ejectable Nose Capsule

slurry, rolling the resultant powder into sheet form, then into "carpet" rolls which are then extruded in a press. The extruded billets, after annealing and X-ray inspection, are machined to final dimensions.

The propellant charge conisted of 12 single perforated uninhibited grains. It was extruded from an initial 1700 lbw slurry on a 15-inch press having a die temperature of approximately 100° F and a ram rate of approximately 1/4 inch per minute. The extruded propellant was then annealed at 140° F, X-rayed, and machined to finished dimensions.

To insure the absence of fissures and voids, the grains were again X-rayed and carefully inspected prior to release for testing. Propellant samples were submitted for chemical analysis and ballistic, stability, and calorimetric tests to insure conformity to quality control standards and to determine specific ballistic parameters of this lot.

The neutral burning characteristics of the single perforated grains were modified by milling of longitudinal slots, increasing the total propellant surface, thereby achieving increased thrust. Thus, the burning surface becomes regressive in proportion to the length of the slot.

Metal Parts

The method of fabrication of the three major components (motor body assembly, forward closure, and nozzle assembly) follows.

Motor Body Assembly - The motor body assembly consists of a cylindrical section, plenum chamber, nozzle boss, and forward and aft mounting lugs. The cylindrical section was machined from a forged tube of 4130 alloy steel. The tube was completely finish-machined with the exception of the ID for the length of the forward closure before welding to the plenum chamber. The plenum chamber contour was finish-machined from a spherical forging of 4130 steel material. The nozzle port boss and motor body cylindrical section were then welded to the plenum chamber. After a stress-relieving operation, the forward and aft mounting lugs were welded to this assembly. The assembly was then heat treated to 150,000 psi minimum yield with an elongation of eight percent in a two-inch gage length. Final machining was then performed.

Forward Head - The forward head was machined from a pancake forging of 4130 alloy steel. The head was rough-machined, heat treated, and then final-machined.

Nozzle Assembly - The nozzle housing was manufactured using the same method as for the forward head. The nozzle insert was finish-machined from a solid billet of ATJ graphite and then pressed in the nozzle housing to form the nozzle assembly.

The motor body assembly and forward head were hydrostatically tested. All critical dimensions were checked before and after hydrotest to insure that dimensional changes had not occurred. The nozzle port boss was plugged with a suitable fixture during this test.

SECTION IV

HYDROSTATIC TEST

When the first motor was completed, an Ordnance team of engineers, technicians, inspectors, and contract specialists conducted a thorough inspection of the motor and compared their inspection report with the contractor's report. Both reports were reconciled immediately and the motor was accepted dimensionally.

Hydrotest was performed successfully by contractor personnel under the direction of the government production engineer. The contractor was then certified as to inspection techniques, including hydrotest of the motor.

The second preproduction motor failed in hydrotest just short of the required three minutes at 2400 psi. A careful investigation of assembly procedures, manufacturing tolerances, and stress analysis of the design was conducted. Deviations of manufacturing tolerances seemed reasonable. From examination of the lock wires and grooves, it appeared that the assembly was made improperly. As a result of

corrective instruction, the contractor experienced no further assembly difficulties. (Repairs were authorized on the damaged motor.)

Results of the stress analysis (Appendix I) review showed that, as initially designed, the parts were satisfactory and a 2000 psi hydrostatic test would insure structural integrity. The 2000 psi test pressure was therefore substituted for the 2400 psi for the remaining motors. In addition, certain minor improvements were made to the design of the head closure area to reduce any possible stress raisers.

Delivery of two motors was waived when material flaws were reported in the body forgings. One of these was the second preproduction motor repaired after head closure failure. The remaining motors were delivered without incident.

SECTION V

STATIC TESTS

In order to evaluate motor performance on the test track, measurements were taken to establish performance by:

1. Acquisition of pressure-time data, taking pressures at the head end and the plenum chamber during static stand firings. (These data give an excellent report on the internal conditions of the motor.)

2. Acquisition of thrust-time data simultaneously with pressure-time data in a multicomponent thrust stand to establish thrust level and thrust direction.

The rocket performance was thus calibrated to chamber pressure data that would be obtained during capsule tests.

Test Stands

The pressure stand is a specially designed low cost unit which was used for the preliminary test firings, including igniter tests and reduced and full charge pressure tests. This stand is of welded steel construction and attaches directly to the main vertical thrust abutment in the firing bay. The rocket motor is supported vertically in a manner simulating actual motor mount conditions, with the body at an angle of 22 degrees to the abutment. This positions the nozzle perpendicular to the abutment for optimum static firing conditions. A detailed report of the design, construction, and use of the test stand is presented in Appendix II. Figure 8 is a drawing of the pressure test stand, and Figures 9, 10, 11, and 12 show various phases of the test arrangement.

The multicomponent stand is a specially designed unit for obtaining resultant thrust levels in addition to thrust misalignment in the vertical or principal plane of the rocket motor. This is accomplished by employing the following three force-measuring components in the required plane:

1. The main (or axial) force component, which is positioned directly in line with the nozzle center line.

2. The head end (or horizontal) component, which is placed approximately 22 inches above and parallel to the axial component.

3. The nozzle end (or vertical) component, which is positioned perpendicular to the other two and in the same plane.

Any small amount of thrust misalignment in the principal plane is observed by components 2 and 3.

The rocket motor is mounted to a special cradle assembly and is supported in the same orientation as in the pressure stand. Cradle support is provided by the three previously mentioned thrust components and three accurately located "dummy" components which provide added capability for measuring thrust misalignment in three mutually perpendicular planes when equipped with live thrust cells.

Each thrust measuring component includes a load cell, two commercially manufactured flexures to minimize interactions, and adjustment fixtures for accurate positioning and alignment. Alignment is

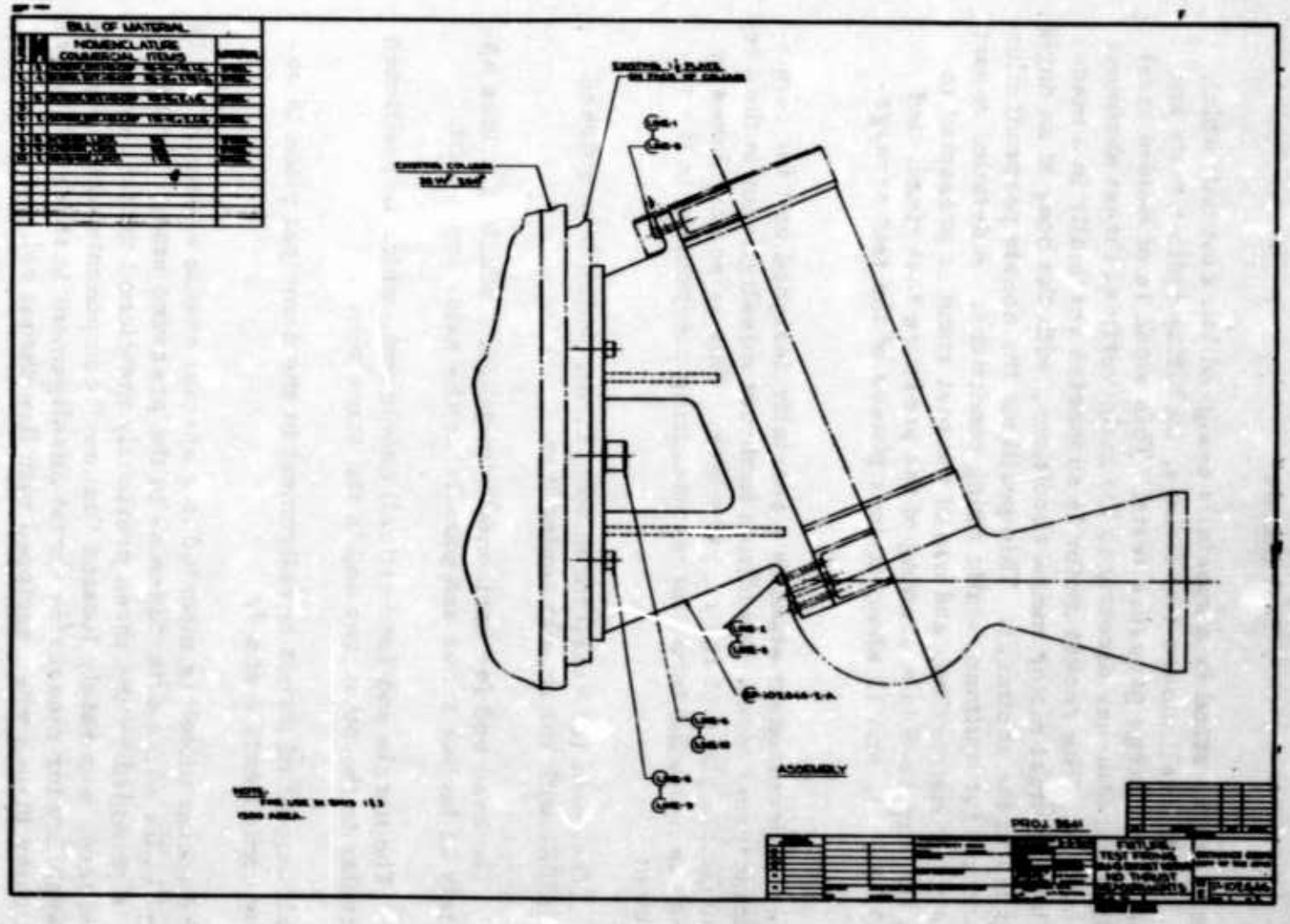

Figure 8. Pressure Test Stand

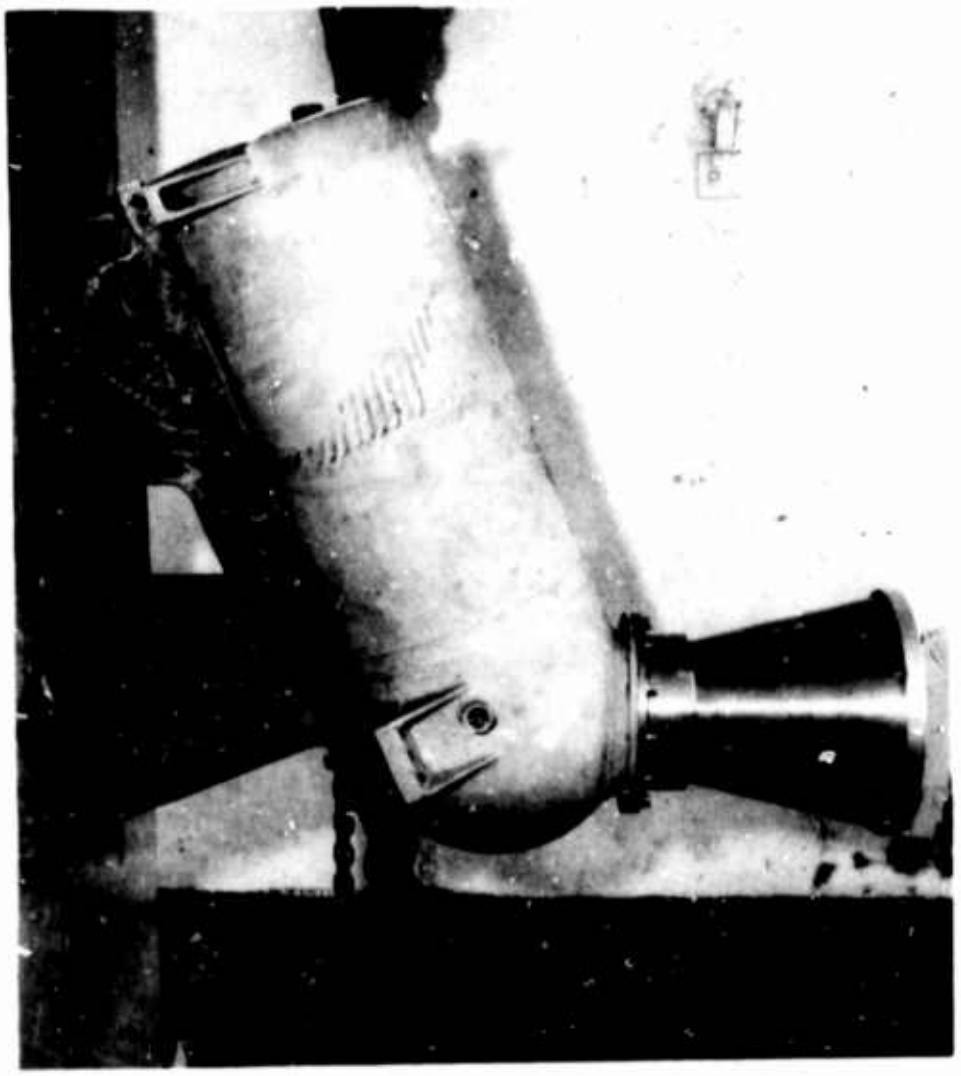

Figure 9. Test Arrangement showing Head and Nozzle End Pressure Ports and associated Mounting Fixture

Figure 10. Test Arrangement showing associated Mounting Fixture and Nozzle Closure Disc

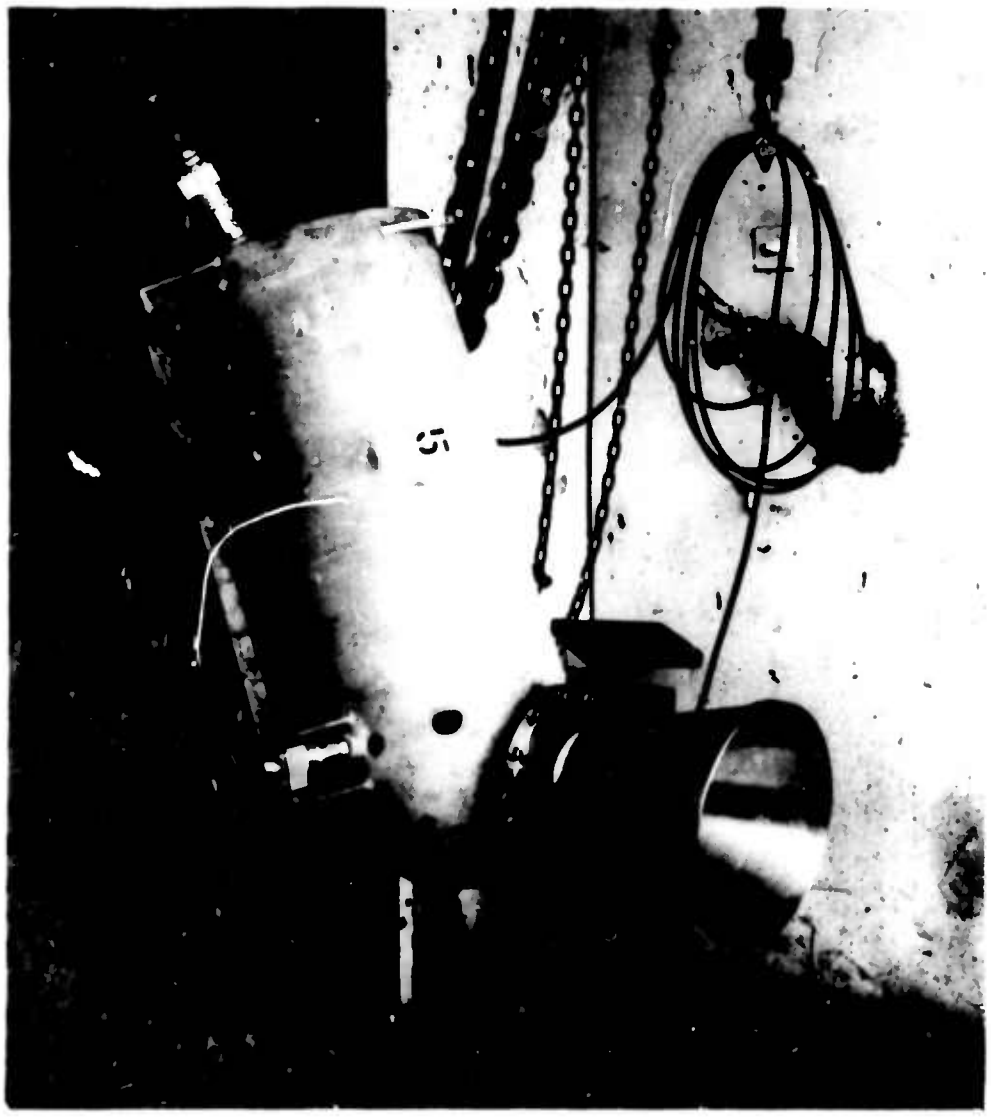

Figure 11. Static Test Setup with Head End and Nozzle End Pressure Gages

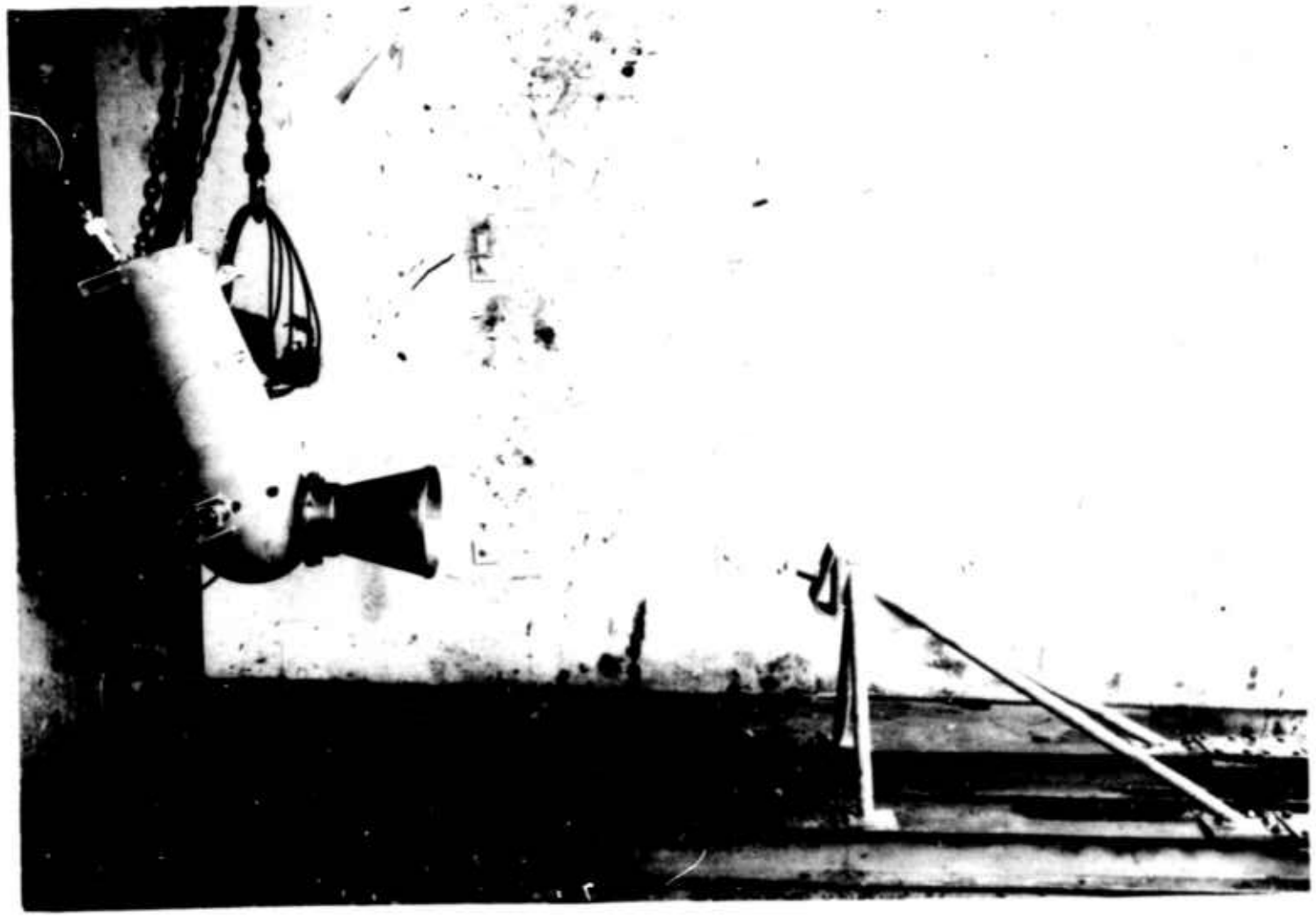

Figure 12. Static Test Setup with Pressure Gages and Rocket Sled Component placed in line with the Exhaust Stream

accomplished by the use of a surveyor's transit. These assemblies terminate at a framework of welded steel construction which is readily adaptable to the configuration of the firing bay. Figures 13 and 14 present drawings of the multicomponent test stand, and Figures 15, 16, 17, and 18 show various phases of the test arrangement.

A third test stand was utilized for preliminary small scale propellant evaluation studies. This is a standard "cart" type stand which is normally employed for conventional static rocket test firings. Two tests (rounds 9 and 10), using the XM37 motor body, were conducted using this stand. These represent the only test firings which did not utilize actual XM15 motor parts.

Instrumentation

Initial test firing data were recorded using an Electronic Tube Corporation model K55 five-beam oscilloscope in conjunction with a ten inch diameter drum type camera (120 mm). All multicomponent test firing data, in addition to data from a number of pressure tests, were recorded using a Midwestern Instruments Incorporated oscillograph, model M1603. Both methods produced a permanent record of the complete burning history of the particular test firing. A block diagram of one recorded instrumentation channel is presented in Figure 19.

Galvanometer, attenuator, and amplifier selection for each recorded channel of information depended on the desired frequency response, expected gage output, desired galvanometer deflection, and the linearity limitations of the system. Linearity of each channel was checked during setup by applying a three-step electrical calibration. A single calibration value was applied to each channel just prior to firing and was used in the thrust and pressure value calculations.

The measuring system utilized standard transducers, including Baldwin SR-4 fluid pressure cells and Alinco dual bridge tension and compression load cells. Each gage utilized bonded resistance wire strain gages in a Wheatstone bridge circuit. High speed (Fastax) and 24 frames/second camera coverage were furnished for all full charge test firings.

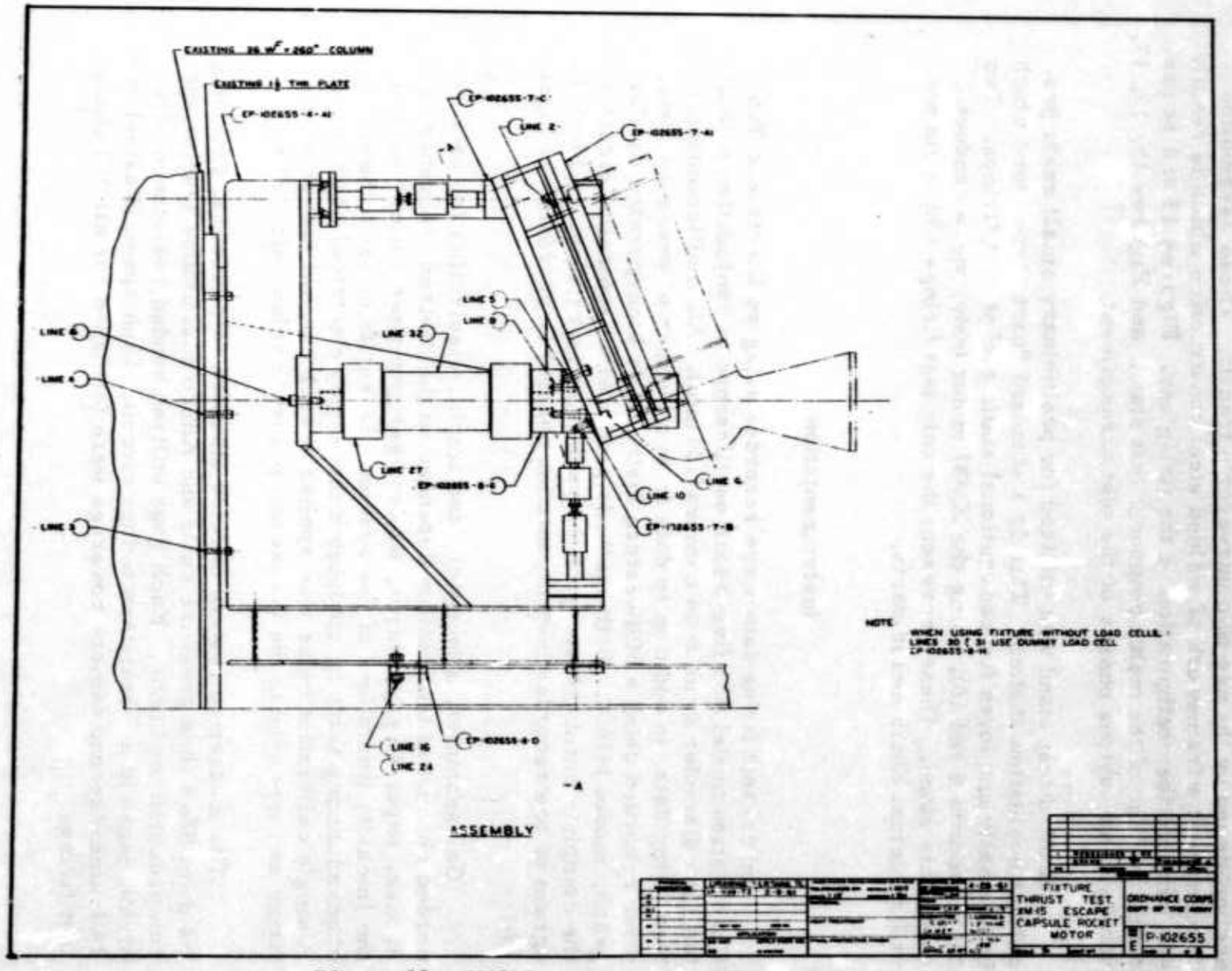

Figure 13. Multicomponent Test Stand Assembly

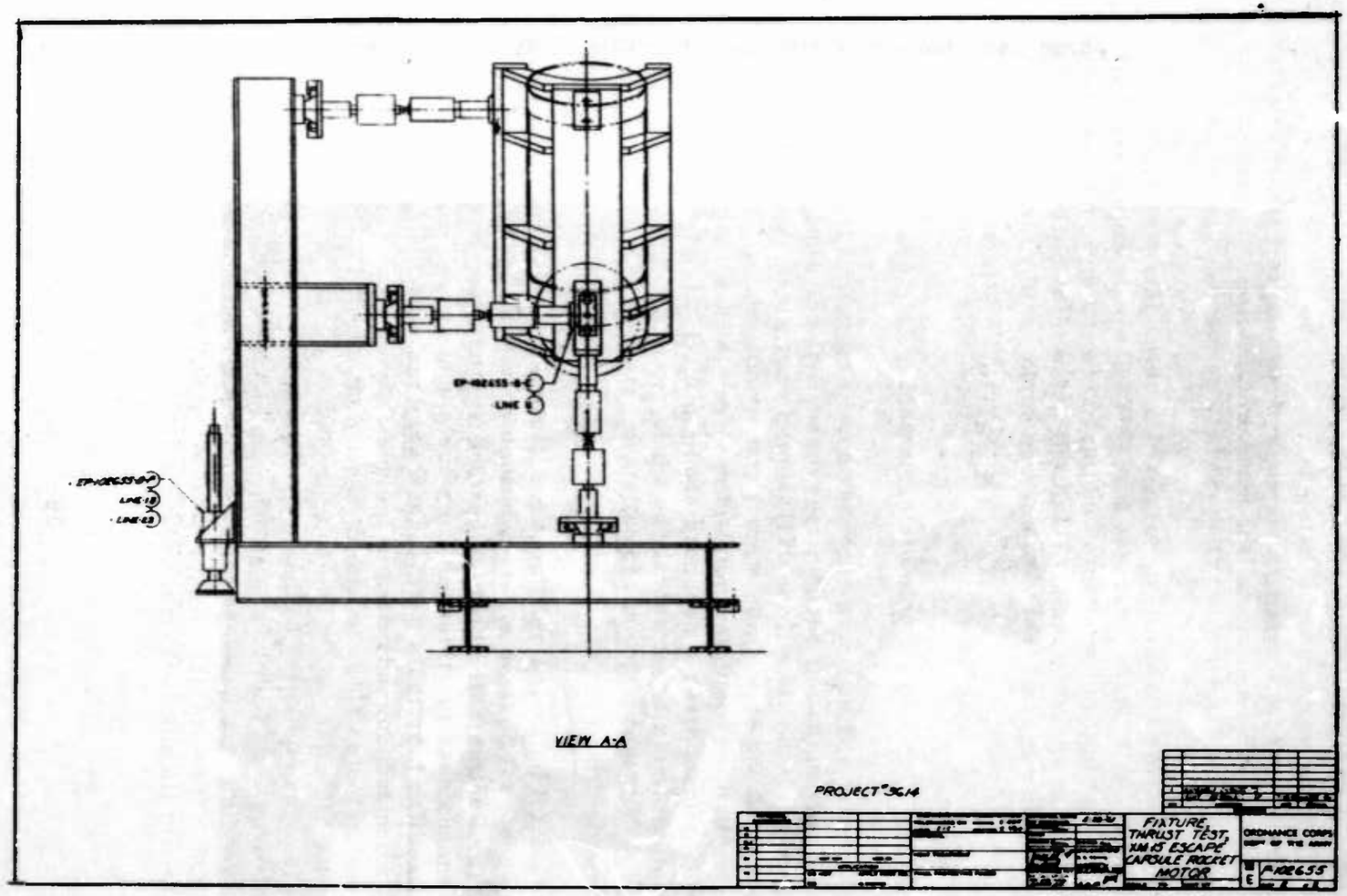

Figure 14. Drawing, Multicomponent Test Stand

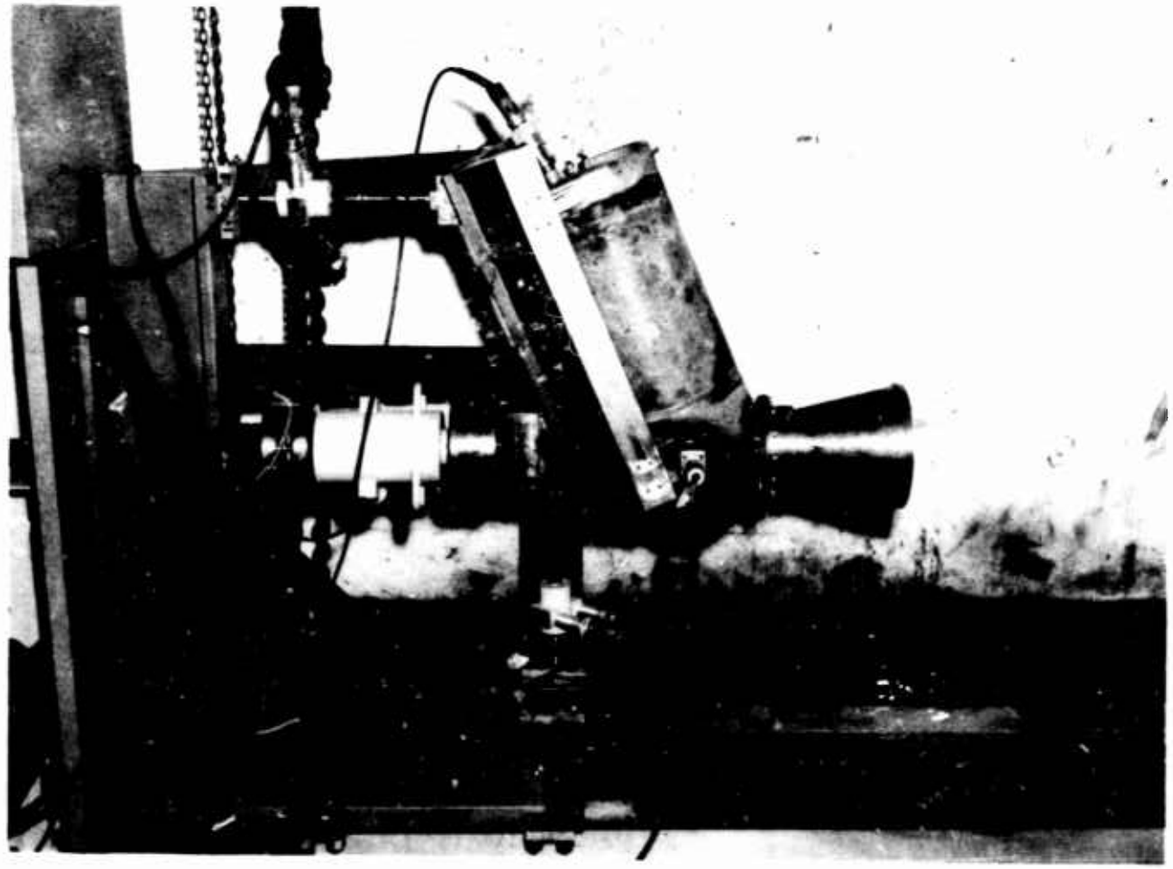

Figure 15. XM15 Escape Rocket Multicomponent Test Stand

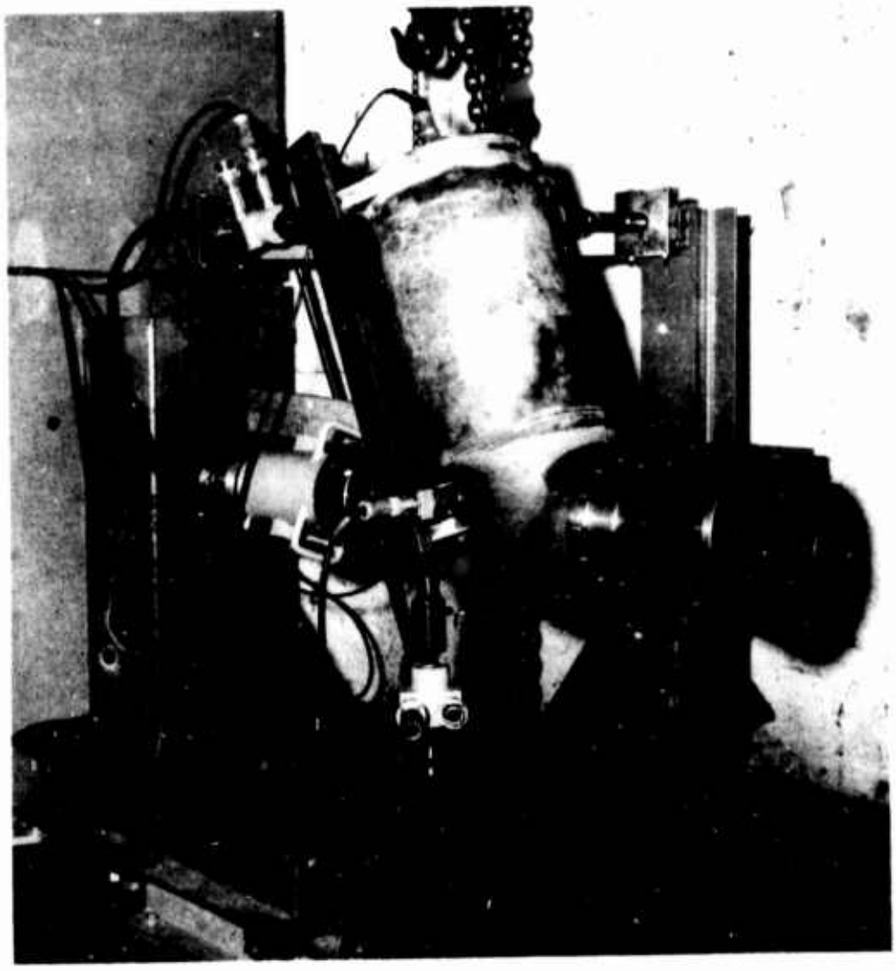

Figure 16. Static Test Setup utilizing Multicomponent Stand

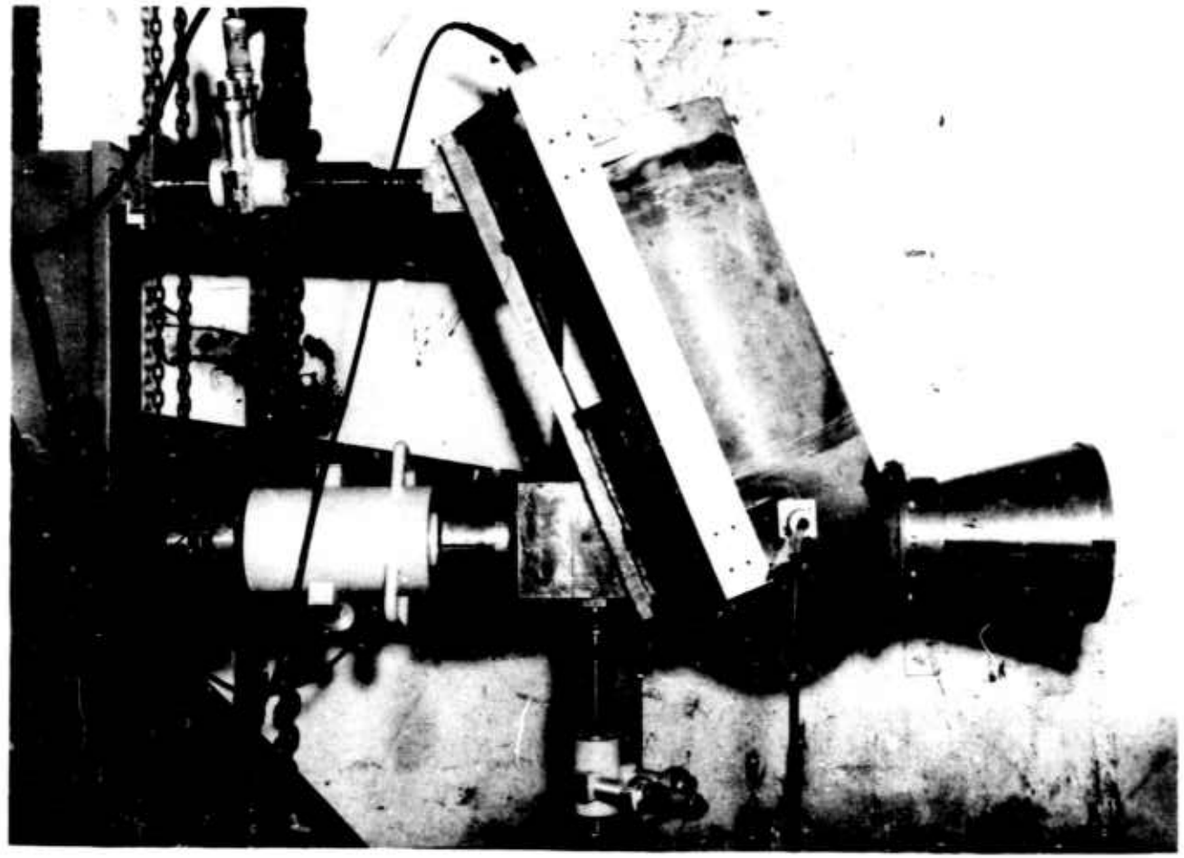

Figure 17. Side view of Static Test Setup utilizing a Multicomponent Stand with Three Thrust-measuring Assemblies

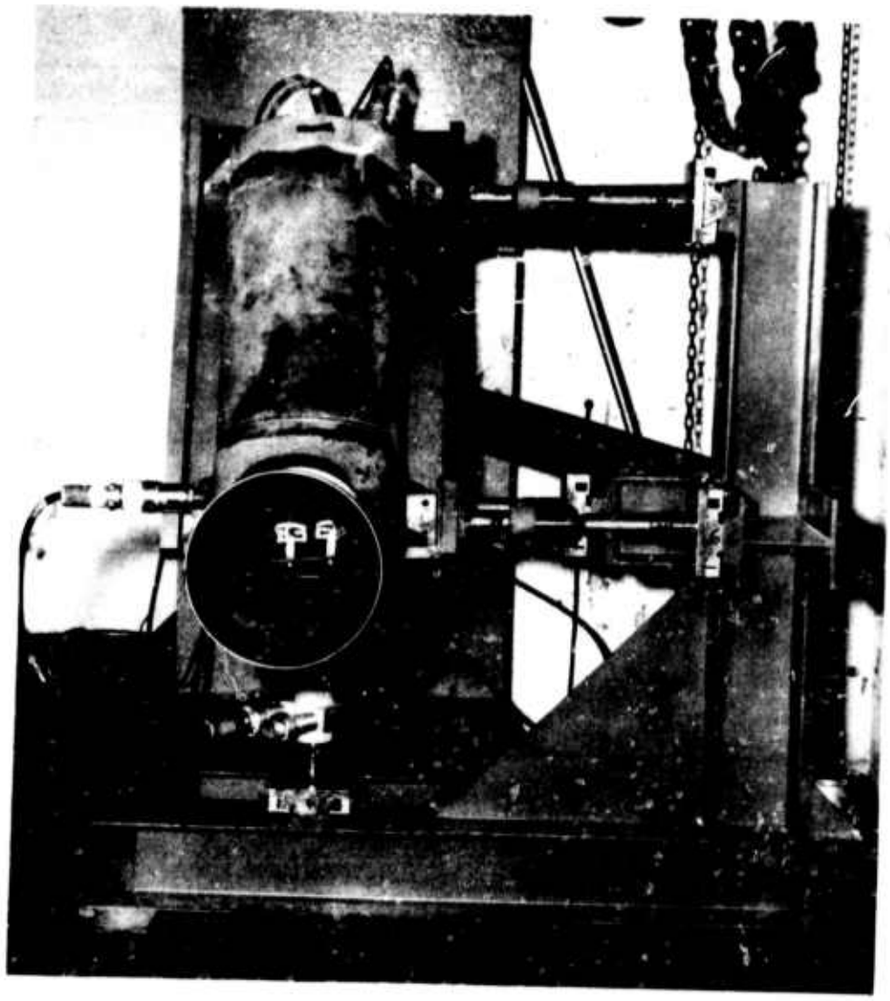

Figure 18. Nozzle End view, Static Test Setup utilizing a Multicomponent Test Stand

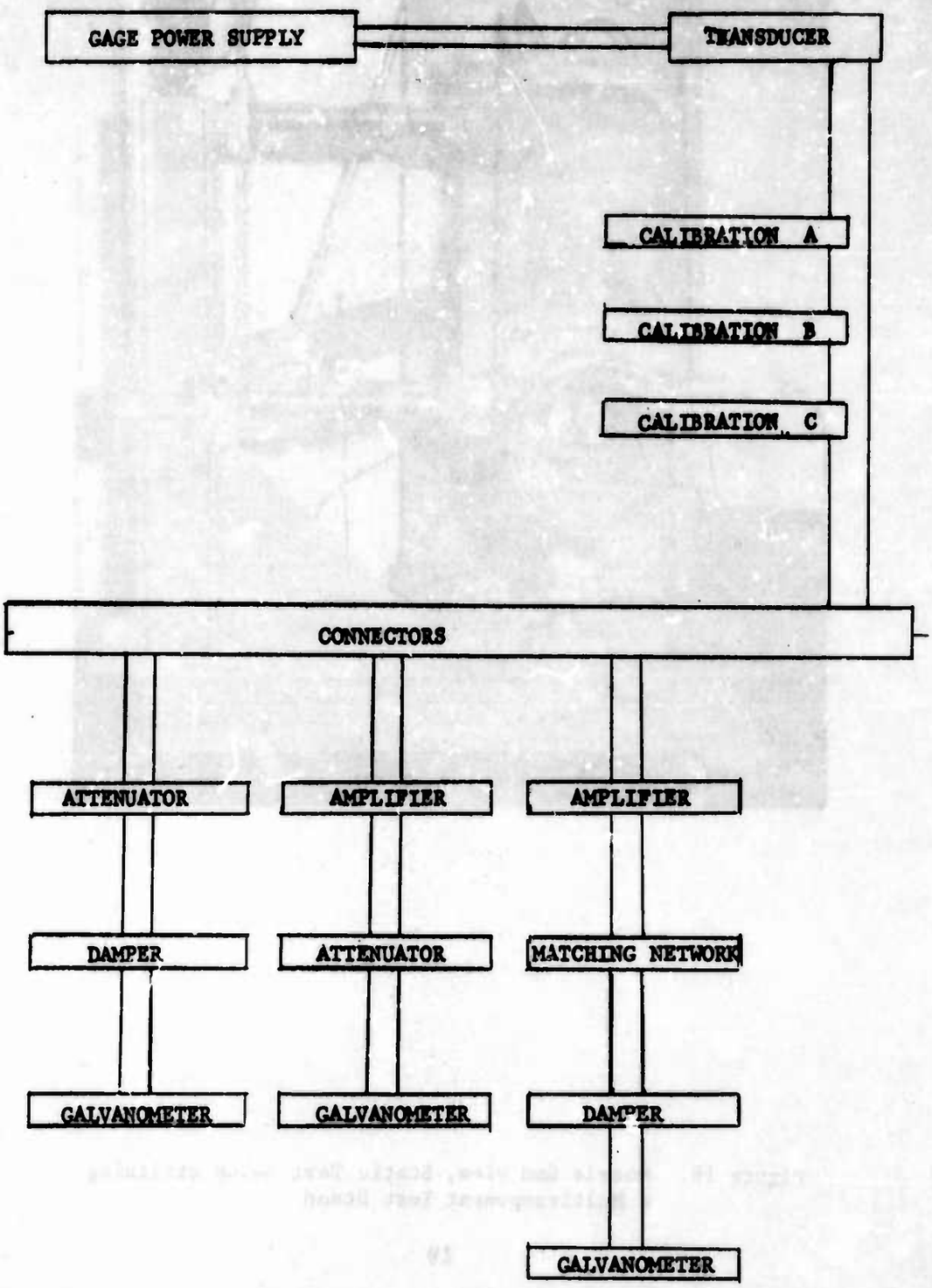

Figure 19. Block diagram of a Recorded Instrumentation Channel

Data Reduction

All data were reduced using standard reduction methods in accordance with MIL-STD-292 (Ord). Point values of pressure, thrust, and temperature were measured with a linear scale, and computed using the calibration scale factor. A planimeter was used in determining the area under the pressure and thrust curves. Where dual bridge thrust gages were used, yielding dual outputs, an average of the two thrust values is reported.

During the thrust misalignment tests, mechanically induced sinusoidal oscillations are evidenced in the thrust-time curves for the head end (horizontal) and nozzle end (vertical) components. These oscillations were bisected during the data reduction process and points on the faired curve were used for actual thrust amplitude determinations. This procedure is employed for accuracy and to avoid misinterpretation wherein observed oscillations are not directly proportional to chamber pressure and are, in fact, caused by the initial excitation of the motor-test stand mechanical system at its natural frequency. Thus determined, the faired curve is considered to be very indicative of the true, developed thrust.

The nozzle component, in addition to sensing a thrust output along the vertical axis, also sensed the decrease in propellant weight during firing. An accurate determination of the thrust misalignment angle required that a correction be made in the vertical thrust-time curve for this decrease in weight. This was accomplished during data reduction by assuming a completely linear burning rate and associated linearly decreasing propellant weight with time during the firing. A complete analysis of the method used for evaluating misalignment angles is given in Appendix II.

Test Results

All ballistic performance data are presented by the following group designations:

Group A - Igniter tests (rounds 1 through 4, 6 through 8, and 12 through 16).

Group B - Propellant evaluation (rounds 9 and 10).

Group C - Reduced charge pressure test (rounds 5 and 11).

Group D - Full charge pressure test (rounds 0 and 17 through 21).

Group E - Pressure, thrust, and misalignment studies (rounds 22 through 27).

The sources of error in these tests are the test stand, instrumentation, and data reduction. Previous investigation of the errors involved in the instrumentation, data reduction equipment, and procedures indicate that these errors are on the order of ± 1.5 percent. The procedures used to resolve the test stand errors are discussed in detail in Appendix II. Although these are mathematical procedures, the data obtained confirm their effectiveness. Thrust angle measurements were very consistent and reproducible at points along the thrust curve for each round and, also, from round to round for all tests. These angles were also very close to the theoretical value for these rounds. It is concluded that the angular results are accurate to about ± 10 minutes.

Group A - Igniter Tests (Table I)

The object of this test was to independently evaluate the performance of various type igniters by utilizing actual round components with inert (wooden) sticks simulating the propellant grain configurations.

Rounds 1, 3, 4, 6, 7, 8 (Composition - 40 gm B-KNO_3 pellets) - Test results revealed low, undesirable pressure levels. Both head end and nozzle end pressure gages produced negligible outputs and, as a result, most values were lost. Estimated values were obtained in a few instances and revealed ignition delays under 0.021 second and no pressures higher than 30 psig. All the simulated (inert) propellant grains were scorched, indicating a satisfactory flash pattern was produced by this igniter. The flash pattern was constantly improved by redesigning metal parts (head section and grain supports) in rounds 6, 7, and 8, with round 8 producing the best flash results. Disassembly and examination of round components after firing revealed no adverse effects on the metal parts.

TABLE I. Test Results, Group A Igniter Tests

Round No.	1	2	3	4	6	7	8	12	13	14	15	16
Film No.	59855	59874	59886	59900	60209	60248	60273	60415	60422	60423	60473	60478
Date fired (1961)	8/28	8/29	8/31	9/1	9/27	9/29	10/5	10/18	10/19	10/20	10/23	10/24
Igniter Composition (gm)												
B-KNO_3 pellets[a]	40	-	40	40	40	40	40	-	-	-	-	50
A5 black powder	-	10	-	-	-	-	-	10	35	71	75	75
A1 black powder	-	39	-	-	-	-	-	39	-	-	-	-
Squib	XM21	XM21	XM21	XM21	XM21	XM21	XM21	XM21	XM21	XM21	XM21	XM21
Pressure gage												
Head end	1K12021	2C8135	2C8135	2C8135	2C8135	2C8135	2C8135	2K12020	2K12020	2K12020	2K12020	2K12020
Nozzle end	1K12033	1C12676	1C12676	1C12676	1C12676	1C12676	1C12676	2K12021	2K12021	2K12021	2K12021	2K12021
Max pressure (psig)												
Head end	30[b]	230	10[b]	10[b]	NR[c]	NR	NR	20[b]	80[b]	40[b]	120[b]	170[b]
Nozzle end	20[b]	220	NR	NR	NR	NR	NR	20[b]	40[b]	30[b]	30[b]	70[b]
Ignition delay (sec)												
Head end	0.006	0.005	0.019	0.021	NR	NR	NR	0.467	0.020	0.046	0.009	0.013
Nozzle end	0.008	0.005	NR	NR	NR	NR	NR	0.492	0.022	0.048	0.016	0.013

[a]Boron potassium nitrate pellets, Type NNP 502, aspirin size (0.250 in. dia and 0.130 in. thick).

[b]These are estimated values because of the low pressure and limited resolution.

[c]NR - data not recorded because of low or negligible pressure.

NOTE: Inert wooden grains, simulating the propellant grain configurations, were painted white before each firing for visual examination of igniter blast pattern.
All igniters were fired under ambient temperature conditions.
Igniter utilized an ethyl cellulose container for all rounds except rounds 15 and 16, which used a cotton bag.

Rounds 2, 12 (Composition - 39 gm A1 and 10 gm A5BP) - Round 2 developed a satisfactory maximum pressure of 230 psig with an ignition delay of 0.005 second. The blast due to the igniter damaged the three center grain supports, which were immediately redesigned. Round 12 developed negligible pressures and, as a result, only estimated values could be obtained. These low pressures were attributed to the fact that the igniter container had failed under the pressure exerted by the squib on the base of the igniter container. Recovery of igniter container pieces revealed that the top and bottom sections were undamaged and the squib failed to penetrate through to the black powder. Container failure occurred at the sides before the black powder had a chance to ignite properly.

Round 13 (Composition - 35 gm A5BP) - This igniter produced undesirable pressure levels (too low), good flash pattern, and no damage to the metal parts.

Round 14 (Composition - 71 gm A5BP) - The relatively low pressure values and excessively long ignition delays were attributed to the container failure, as in round 12. Both top and bottom sections were recovered, revealing the squib did not penetrate the etnyl cellulose container, which failed due to the pressure on the base section.

Round 15 (Composition - 75 gm A5BP) - Because of the ethyl cellulose container failure in rounds 12 and 14, this igniter utilized a cotton bag container. Pressure was still too low (120 psig), but the igniter performed satisfactorily in all other respects.

Round 16 (Composition - 75 gm A5BP and 50 gm B-KNO_3 pellets) - This igniter, utilizing a cotton bag container, produced the best flash results, a short ignition delay (0.013 sec), and a maximum head end pressure of 170 psig. Figure 20 is the oscillograph record of this firing. Metal parts suffered no adverse effects. It was decided that since this igniter produced satisfactory results, it would be used in all future firings.

Group B - Propellant Evaluation (Rounds 9 and 10, Table II)

The object of this test was to evaluate the ballistic performance of HE-N12 propellant by utilizing an XM37 motor body. No useful data were obtained because of poor round functioning. Further

Figure 20. Oscillograph Record, Round 16

TABLE II. Test Results, Group B, Propellant Evaluation

Round No.	9	10
Film No.	60334	60344
Date fired	10/9/61	10/11/61
Igniter composition (gm)		
A5 black powder	1.5	1
A1 black powder	6.5	-
B-KNO_3 pellets	-	7
Squibs (two in parallel)	M1A1	M1A1
Propellant		
Type	HE-N12	HE-N12
Weight (lb)	2.18	2.16
Pressure		
Gage	2K2923	2K2923
Results	a	b
Thrust		
Gage	2-1336	2-1336
Results	a	b
Nozzle diameter before firing (in.)	1.100	1.107

[a]Round did not function properly. Poor ignition, with approximately one-second hangfire. Propellant then chuffed for approximately ten seconds. No valid data obtained.

[b]Round ignited properly, but burned erratically. No useful data obtained.

NOTE: Firing were conducted under ambient temperature conditions, utilizing an XM37 motor body.

investigation for obtaining preliminary performance data on the HE-N12 propellant utilizing the XM37 motor body was discontinued.

Group C - Reduced Charge Pressure Test (Table III)

The object of this test was to obtain the ballistic characteristics (pressure only) of a reduced charge of multiple extruded double base propellant grains (HE-N12).

Round 5 (Composition - 3 gr HE-N12, 20.85 lb) - Propellant burned for approximately 20 seconds at a very low pressure (too low for adequate resolution). The recording equipment was set up for a 2.7-second functioning time; therefore, most of the burning was missed. Camera coverage verified the 20-second burning time. Nine inert grains were utilized in this firing. Metal parts suifered no adverse effects.

Round 11 (Composition - 12 gr HE-N12, 52.40 lb) - This firing produced approximately a 0.5-second hangfire. The igniter functioned 0.020 second after fire pulse. Two distinct, audible reports during the firing verified the hangfire. Figure 21 is an oscillograph record of this firing. The round performed satisfactorily subsequent to the hangfire.

Group D - Full Charge Pressure Tests (Table IV)

The object of this test was to obtain the ballistic characteristics (pressure only) of a full charge of multiple extruded double base propellant grains (HE-N12).

Round 0 - This was the first static functioning test of the XM15 round. Normal operation was not achieved and the unit failed from over-pressure. After data analysis was conducted, a test program was initiated to correct: (1) local port inbalance; (2) concentration of the igniter on the three central grains; and (3) insufficient grain support.

Round 17 - At the conclusion of the igniter test program, a full round (round 17) functioned normally except for a trap which eroded away at about the 2/3 point of burn time. Pressures were slightly higher and burning time slightly faster than expected. Temperature-sensitive paint on the external center section of the motor body revealed

TABLE III. Test Results, Group C, Reduced Charge Pressure Test

Round	5		11	
Film No.	59953		60386	
Date fired	9/12/61		9/13/61	
Igniter composition, B-KNO_3 pellets (gm)	40		40	
Squib	XM21		XM21	
Propellant				
Type	HE-N12		HE-N12	
No. of sticks	3[a]		12	
Weight (lb)	20.85		52.40	
End	Head	Nozzle	Head	Nozzle
Pressure				
Gage	1K305	1K1448	2K12209	2K12212
Maximum (psi)	Lost[b]	Lost[b]	860	860
At burnout (psi)	Lost[b]	Lost[b]	380	380
Mean, at action time (psi)	Lost[b]	Lost[b]	580	610
Mean, at burning time (psi)	Lost[b]	Lost[b]	610	630
Time (sec)				
Ignition delay, pulse to 10% maximum pressure	Lost[b]	Lost[b]	0.536[c]	0.532
10% max pressure to max pressure	Lost[b]	Lost[b]	0.051	0.053
Action, 10% to 10%	Lost[b]	Lost[b]	0.681	0.675
Burning, 10% to burnout	Lost[b]	Lost[b]	0.632	0.630
Conditioning				
Temperature (°F)	70		70	
Minimum hours	8		24	
Nozzle diameter before firing (in.)	4.763		4.780	

[a]Three live propellant sticks placed in center of motor. The nine surrounding grains were inert (wood).

[b]Round 5 burned for approximately 20 seconds at a pressure too low to record with adequate resolution.

[c]Round 12 had approximately a 0.5-second hangfire. Slight pressure evident approximately 0.020 second after fire pulse, indicating igniter fired at this time.

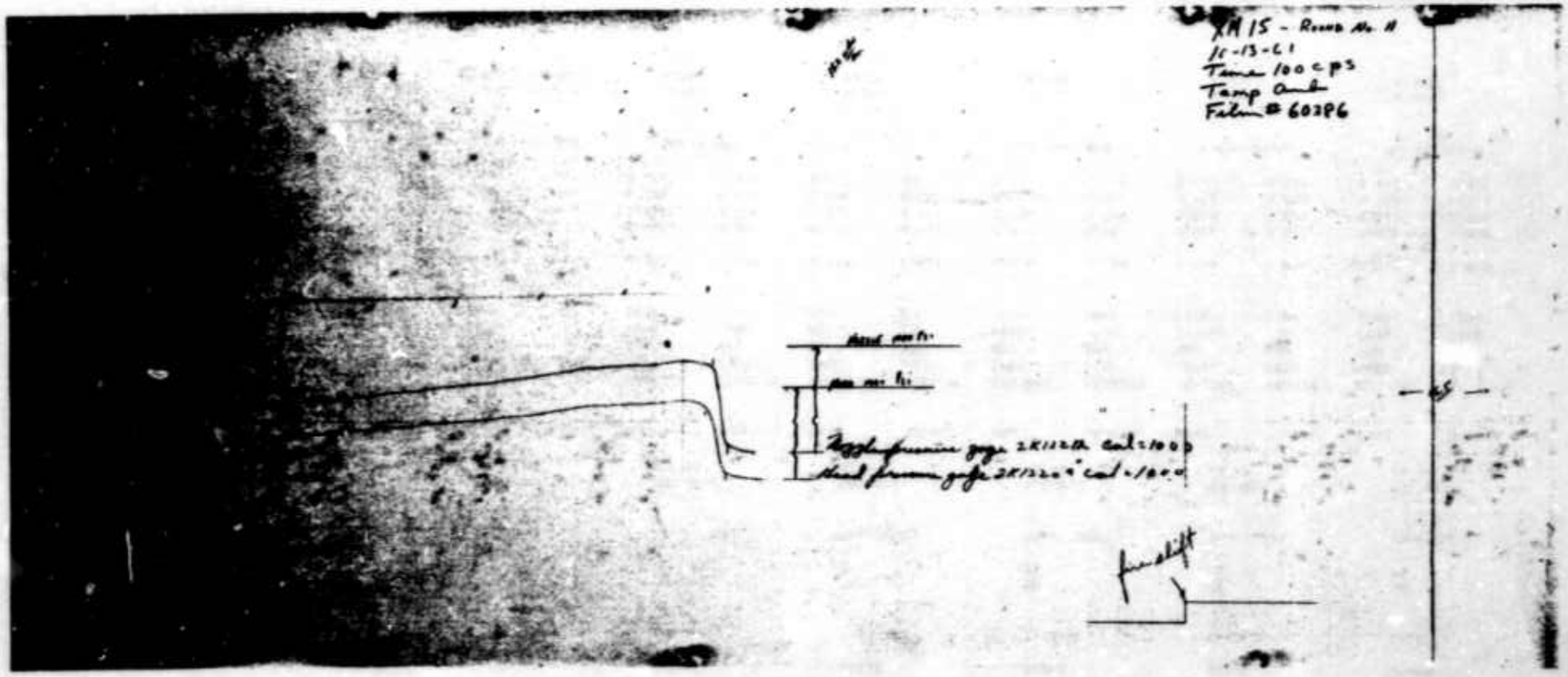

Figure 21. Oscillograph Record, Round 11

TABLE IV. Test Result, Group D, Full Charge Pressure Test

Round No.	0		17		18		19		20[a]		21	
Film No.	59640		60486		60712		61280		63252		63409	
Date fired	8/1/61		10/26/61		11/27/61		1/12/62		6/5/62		6/20/62	
Igniter composition (gm)												
B-KNO_3 pellets	40		50		50		50		50		50	
AS black powder	-		75		75		75		75		75.	
Squib	XM21		Two XM21		Two XM21		Two XM21		Two XM21		Two XM21	
Propellant												
Type	HE-N12		HE-N12		HE-N12		HE-N12		HE-N12		HE-N12	
Weight (lb)	85.00		82.50		82.04		80.49		80.53		79.94	
End	Head	Nozzle	Head	Nozzle	Head	Nozzle	Head	Nozzle	Head	Nozzle	Head	Nozzle
Pressure												
Gage	2KB661	2KB943	2K12211	2K12212	5K12536	5K12537	2K12208	2K12213	2K12208	2K12209	2K12208	2K12209
Maximum (psi)	Lost[b]	Lost	2010	1900	1960	1910	1420	1330	1480	1400	1640	1550
At burnout (psi)	Lost	Lost	850	840	330	310	830	800	700	680	770	760
Mean, at action time (psi)	Lost	Lost	1450	1400	860	830	1090	1040	1090	1060	1190	1150
Mean, at burning time (psi)	Lost	Lost	1510	1460	NR[c]	NR	1130	1080	1130	1100	1250	1200
Time (sec)												
Fire pulse to initial rise	0.017	0.017	0.036	0.037	0.017	0.017	0.029	0.029	0.014	0.014	0.010	0.010
Ignition delay, fire pulse to 10% maximum pressure	0.506	0.506	0.042	0.047	0.029	0.029	0.033	0.033	0.026	0.026	0.028	0.028
10% max pressure to max pressure	Lost	Lost	0.026	0.038	0.147	0.147	0.036	0.036	0.029	0.029	0.021	0.031
Action, 10% to 10%	Lost	Lost	0.475	0.475	0.600	0.600	0.561	0.561	0.558	0.558	0.514	0.514
Burning, 10% to burnout	Lost	Lost	0.440	0.449	NR	NR	0.525	0.525	0.526	0.526	0.475	0.475
Motor body temperature (°F)	Not recorded		500 to 600		d		Not recorded		Not recorded		Not recorded	
Nozzle diameter (in.)												
Before firing	Not recorded		4.766		4.775		4.943		4.946		4.964	
After firing	Not recorded		4.764		4.775		4.946		4.952		4.987	

[a] Section of rocket sled structure was in direct line with nozzle exhaust in this firing (round 20).

[b] Round 0 malfunctioned; records indicated igniter functioned 0.017 second after fire pulse, but round experienced approximately 0.5-second hangfire. Last recorded pressure exceeded 2600 psi; this occurred as soon as the propellant started to burn.

[c] Round 18 burned erratically. Certain data were not required.

[d] Maximum surface temperature data from round 18 (thermocouples): (1) Center of motor body, nozzle side - 800° F
(2) Center of motor body, 180° from (1) - 875° F
(3) Curved section at nozzle, or aft end - 350° F.

NOTE: All rounds were preconditioned at 70° F for a minimum of 16 hours. Camera coverage (high speed and 24 frames per second) was utilized on all firings.

temperatures between 500° and 600 F. Figure 22 is the oscillograph record of this firing.

Round 18 - In this round the six grains near the nozzle entrance were shortened two inches to remove them from the transverse high velocity flow region, and the six grains near the opposite (forward) side were lengthened two inches in compensation. The charge was established; however, the record showed a trap failure similar to the previous round. Figure 23 is the oscillograph record of this firing. Thermocouples placed on the motor body at the center and curved aft end sections revealed acceptable temperature levels. An attempt at sound level readings seven feet from the nozzle was unsuccessful.

Round 19 - This round functioned satisfactorily. The pressure-time curves were very smooth, with good regression and no evidence of propellant break-up. Figure 24 is the oscillograph record of this firing. Theoretical thrust values were obtained from the pressure time curves by using the expression:

$$F = C_D I_{SP} A_t P_c$$

where

F = thrust (lb)

C_D = discharge coefficient (lbm/sec)

I_{SP} = specific impulse (lbf-sec/lbm)

A_t = nozzle throat area ($in.^2$)

P_c = chamber pressure (psi).

A_t and P_c are known, and various values were assumed for C_D and I_{SP}. The following theoretical results were obtained for total impulse.

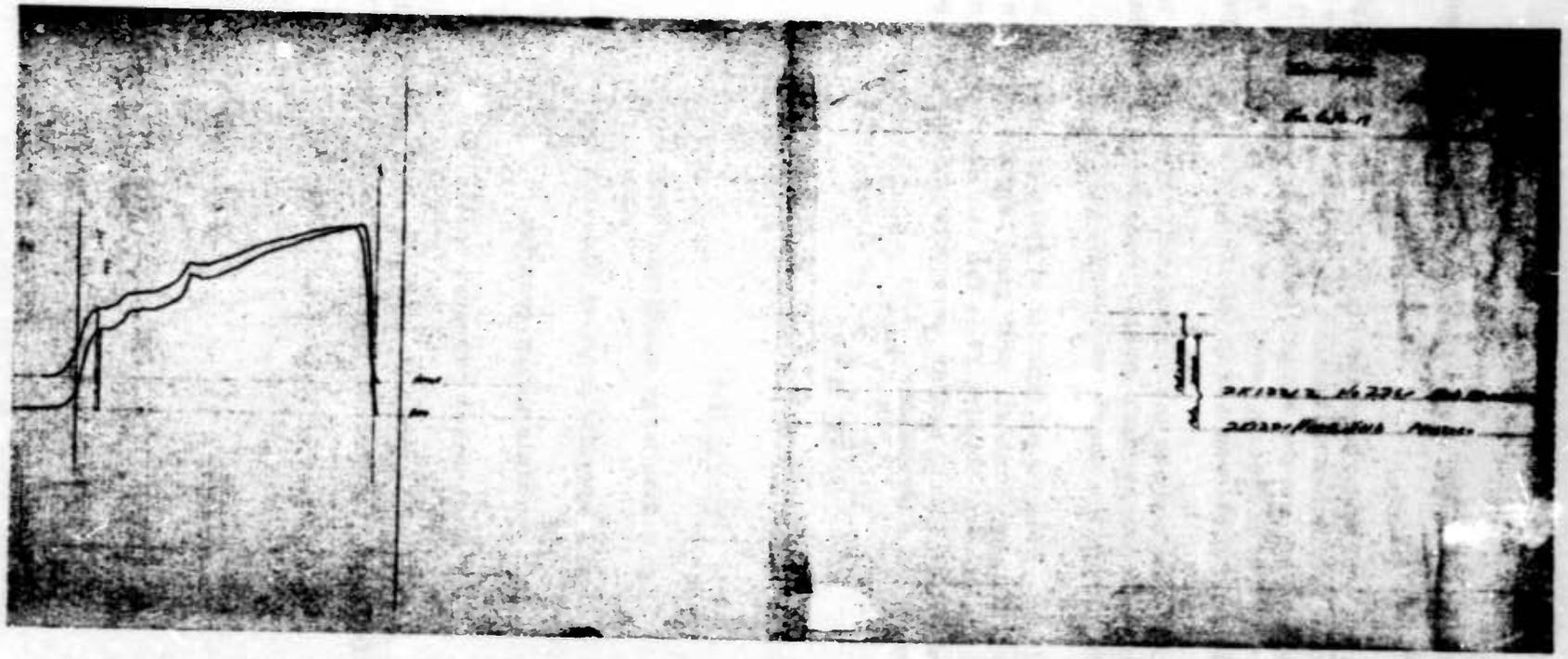

Figure 22. Oscillograph Record, Round 17

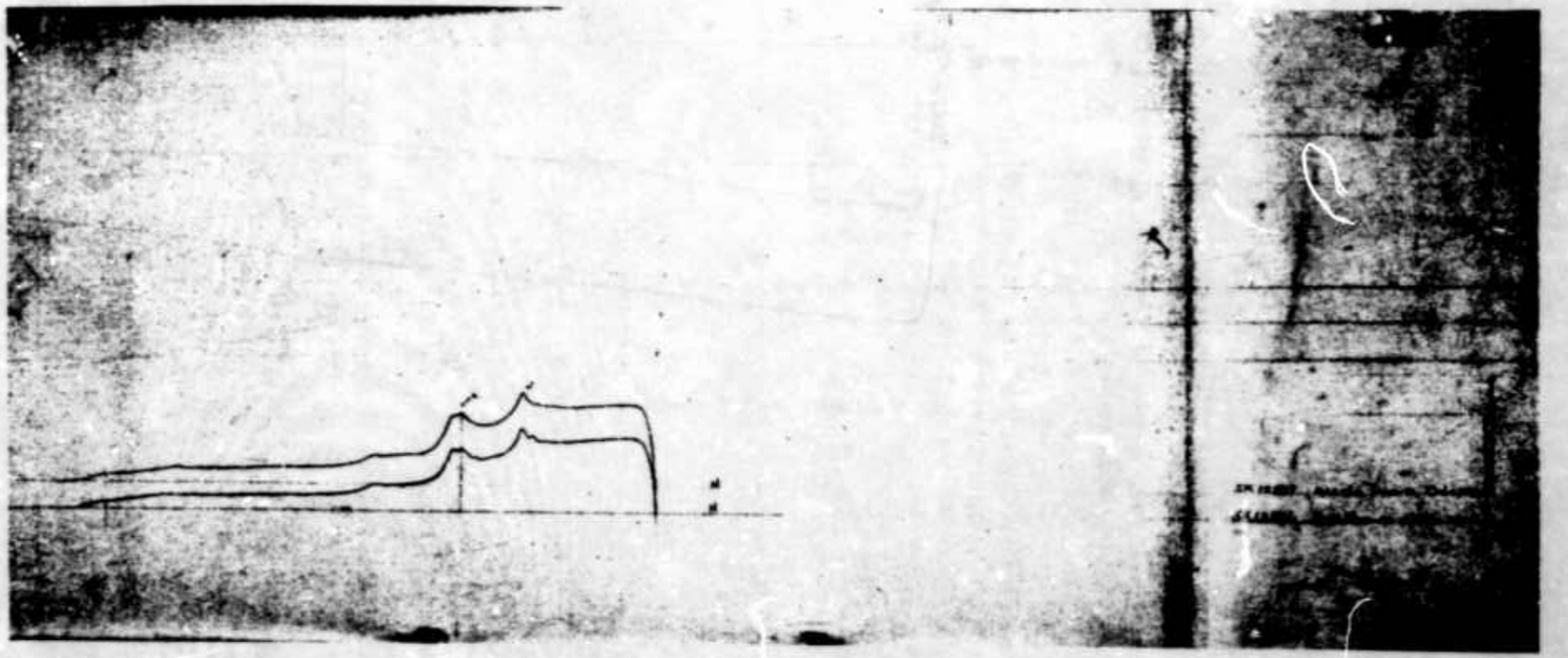

Figure 23. Oscillograph Record, Round 18

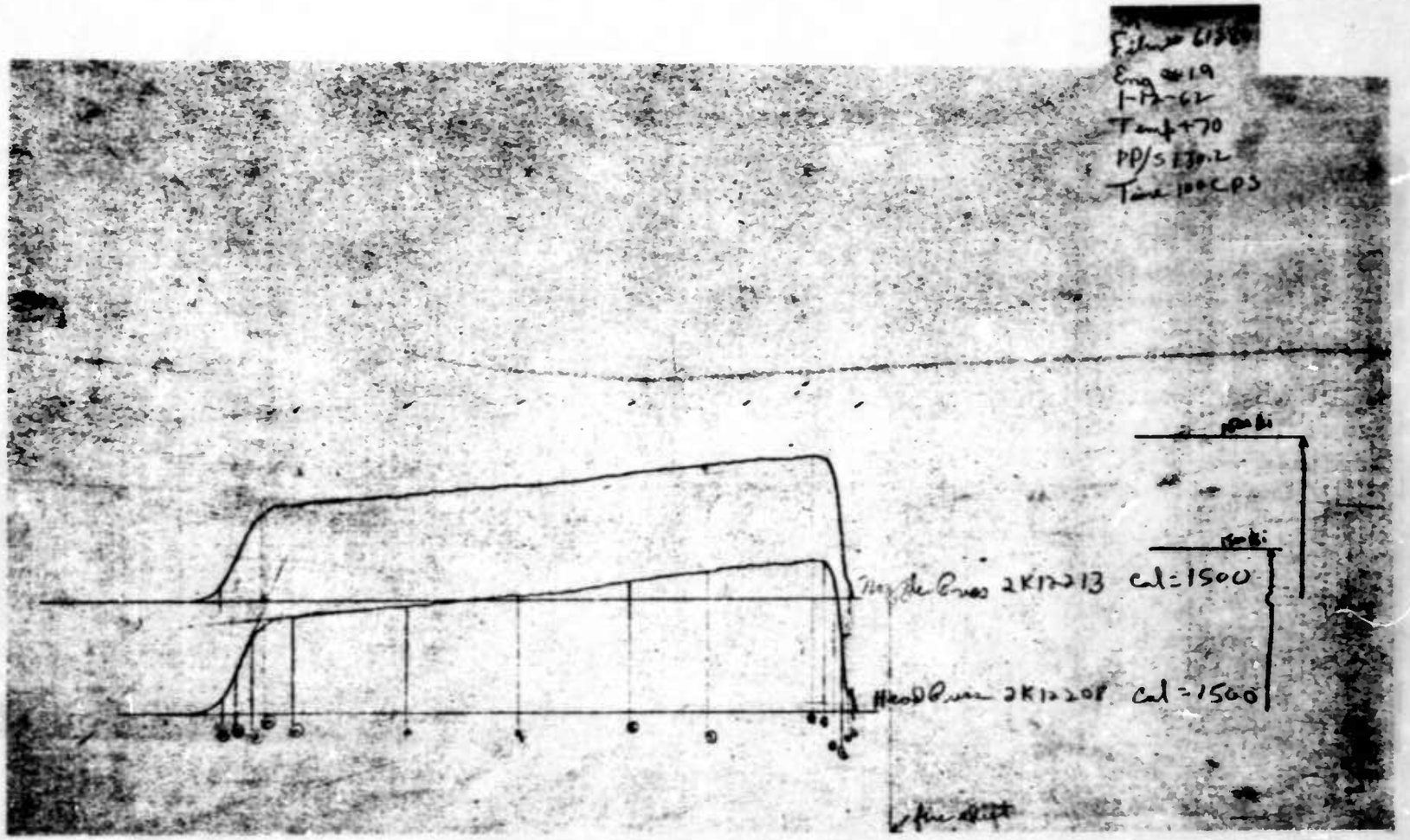

Figure 24. Oscillograph Record, Round 19

C_D (lbm/lbf-sec)	I_{SP} (lbf-sec/lbm)	Total Impulse (lbf-sec)
0.0066	210	16,200
0.0066	215	16,800
0.0066	220	17,200
0.00686*	215	17,700

*C_D calculated from test results.

In this round, transverse trap supports were incorporated and ceramic coatings were used on the trap subjected to high erosion. Slots were machined only in the six grains furthest from the nozzle entrance. The nozzle diameter was enlarged slightly. Mechanical integrity for the action time was established.

Consideration now shifted to preparation for obtaining thrust data.

Rounds 20 and 21 - Both of these rounds functioned satisfactorily. Figures 25 and 26 are the oscillograph records of these firings. A section of the sled structure which would be used in future rocket sled tests was placed at a distance of three feet from and in direct line with the nozzle to observe nozzle blast effects. The sled structure was rigidly secured to the rails of the firing bay (see Figure 12). No adverse effects were encountered.

Rounds 20 and 21, with additional parts coated with ceramic, provided the confidence to schedule rounds in the multicomponent thrust stand. In addition, the thrust appeared to be properly directed, as observed in the flame pattern viewed against a reticle on high speed film. Pertinent details of the charge at this point were:

Initial surface area	3440 sq. in.
Initial thrust	42,500 lbf
Final surface area	2900 sq in.
Final thrust	23,000 lbf
Specific impulse	215 lbf-sec/lbm
Density	0.0586 lbm/cu in.
Nozzle throat area	19.25 sq in.
Coefficient of discharge	0.0067 lbm/lbf-sec

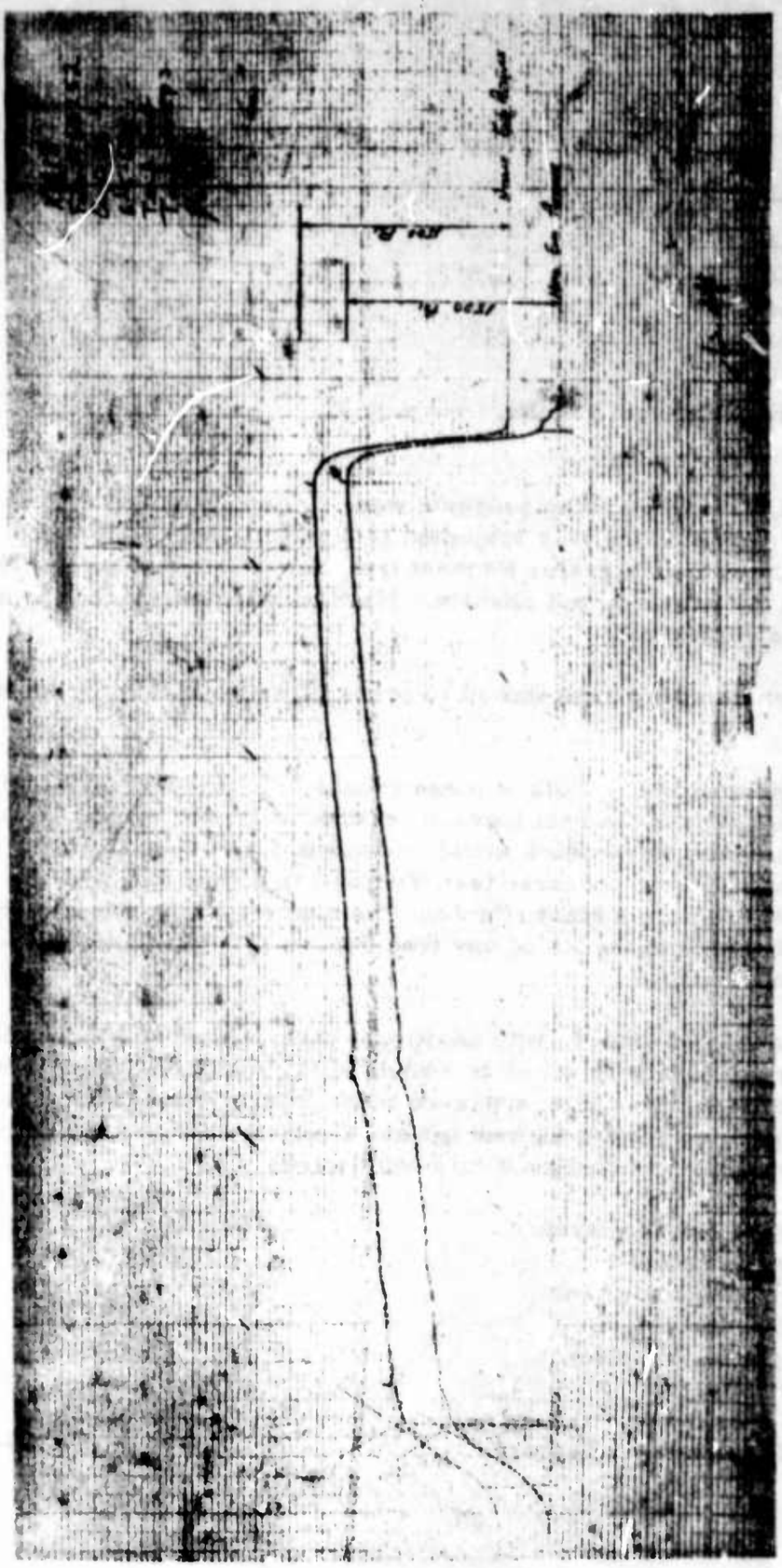

Figure 25. Oscillograph Record, Round 20

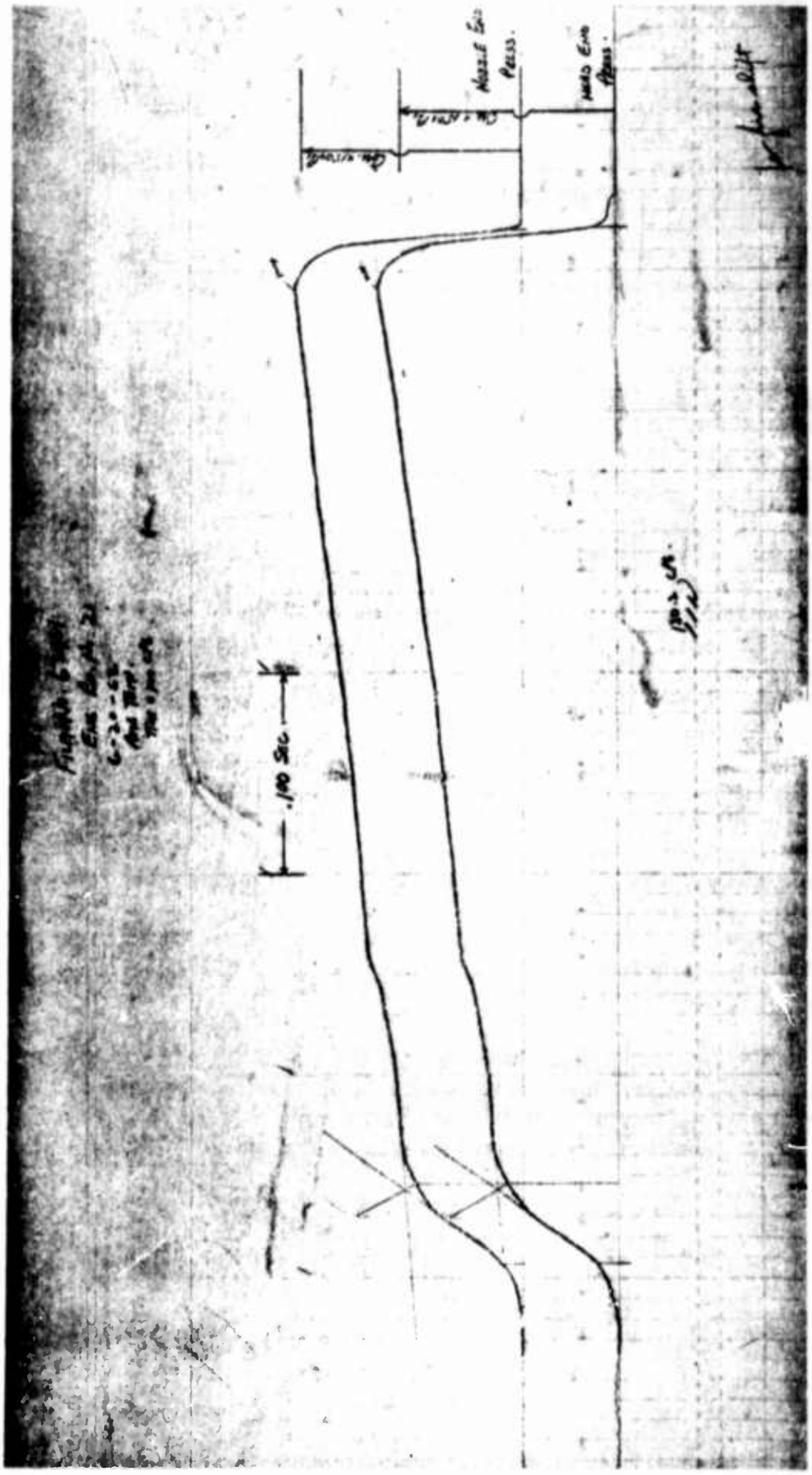

Figure 26. Oscillograph Record, Round 21

Chamber pressure	1500 psi
Burning rate	0.98 in./sec
Total impulse, avg	17,300 lbf-sec
Propellant weight	80 lbm.

Photographs of the motor after firings are shown in Figures 27 through 31.

Group E - Pressure, Thrust, and Misalignment Studies (Tables V and VI).

Rounds 22 through 26 - All rounds functioned satisfactorily. Figures 32 through 36, respectively, are the oscillograph records of these firings. The maximum average misalignment for any of the rounds was +7 minutes on round 24. Point by point determinations revealed that this round developed the maximum observed misalignment (+14 minutes) of all the tests. The positive misalignment angle indicates that the resultant thrust vector contains a vertical component acting in a downward direction. (An example for calculating the thrust misalignment is given in Appendix II in addition to the derivation of the formula used.)

Round 27 - The A. F. Flight Dynamics Laboratory requested a unit for the 900 KEAS ejection with peak thrust increased to 50,000 lbf maximum to assure lift off of the capsule at the high Q forces. Figure 37 is the oscillograph records of this firing. The increased thrust was achieved by increasing the length of the slots in the grains to increase the total propellant surface. Total impulse was reduced concomitant with the increase of surface. Round 27 developed 48,360 lbf and a total impulse of 16,370 lbf-sec.

Thrust output and variations of thrust in the pitch plane were determined by reading three components of a stand equipped to acquire six components. Summary of the data for the six rounds of Group E follows and a graphical presentation is given in Figure 38.

Maximum Thrust -		
No. of rounds	5	1
Avg thrust (lb)	42,330	48,360
Thrust range (lb)	± 1,200	-
Max target thrust (lb)	45,000	50,000

Figure 27. XM15 Escape Rocket, After Firing

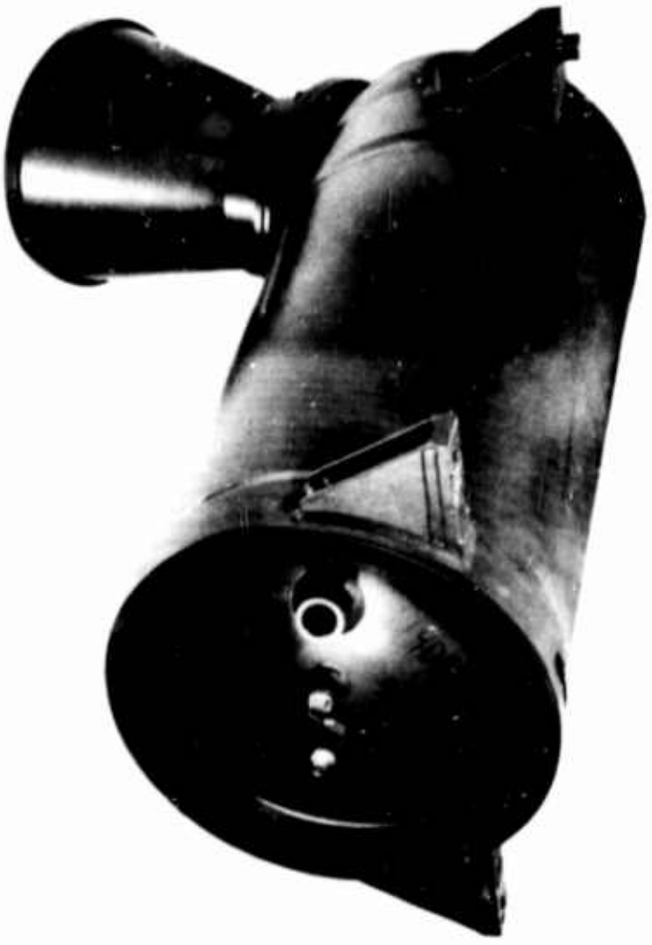

Figure 28. Head End view, XM15 Escape Rocket, After Firing

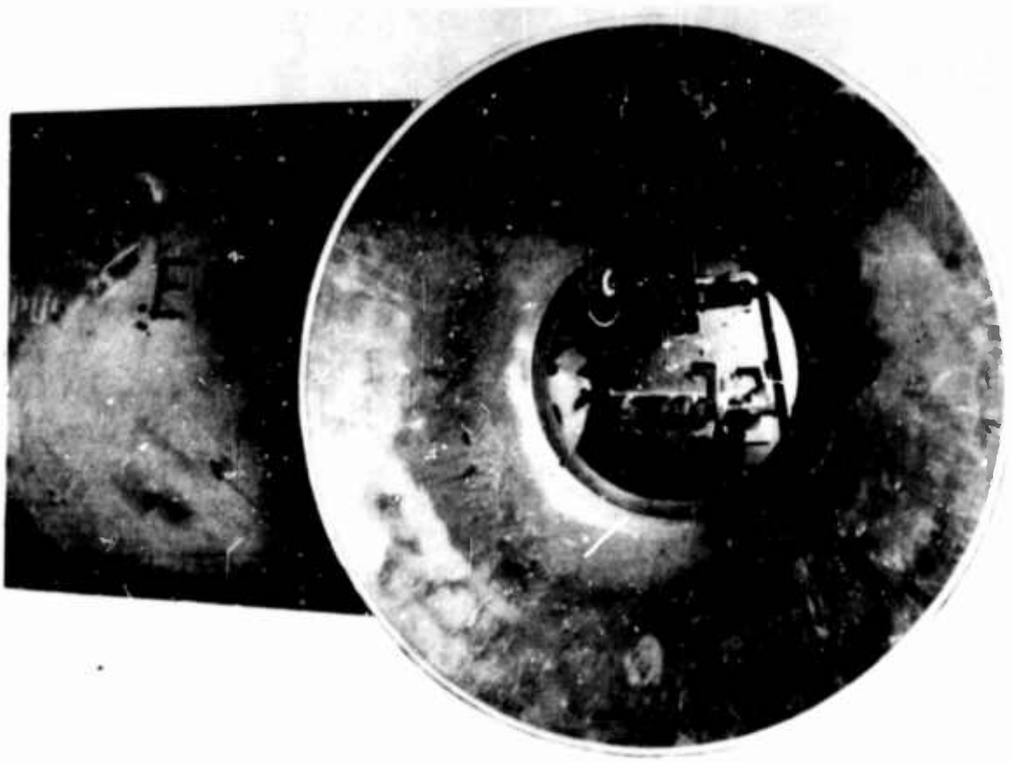

Figure 29. Nozzle and Interior view, XM15 Escape Rocket, After Firing

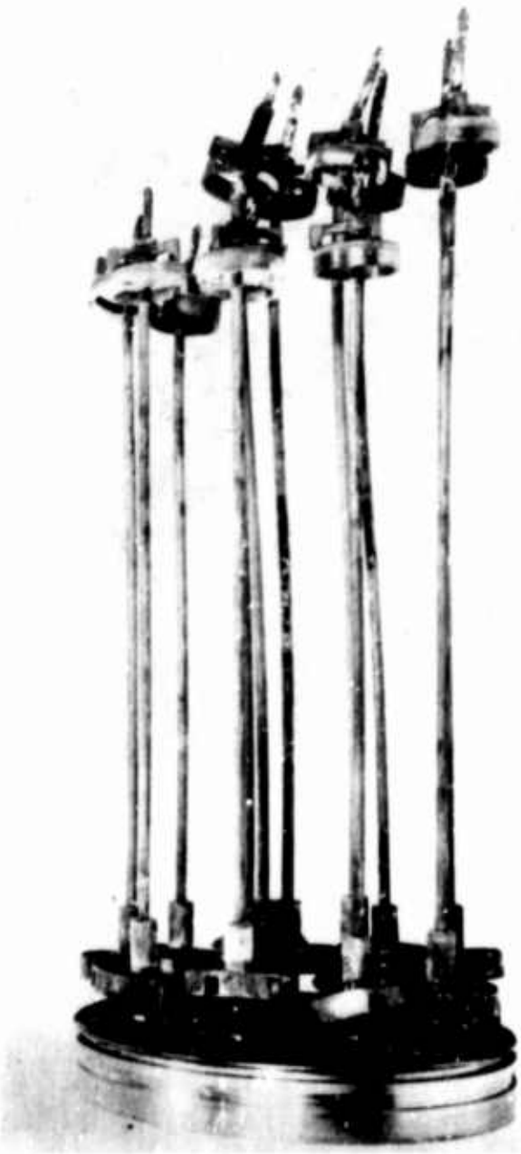

Figure 30. Head End and Suspension Assembly, XM15 Escape Rocket, After Firing

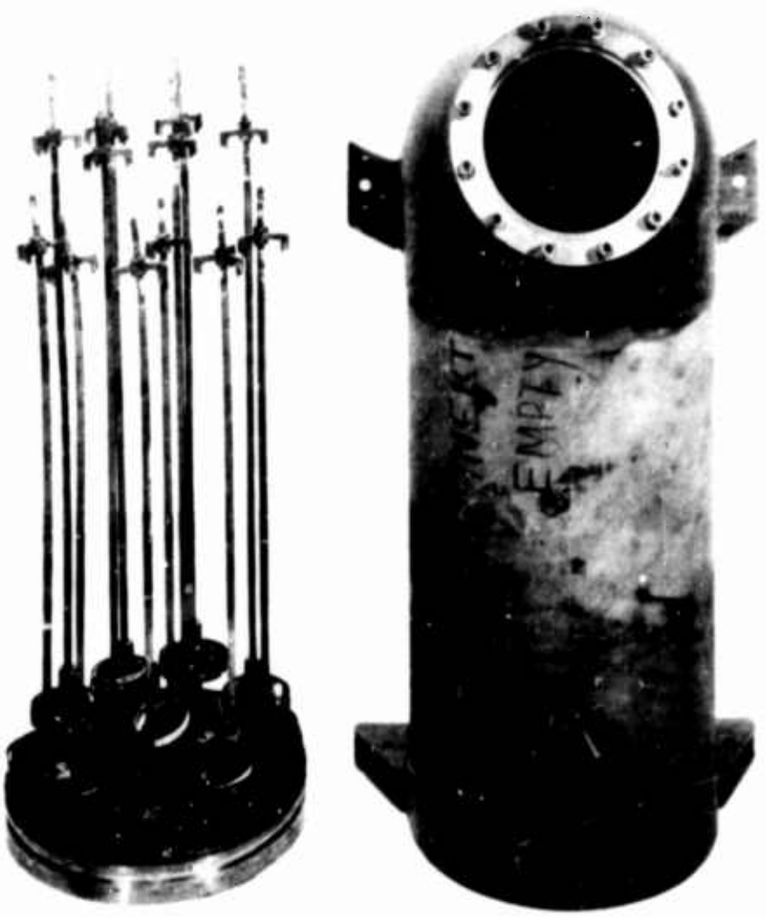

Figure 31. Head End and Suspension Assembly with Case, XM15 Escape Rocket, After Firing

TABLE V Test Results, Group E - Thrust and Pressure Determinations (Multicomponent Stand)

		F/P[a]		F/P		F/P		F/P		F/P		F/P
Round No.	22		23		24		25		26		27[b]	
Film No.	63771		63880		63973		64028		64058		64962	
Date fired	7/31/62		8/10/62		8/21/62		8/30/62		9/6/62		1/24/63	
Conditioning temperature (°F)	70		70		70		90		90		70	
Minimum conditioning time (hr)	24		24		24		24		24		24	
Propellant weight (lb)	80.69		80.86		80.65		80.45		80.60		79.37	
Time (sec)												
Fire pulse to initial rise	0.010		0.010		0.010		0.009		0.007		0.004	
Fire pulse to 10%	0.017		0.017		0.014		0.017		0.012		0.016	
Fire pulse to maximum	0.043		0.044		0.047		0.037		0.034		0.052	
10% to maximum	0.026		0.027		0.033		0.020		0.022		0.036	
Burning time	0.492		0.498		0.516		0.489		0.488		0.485	
Action time	0.543		0.545		0.549		0.532		0.531		0.512	
Head end pressure (psi)												
Maximum	1500	28.50	1520	28.01	1500	27.42	1510	27.60	1520	28.64	b	
Burnout	790	29.44	810	28.44	650	27.58	790	28.13	850	27.95	b	
Burning time avg	1170		1190		1170		1220		1220		b	
Action time avg	1100		1120		1130		1160		1160		b	
Nozzle end pressure (psi)												
Maximum	1440	29.69	1420	29.99	1390	29.59	1430	29.14	1420	30.65	1650	29.31
Burnout	770	30.21	770	29.92	610	29.39	760	29.24	840	28.29	490	26.33
Burning time avg	1160		1130		1100		1160		1190		1180	
Action time avg	1090		1080		1060		1110		1130		1130	
$\int Pdt$[c] (psi-sec)												
Head end	599		611		619		616		618		b	
Nozzle end	594		586		582		591		599		578	
Main thrust, R_{1R} (lb)												
Maximum	42750		42580		41130		41670		43530		48360	
Burnout	23260		23040		17930		22220		23760		12900	
Burning time avg	34080		33720		32470		33960		33940		33500	
Thrust, action time avg (lb)												
Main, R_{1R}	32160		31910		31170		32290		32320		31980	
Horizontal head end, R_{2R}	22		60		55		42		20		7	
Vertical, R_{3R}	-106		-124		-53		-157		-156		-153	
Resultant, T	32180		31970		31230		32330		32340		3,990	
Total impulse, resultant thrust (lb-sec)	17500		17400		17200		17200		17200		16370	
Specific impulse, resultant thrust (sec)	216		215		213		214		213		206	
Misalignment, action time avg, θ (min)	1		-1		7		-4		-4		-3	
Nozzle diameter (in.)												
Before firing	4.941		4.951		4.947		Not recorded		4.944		4.945	
After firing	4.947		4.950		4.945		Not recorded		4.944		4.950	

[a] F = thrust
P = pressure

[b] Increased thrust level.

[c] $\int Pdt$ = Integral of pressure with respect to time.

TABLE VI. Test Results, Group E - Thrust Misalignment Studies

ΔP	Time (sec)	Head Pressure (psi)	F/P	Nozzle Pressure (psi)	F/P	Thrust[a] (lb) R_{1R}	R_{2R}	R_{3R}	Resultant	Misalignment Angle (min)
					Round No. 22					
30	0.126	1390	28.98	1360	29.62	40280	50	-130	40300	+5
10	0.219	1230	28.09	1220	29.33	35780	30	-120	35800	+3
10	0.326	1100	29.35	1090	29.62	32290	10	-100	32300	+2
0	0.425	980	29.40	980	29.40	28810	30	-140	28800	-5
					Round No. 23					
60	0.100	1450	28.23	1390	29.45	40940	80	-240	41000	-4
60	0.200	1280	28.47	1220	29.87	[illegible]	20	-150	36500	0
50	0.300	1120	28.59	1070	29.93	32020	50	-90	32100	+3
40	0.400	1020	28.53	980	29.69	29100	10	-110	29100	-2
					Round No. 24					
100	0.100	1460	27.16	1360	29.16	39660	100	-20	39800	+14
60	0.200	1310	28.12	1250	29.47	36840	60	-70	37200	+8
70	0.300	1150	28.06	1080	29.88	32270	60	-70	32300	+6
40	0.400	1030	27.58	990	28.70	28410	50	-90	28500	+1
					Round No. 25					
60	0.100	1420	28.27	1360	29.51	40140	90	-210	40200	-2
30	0.200	1330	28.14	1300	28.79	37430	50	-210	37500	-5
20	0.300	1200	28.82	1180	29.31	34580	-10	-160	34600	-2
20	0.400	940	27.63	920	28.23	25970	0	-150	26000	-12
					Round No. 26					
60	0.100	1440	27.65	1380	28.85	39810	20	-180	39800	0
30	0.200	1300	28.20	1270	28.87	36660	30	-180	36700	-2
10	0.300	1160	28.58	1150	28.83	33150	0	-120	33200	0
10	0.400	990	31.29	980	31.61	30980	-10	-110	3100	+1
					Round No. 27[c]					
	0.100	Lost[d]		1570	28.39	44580	25	-210	44600	+1
	0.200	"		1330	28.25	37570	0	-190	37600	-2
	0.300	"		1080	27.78	30000	36	-150	30000	-6
	0.400	"		890	27.72	24670	0	-140	24700	-10

[a] R_{1R} = Main or axial thrust.
R_{2R} = Head end (horizontal) thrust.
R_{3R} = Nozzle end (vertical) thrust.

[b] Misalignment angle: + θ, X, − θ. X at nozzle throat area of nozzle center line.

[c] Increased thrust level.

[d] Head end pressure lost due to gage failure.

NOTE: All times are taken from 10 percent of maximum pressure

CODE: ΔP = Difference in pressure (psi) between head end and nozzle end.
F/P = Ratio between thrust (F) and pressure (P).

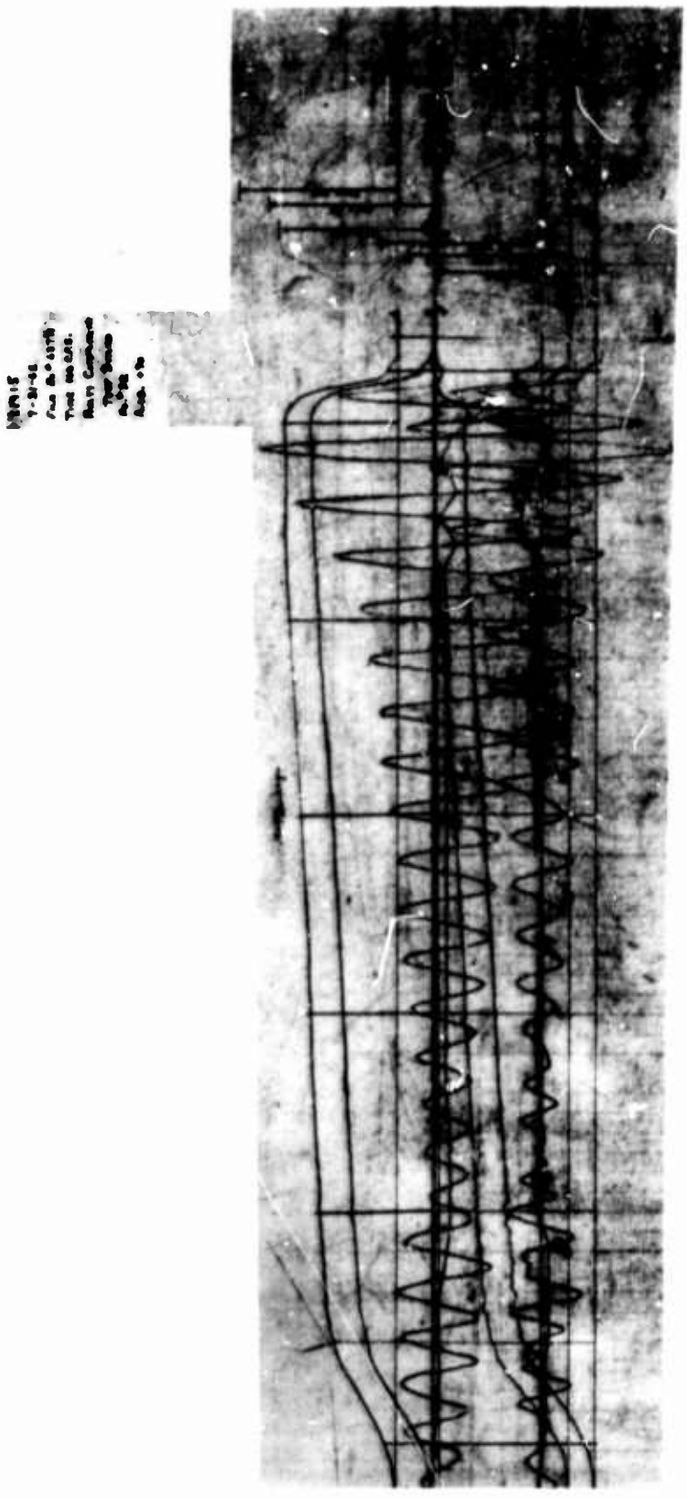

Figure 32. Oscillograph Record, Round 22

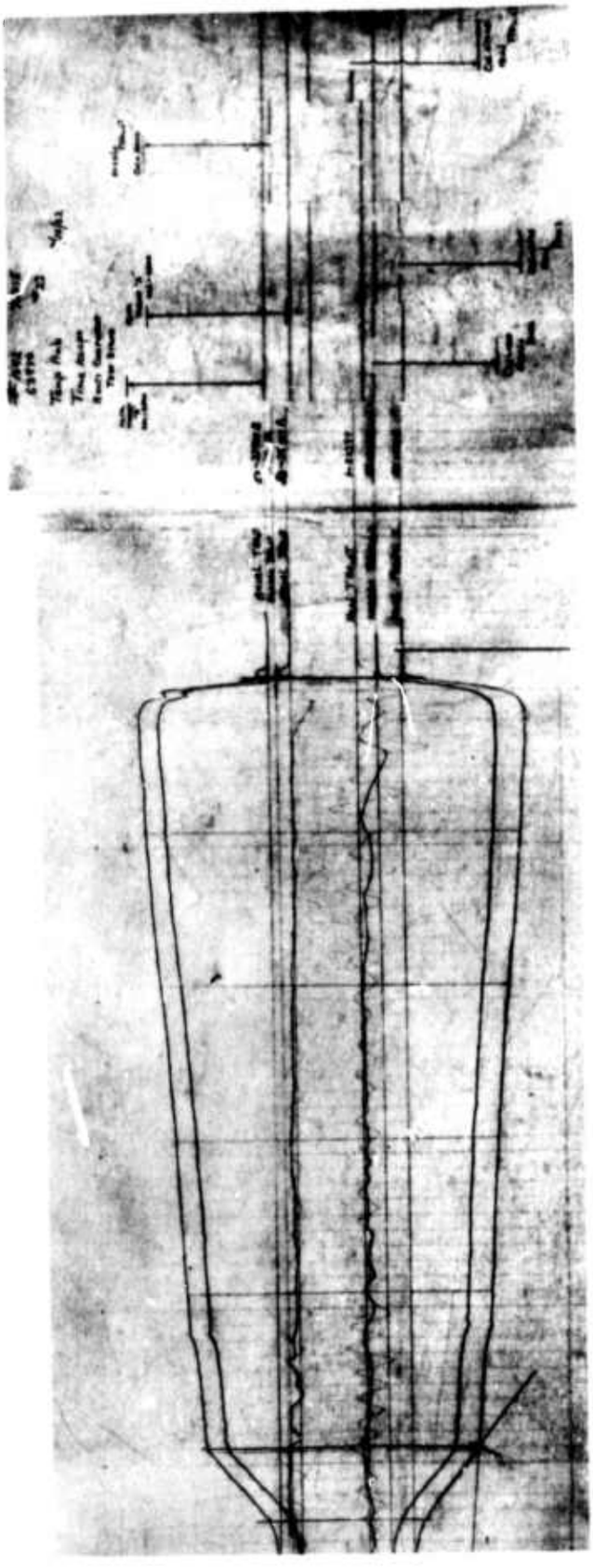

Figure 33. Oscillograph Record, Round 23

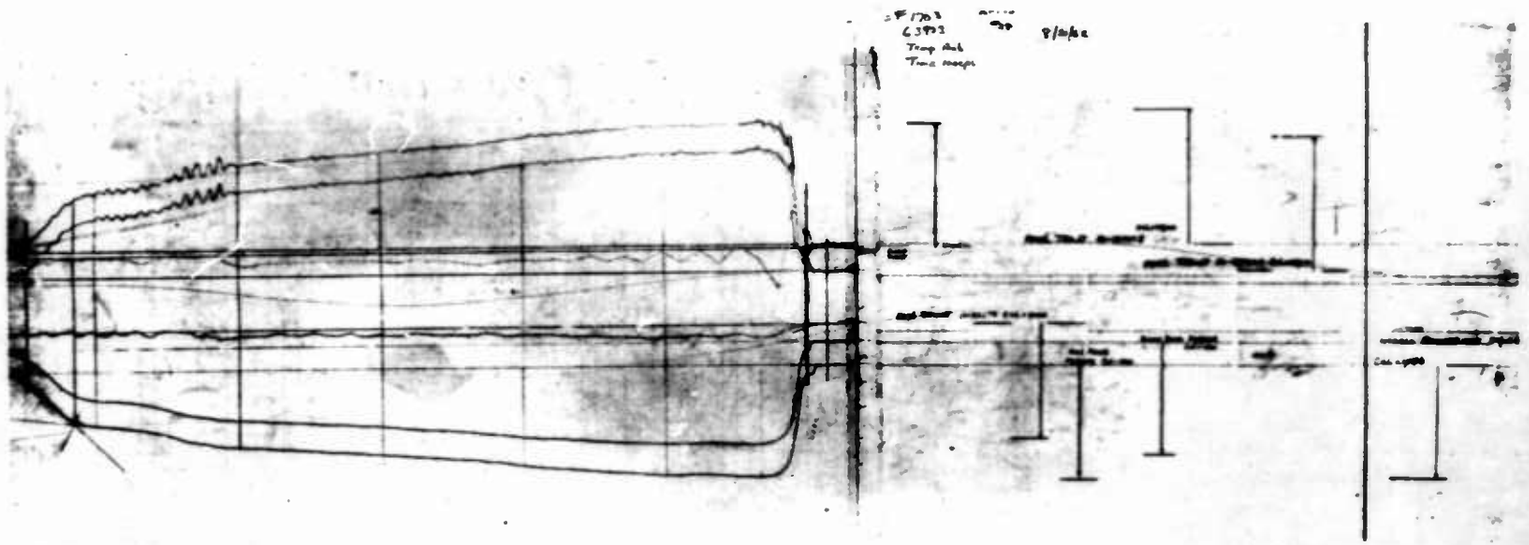

Figure 34. Oscillograph Record, Round 24

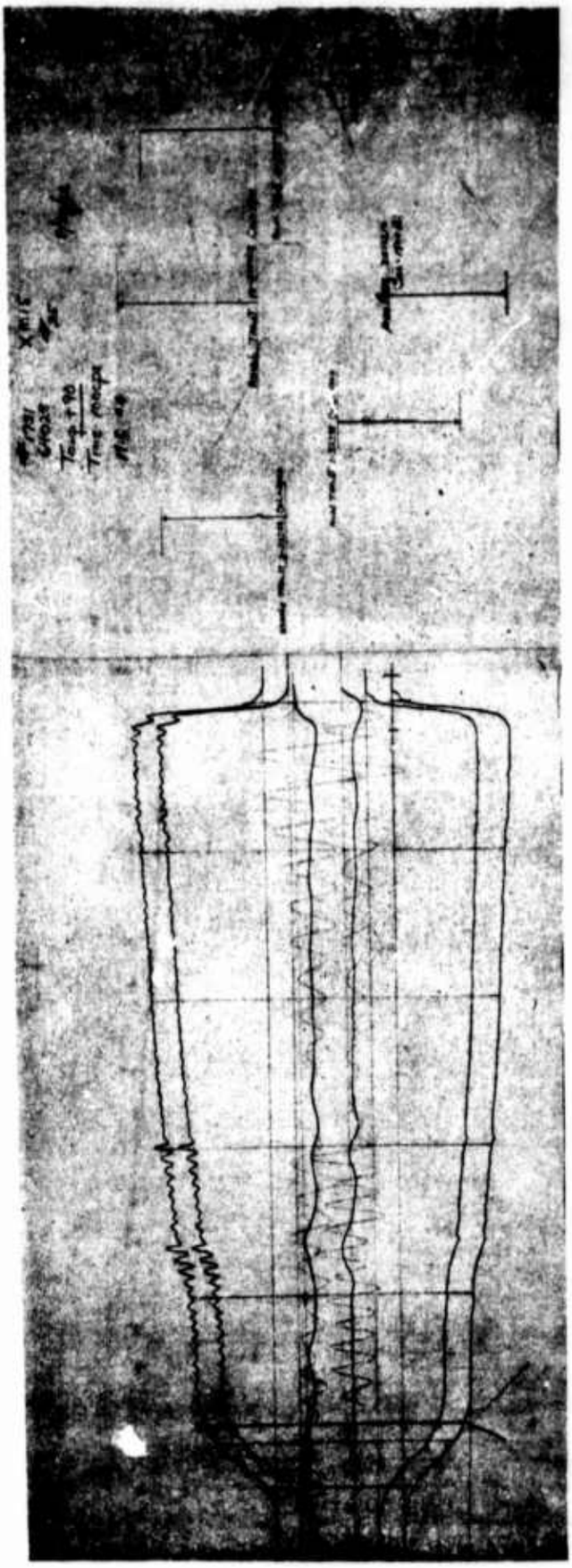

Figure 35. Oscillograph Record, Round 25.

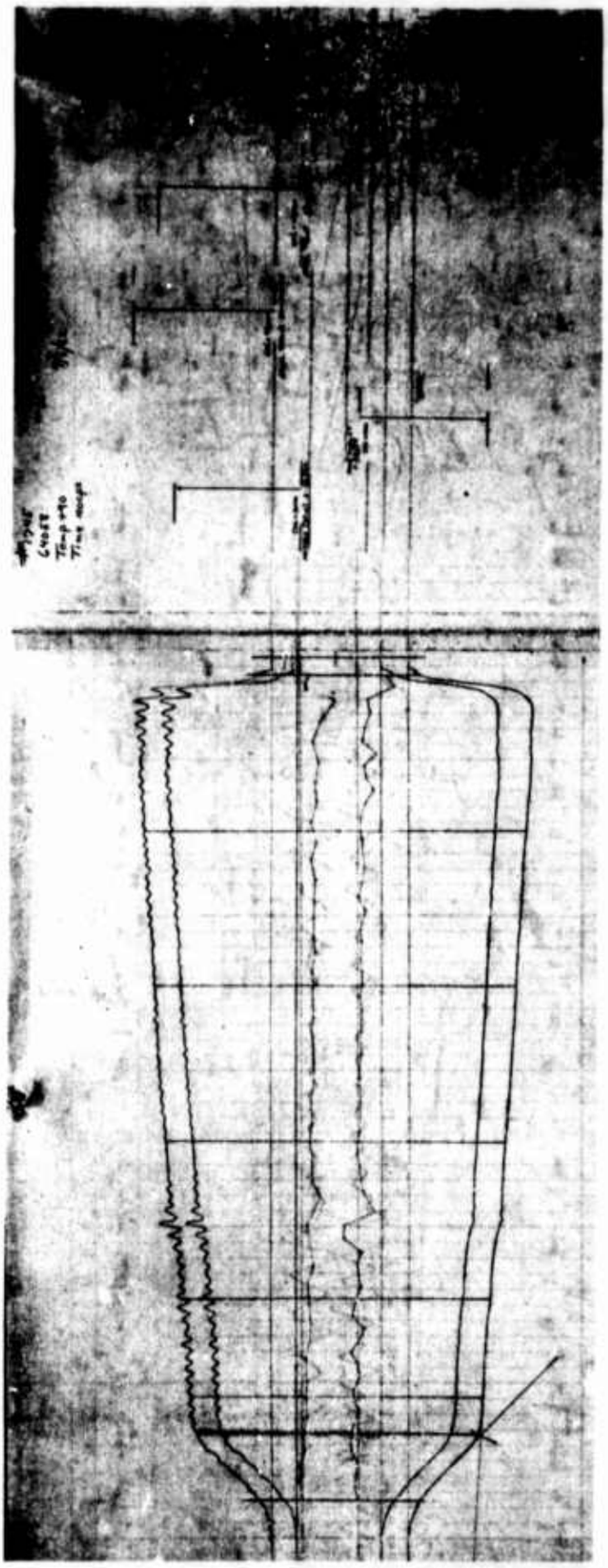

Figure 36. Oscillograph Record, Round 26

Figure 37. Oscillograph Record, Round 27

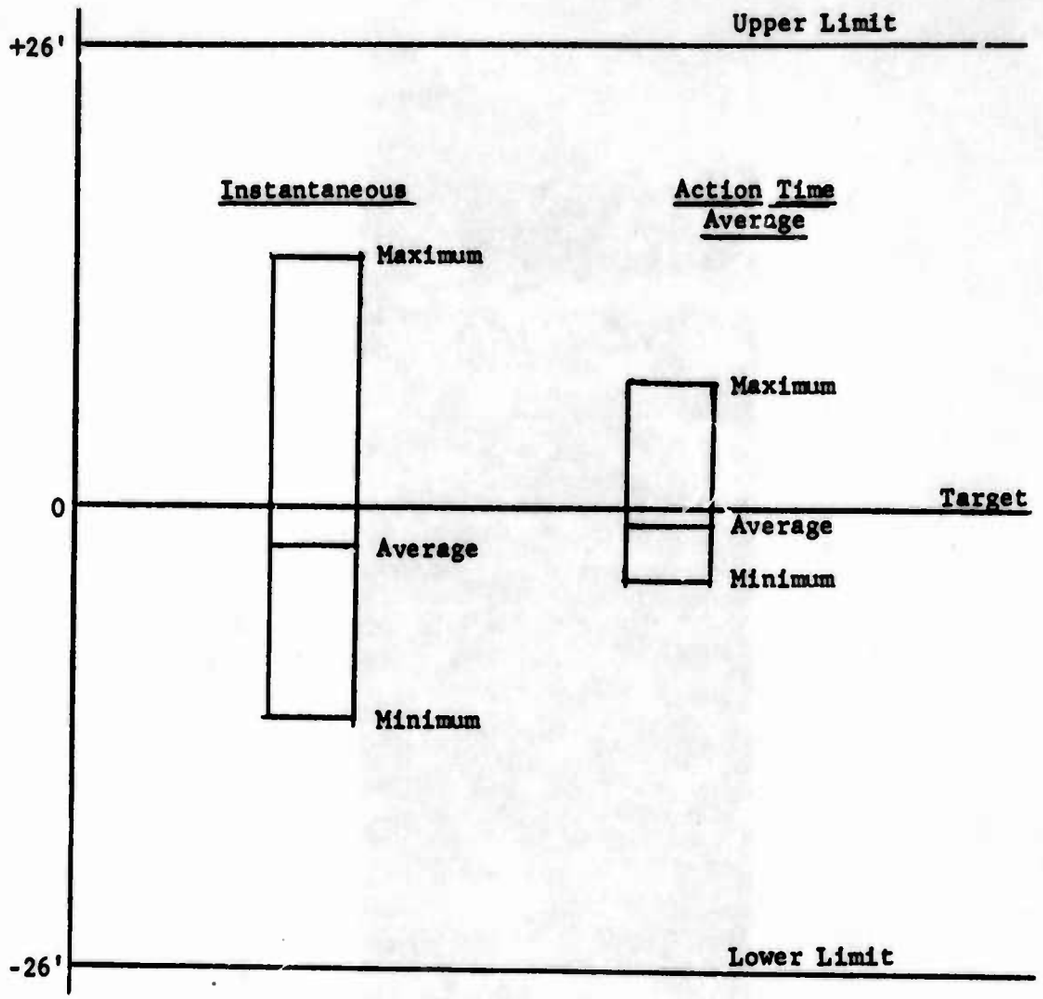

Plotted from data on rounds 22 through 27.
Plus value on the angle indicates nose up pitch; minus value indicates nose down.

Figure 38. Graphical presentation of Data, Group E Firings

Thrust Dispersion Angle	
No. of rounds	6
Action time average	
Average	-0° 1'
Pitch down, max	-0° 4'
Pitch up, max	0° 7'
Target	±0° 26'*
Instantaneous	
Average	-0° 2'
Minimum	-0° 12'
Maximum	0° 14'
Target	±0° 26'*

*Based on a misalignment of 0.250 inch at the capsule center of gravity.

The angular deviation is of such a low order of magnitude that the effect of thrust misalignment is assumed insignificant to the flight path and attitude of the capsule. Total impulse, summarized below, meets the requirements of the work statement.

Total Impulse (lbf-sec)			
Avg of 5 Rd	Minimum	Maximum	Calculated Nominal
17,300	17,200	17,500	17,390

Figure 39 shows the method used to calculate nominal impulse.

Summary of the results of the full scale tests is presented in Table VII.

For information purposes, two tests were conducted to determine the pressure level at which the styrofoam nozzle closure would be expelled from the motor. Results indicated that expulsion occurred at 8 psig. The test motors had been statically pressurized with nitrogen and a conductive break paper arrangement was used to sense the first closure movement.

Calculation of Nominal Impulse from para 1.1.5 of Work Statement, Rev IIIA

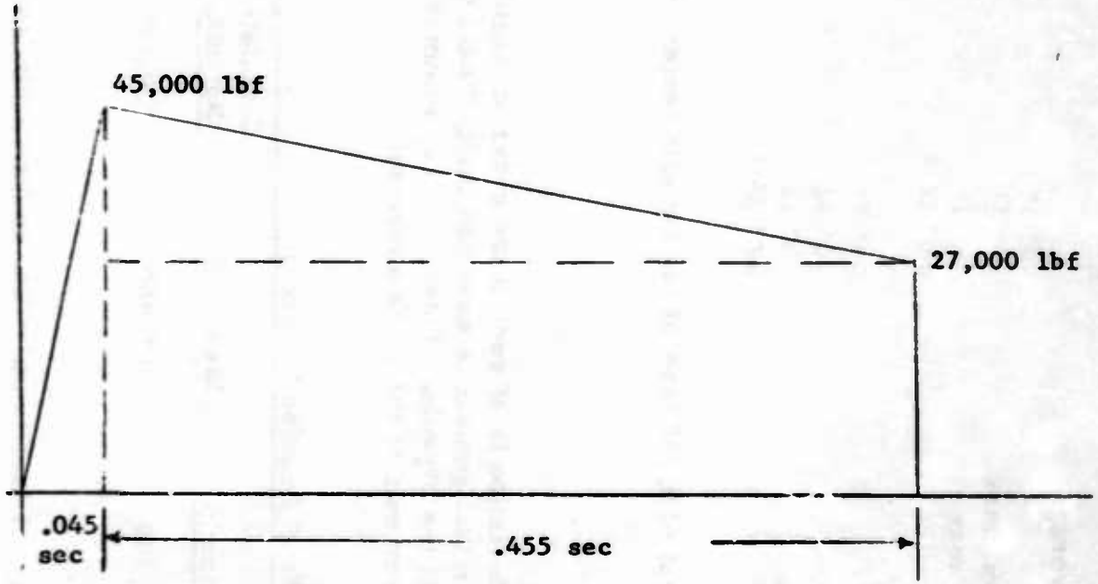

(27,000 lbf)(.455 sec) = 12,285 lbf-sec

$\frac{1}{2}$ (45,000 lbf)(.045 sec) = 1,012 lbf-sec

$\frac{1}{2}$ (18,000 lbf)(.455 sec) = 4,095 lbf-sec

17,392 lbf-sec Nominal

Figure 39. Method of Calculation of Nominal Impulse

TABLE VII. Summary of Results, Full Scale Tests

Round No.	17	18	19	20	21	22	23	24	25	26	27
Film No.	60486	60712	61280	63252	63409	63771	63880	63973	64028	64058	64962
Date fired	10/26/61	11/27/61	1/12/62	6/5/62	6/20/62	7/31/62	8/10/62	8/21/62	8/30/62	9/6/62	1/24/63
Conditioning temperature (°F)	70	70	70	70	70	70	70	70	90	90	70
Propellant weight (lb)	82.50	82.04	80.49	80.53	79.94	80.69	80.86	80.65	80.45	80.60	79.37
Time (sec)											
Ignition delay	0.042	0.029	0.033	0.026	0.028	0.017	0.017	0.014	0.017	0.012	0.016
Burning	0.440	NR[a]	0.525	0.526	0.475	0.492	0.498	0.516	0.489	0.488	0.485
Action	0.475	0.600	0.561	0.558	0.514	0.543	0.545	0.549	0.532	0.531	0.512
Pressure (psi)											
Maximum, head end	2010	1960	1420	1480	1640	1500	1520	1500	1510	1520	Lost[b]
Burnout, head end	850	330	830	700	770	790	810	650	790	850	Lost
Mean, burning time	1510	NR	1130	1130	1250	1170	1190	1170	1220	1220	Lost
Mean, action time	1450	860	1090	1090	1190	1100	1120	1130	1160	1160	Lost
Thrust (lb)											
Maximum	-	-	-	-	-	42750	42580	41130	41670	43530	48360
Burnout	-	-	-	-	-	23260	23040	17930	22220	23760	12900
Mean, burning time	-	-	-	-	-	34080	33720	32470	33960	33940	33500
Mean, action time	-	-	-	-	-	32160	31910	31170	32290	32320	31980
Total impulse (lb-sec)	-	-	-	-	-	17500	17400	17200	17200	17200	16370
Specific impulse (sec)	-	-	-	-	-	216	215	213	214	213	206
Avg misalignment-action time (min)	-	-	-	-	-	1	-1	7	-4	-4	-3

[a]Burnout difficult to distinguish on round 18.

[b]Round 27 - head end pressure data lost due to gage failure.

NOTE: Round 27 functioned at a higher thrust level because of propellant modifications.

SECTION VI

TRACK TEST PERFORMANCE

Sled Testing Preparation

In order to insure compatibility of the XM15 with the capsule, a wooden mock-up (Figure 40), simulating package only, was supplied to Lockheed California Company. Five capsules were used in this test series. Unit compatibility was demonstrated by installing and removing the mock-up in capsule #1. Firing circuits were discussed and various systems evaluated.

The A. F. Flight Dynamics Laboratory decided to connect the rocket igniter and the four separating nuts in a parallel circuit to the knife blades installed on the sled. 600 volt, 85 ampere, DC power was to be supplied from a track-side location to the screen box. Hence, in the event of a power failure, no igniters would fire and the test would be a fail safe "no go." Two complete and independent electrical systems to each explosive device were requested for reliability. Accordingly, the head closure of the XM15 was redesigned to accommodate two ignition elements. A schematic of the circuit is shown in Figure 41.

The XM21 electric ignition element was specified and supplied by Frankford Arsenal for ignition of the XM15 catapult. The no-fire amperage is 1.73 amperes, and all-fire is 3.57 amperes, with a supply voltage of 28 volts DC. Energy-time characteristics (amperes vs time to fire) are:

5 amperes	0.060 ± 0.010 sec
10 amperes	0.0075 ± 0.0025 sec
25 amperes	0.002 ± 0.001 sec.

Frankford Arsenal sent twelve XM21 electric ignition elements to Edwards Air Force Base in advance, for use in parasite sled tests, to check ignition timing. Subsequent performance of the ignition initiation system on the test track was satisfactory.

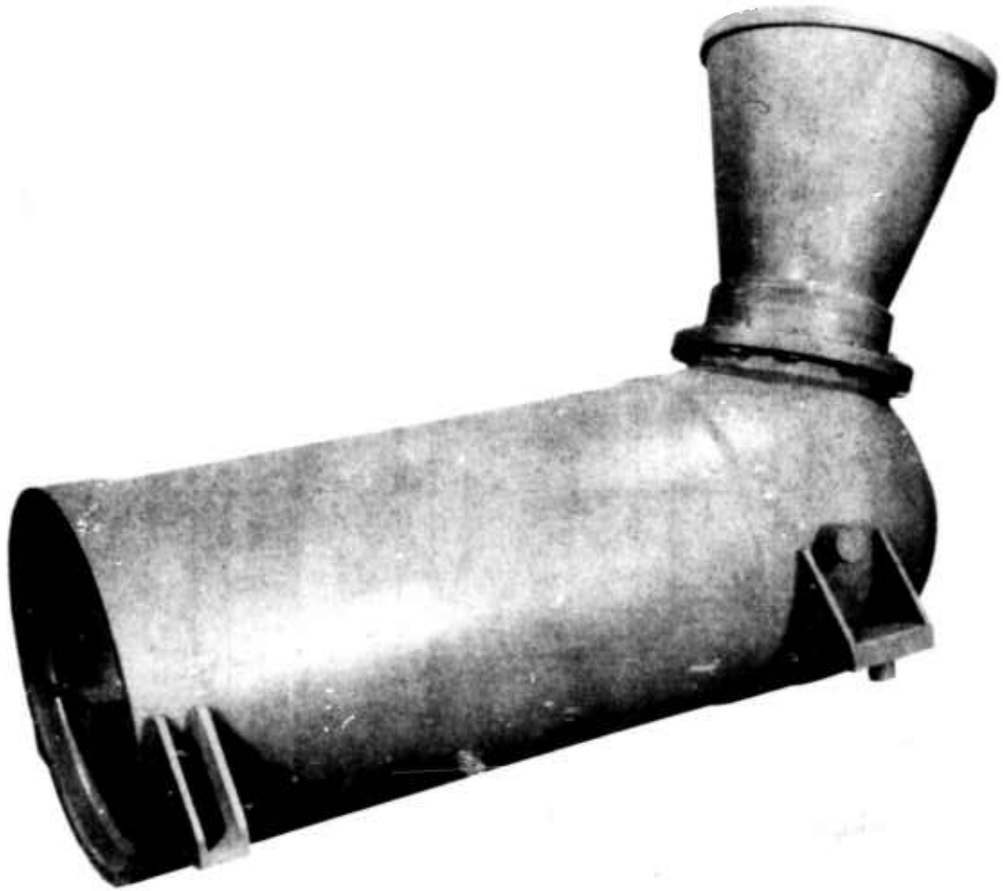

Figure 40. Mock-up, XM15 Escape Rocket

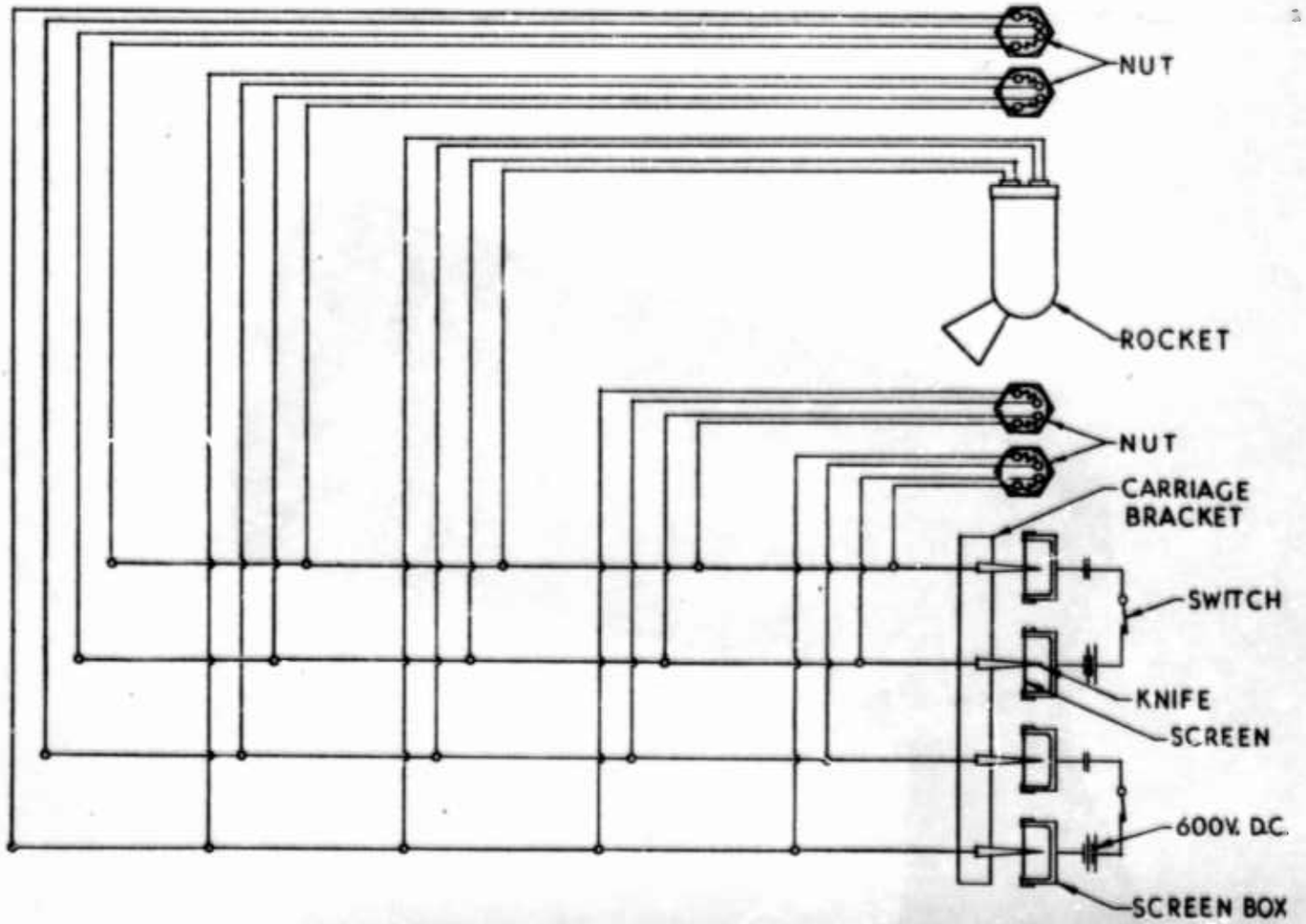

Figure 41. Schematic, Firing Circuit

Weight and balance data were forwarded to Lockheed California Co. (See Figures 42 and 43.) A weighted XM15 escape rocket with inert grains was shipped to Edwards Air Force Base for use in the weight and balance determination of capsule 1 by actual measurments.

Preliminary A. F. Flight Dynamics Laboratory inspection was held at the contractor's plant. During this inspection it was demonstrated that the actual XM15 escape rocket was compatible with the capsule and that capsule No. 1 could be balanced. To simplify installation, slight modifications to the rocket motor were proposed by Lockheed, with Frankford Arsenal concurrence. Changes to the motor are shown in Figure 44.

Concurrent with the motor changes, Lockheed fabricated a matching lifting yoke which was delivered with the capsules. Under Lockheed procedures, the motor installed quickly and easily before the dummy and instrumentation were installed. However, safety considerations at Edwards AFB required the dummy and instrumentation to be installed prior to the live XM15 unit. Since access was severely restricted for the mechanics, the installation system and procedures were revised further. (This is described under Sled Testing, page 83.)

Prior to the 500-KEAS ejection, a calibration run was planned with an unarmed rocket instrumented with accelerometers for vibration data. The major problem was the cantilever structure of the capsule-sled assembly, whose vibration characteristics are indeterminate. During low speed and zero speed firings it was believed that vibration was not a serious problem. At that time, track vibrations could not be defined. Careful disassembly and examination of the motor was scheduled after the run.

Sled Testing

Run No. 1 (10 Aug 62) - 500 KEAS Calibration

Installation of the motor was completed and the run at 500 KEAS, with no scheduled ejection, was made. No acceleration records were obtained to evaluate vibration. Preliminary examination of the motor immediately after the run and at disassembly showed no damage because of the run. Post-run X-ray assessment made of the grains after their return to Picatinny Arsenal also showed no damage.

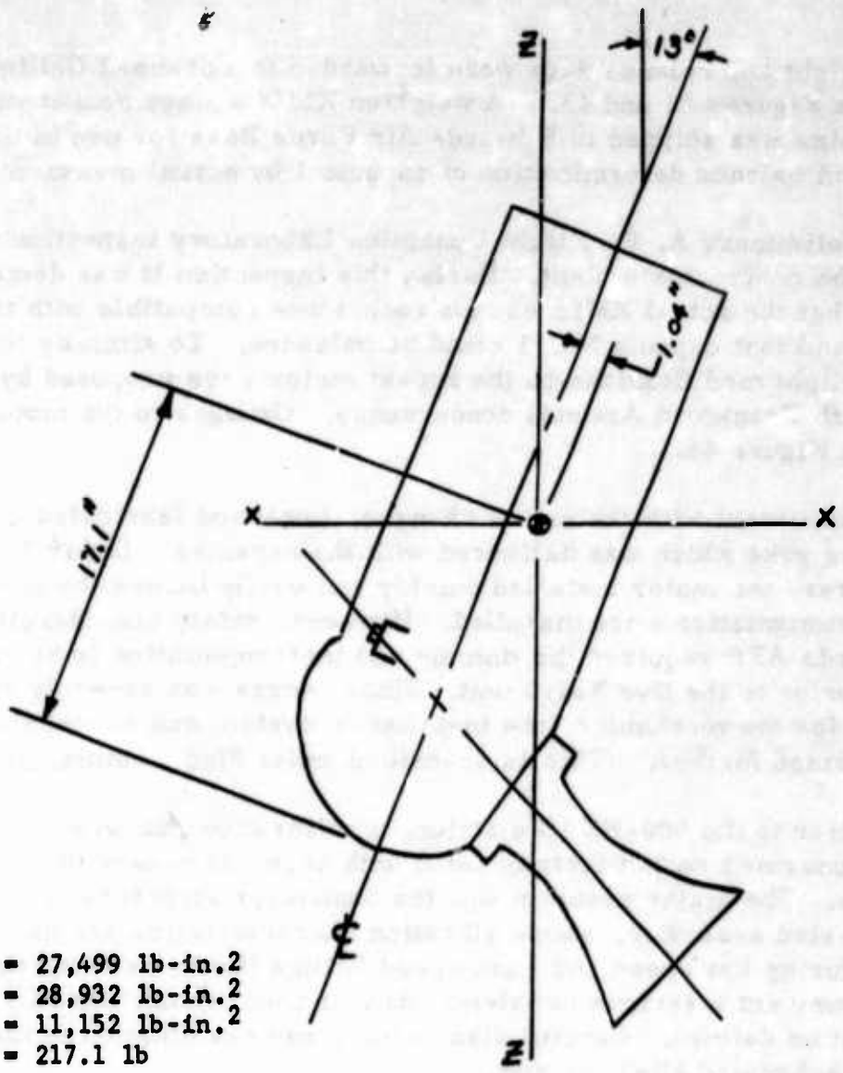

I_{xx} = 27,499 lb-in.^{2}
I_{yy} = 28,932 lb-in.^{2}
I_{zz} = 11,152 lb-in.^{2}
WT = 217.1 lb

Figure 42. Weight and Balance Data, XM15 Escape Rocket, Loaded

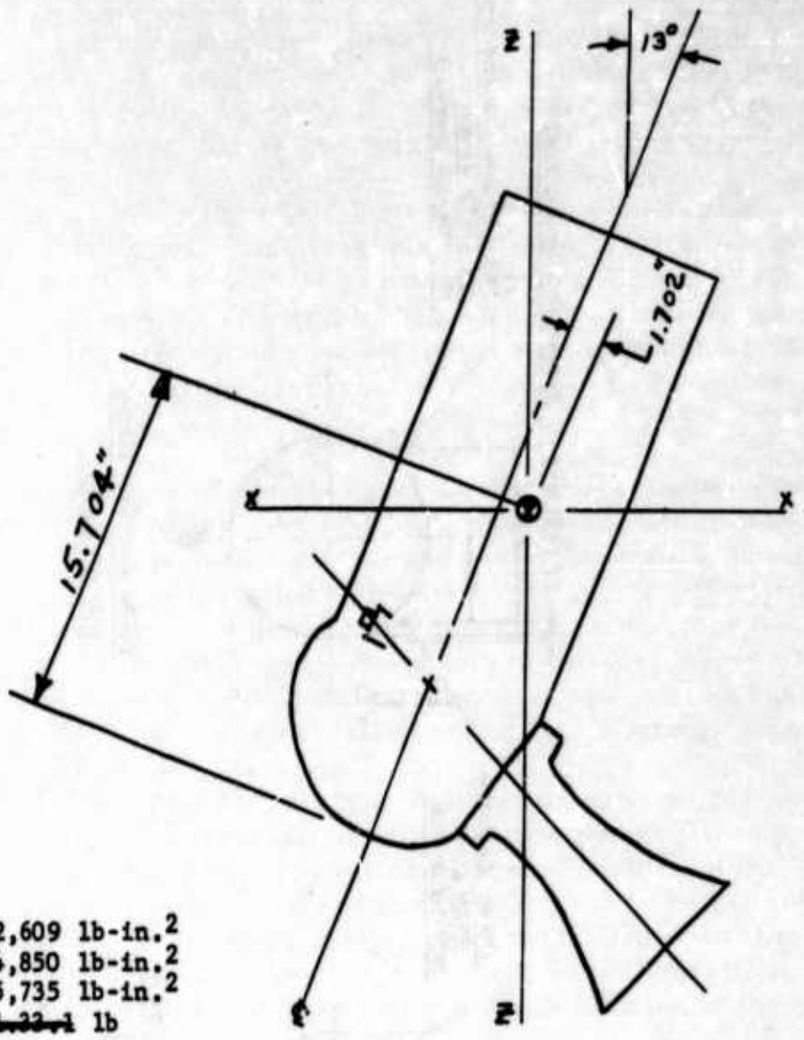

I_{xx} = 22,609 lb-in.^{2}
I_{yy} = 24,850 lb-in.^{2}
I_{zz} = 5,735 lb-in.^{2}
WT = ~~1,331~~ 1,335 lb

Figure 43. Weight and Balance Data, XM15 Escape Rocket, Burnt

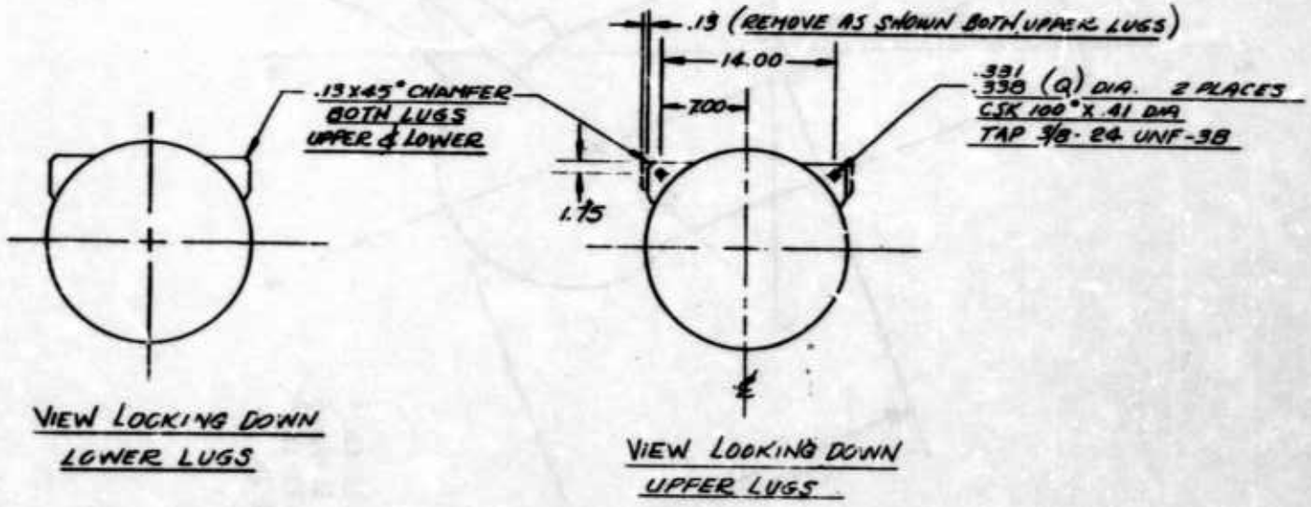

Figure 44. Modification, XM15 Motor

Run No. 2 (19 Sep 62) Zero-Zero, Horizontal (Figures 45, 46, 47)

The first free-flight firing of an XM15 escape rocket was successfully completed on 19 Sep 62. Pressure-time records indicated normal rocket function.[11] Ejection was made with the sled at rest and situated on a promontory approximately 300 feet above the planned recovery area.

Post-run examination showed that the two upper motor attachment bolts had failed prior to or during ejection because of excessive torque applied at the time of motor installation in the capsule. The four lower bolts also showed signs of incipient failure from the same cause. (See Reference 12 for other USAF test data on all track tests.)

Run No. 3 (9 Oct 62) - 100 KEAS (Figures 48, 49, 50)

Nose capsule No. 1 was successfully ejected from the sled vehicle traveling on the track. The motor mounting bolts, now changed to remachined aircraft bolts, showed distress similar to the previous runs because of the mounting difficulties.

Run No. 4 (31 Oct 62) - 500 KEAS (Figures 51, 52, 53)

A successful launch was made from a sled traveling at a velocity of 500 KEAS. Examination of the XM15 escape rocket and the traces show normal function of the unit. Height of trajectory was limited because of an adverse angle of attack.

Rocket factors reviewed as the possible cause of the adverse angle of attack were: the high mass rate of flow of gases from the XM15 escape rocket; rocket thrust misalignment because of deflection of the bulkhead; the failure of the upper attachment at installation; misalignment of the thrust vector within the XM15; and shifting of receiver holes because of natural settling of the capsule.

The suggested causes were considered and discounted. Bulkhead deflection was discarded on the basis of stress analysis and strain gage data. Failure of the upper attachment bolts was discarded, as a free body diagram shows this would not affect motor position. Vector

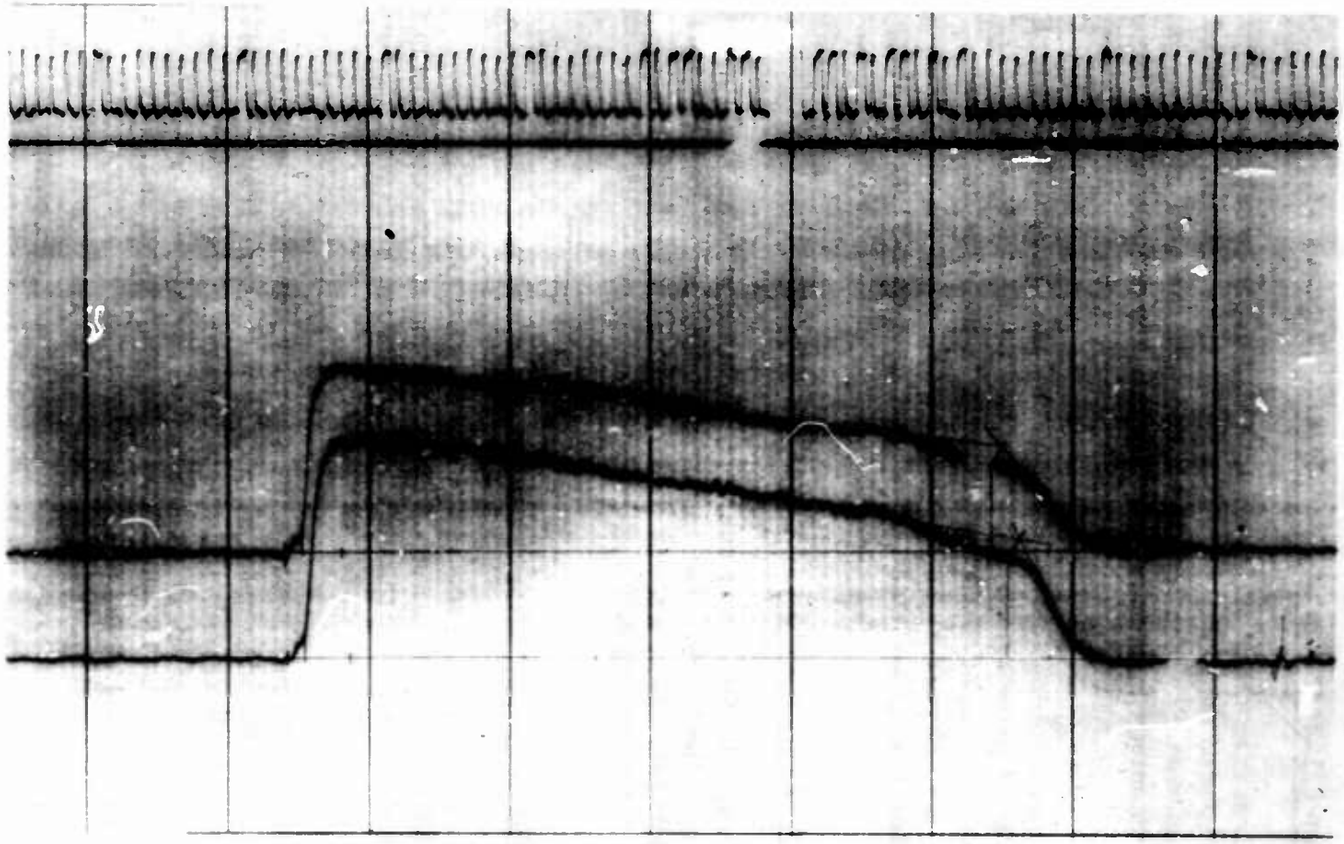

Figure 45. Oscillograph Record, Run 2

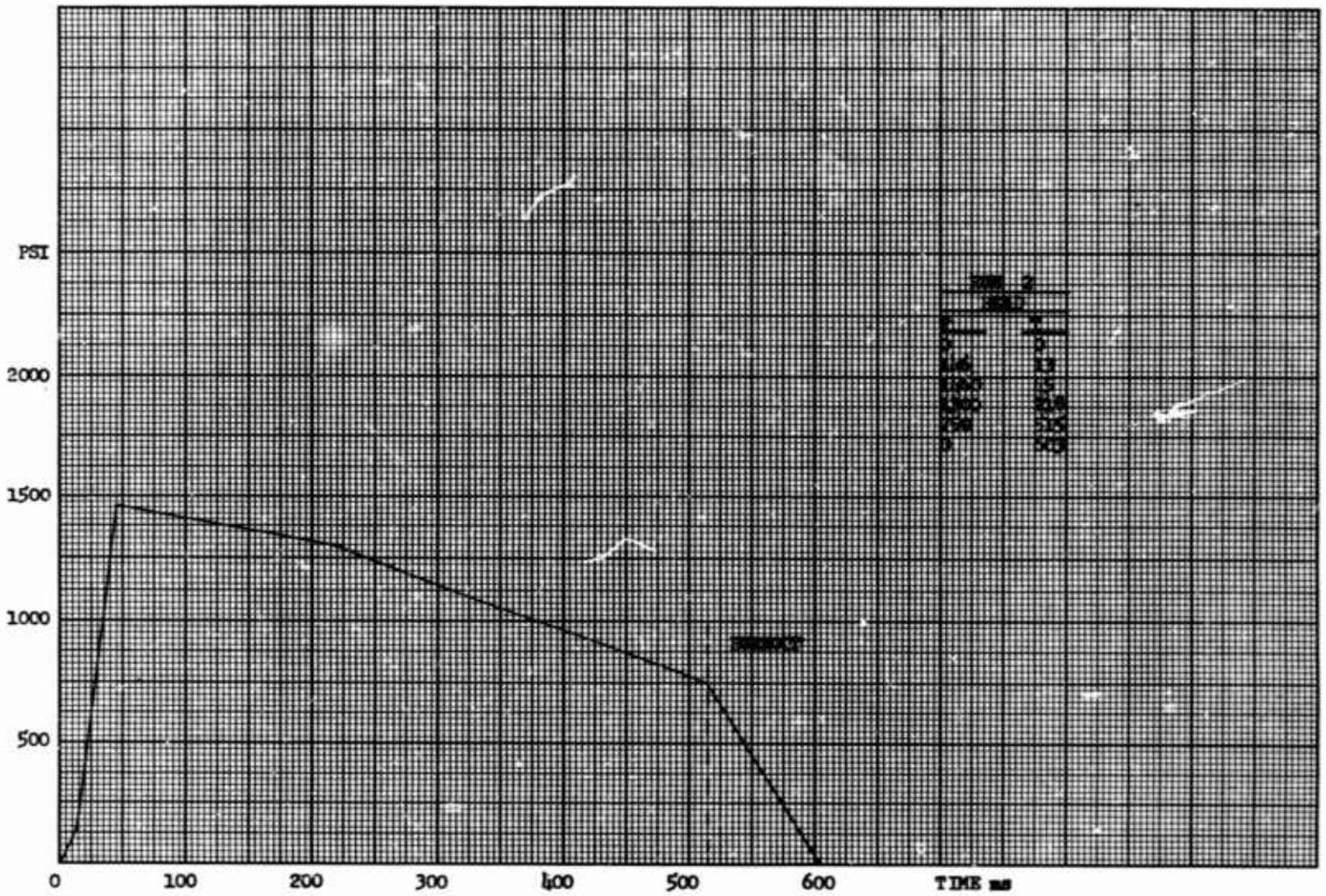

Figure 46. Linear replot, Pressure vs Time, Run 2

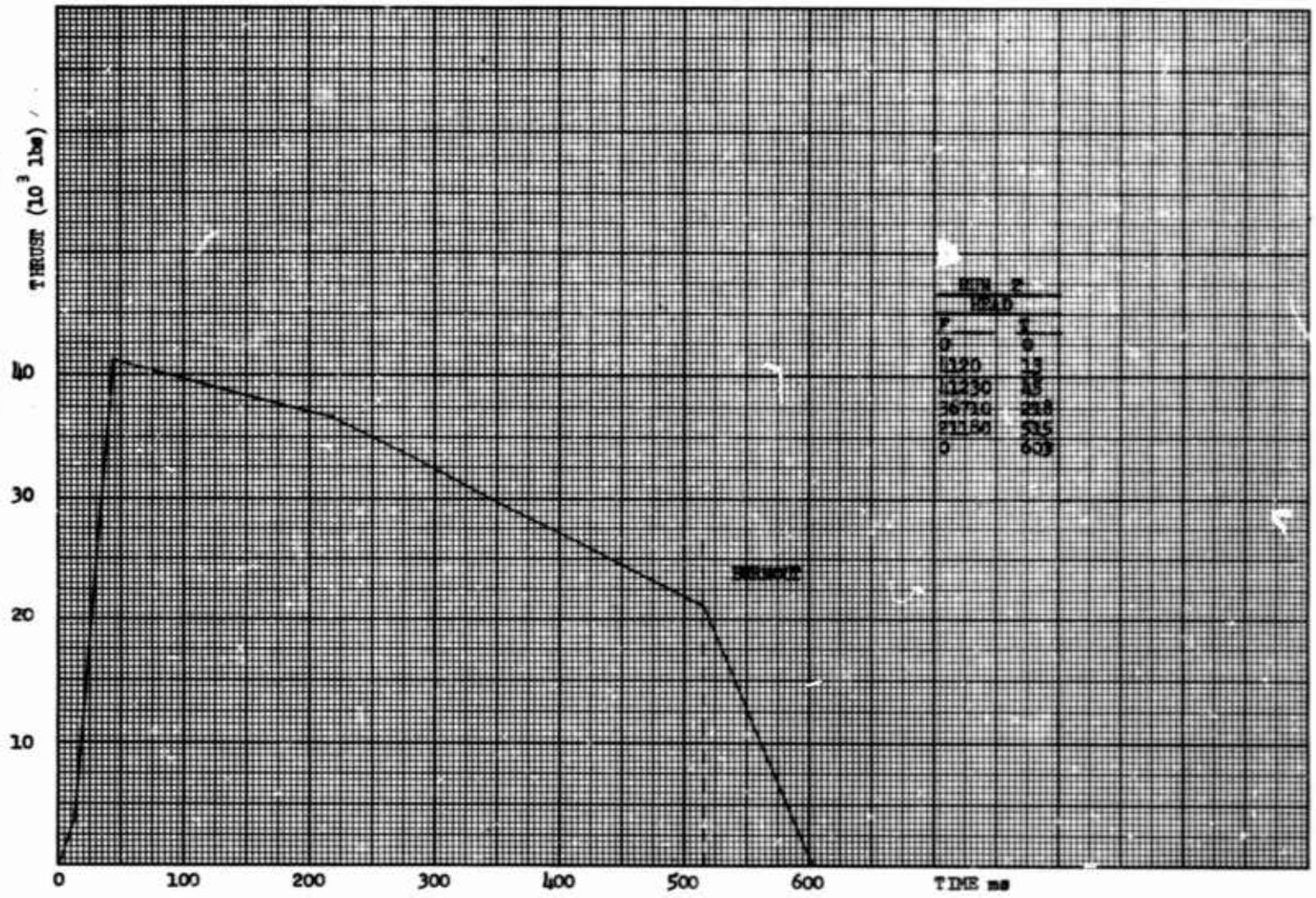

Figure 47. Estimated Thrust vs Time, Run 2

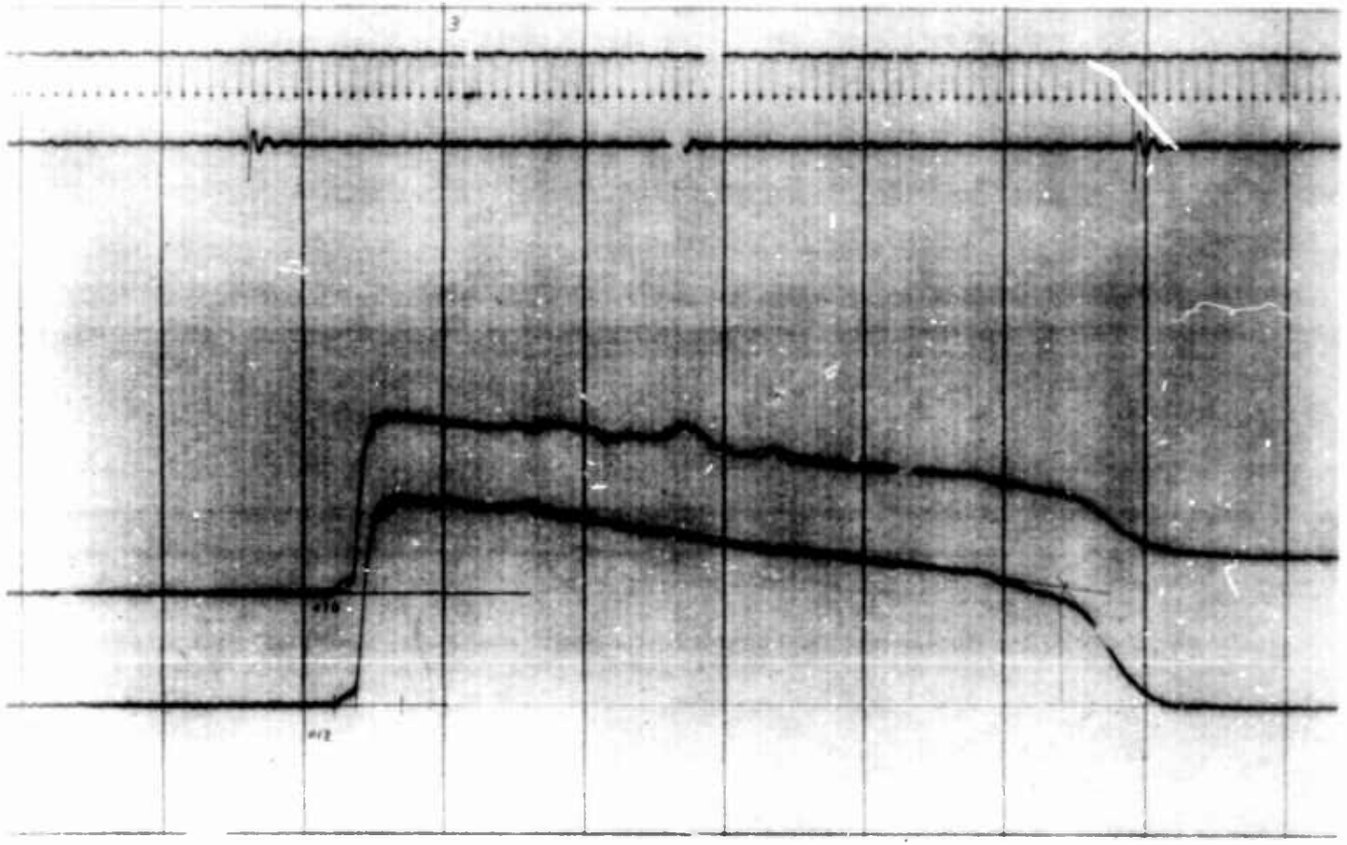

Figure 48. Oscillograph Record, Run 3

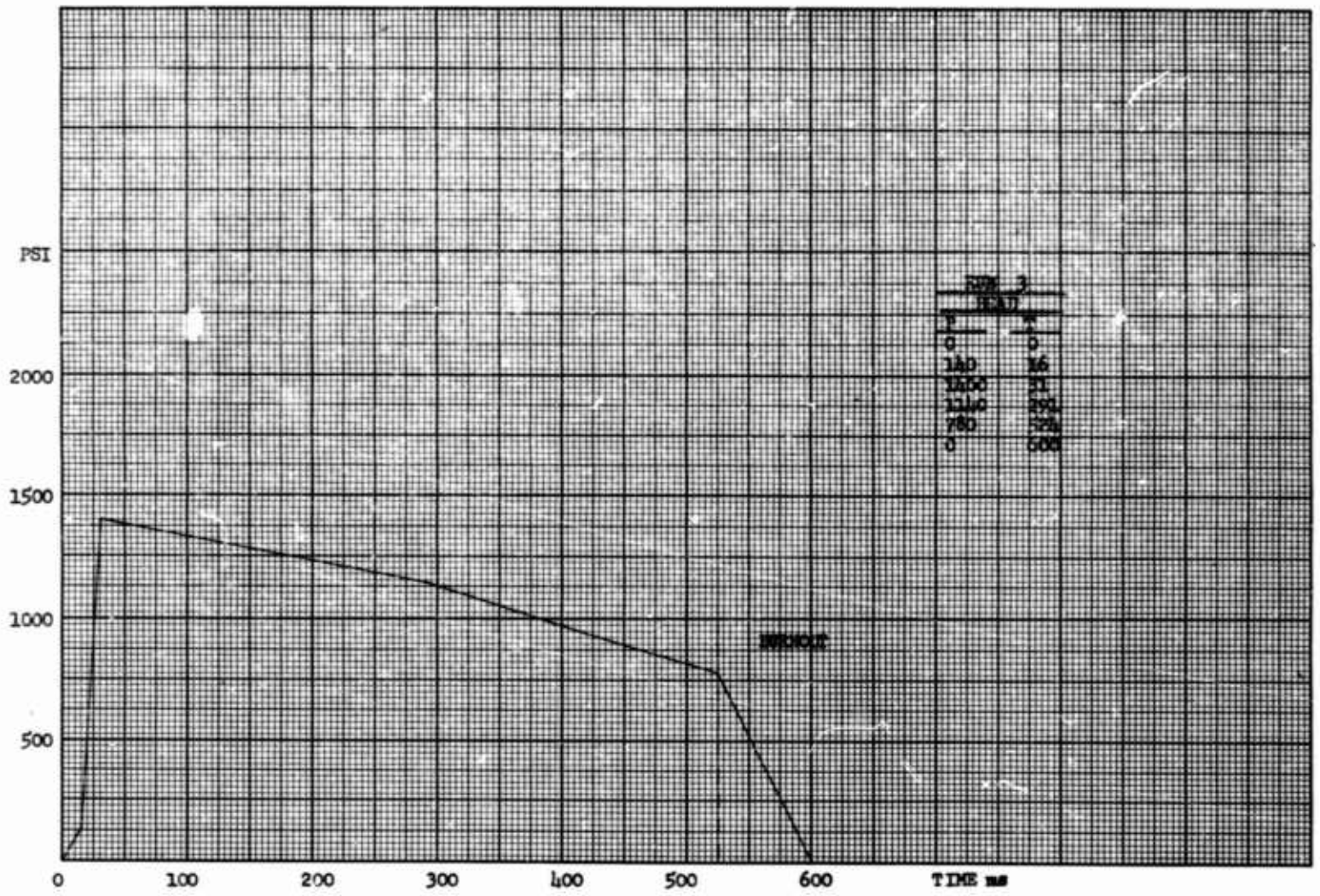

Figure 49. Linear replot, Pressure vs Time, Run 3

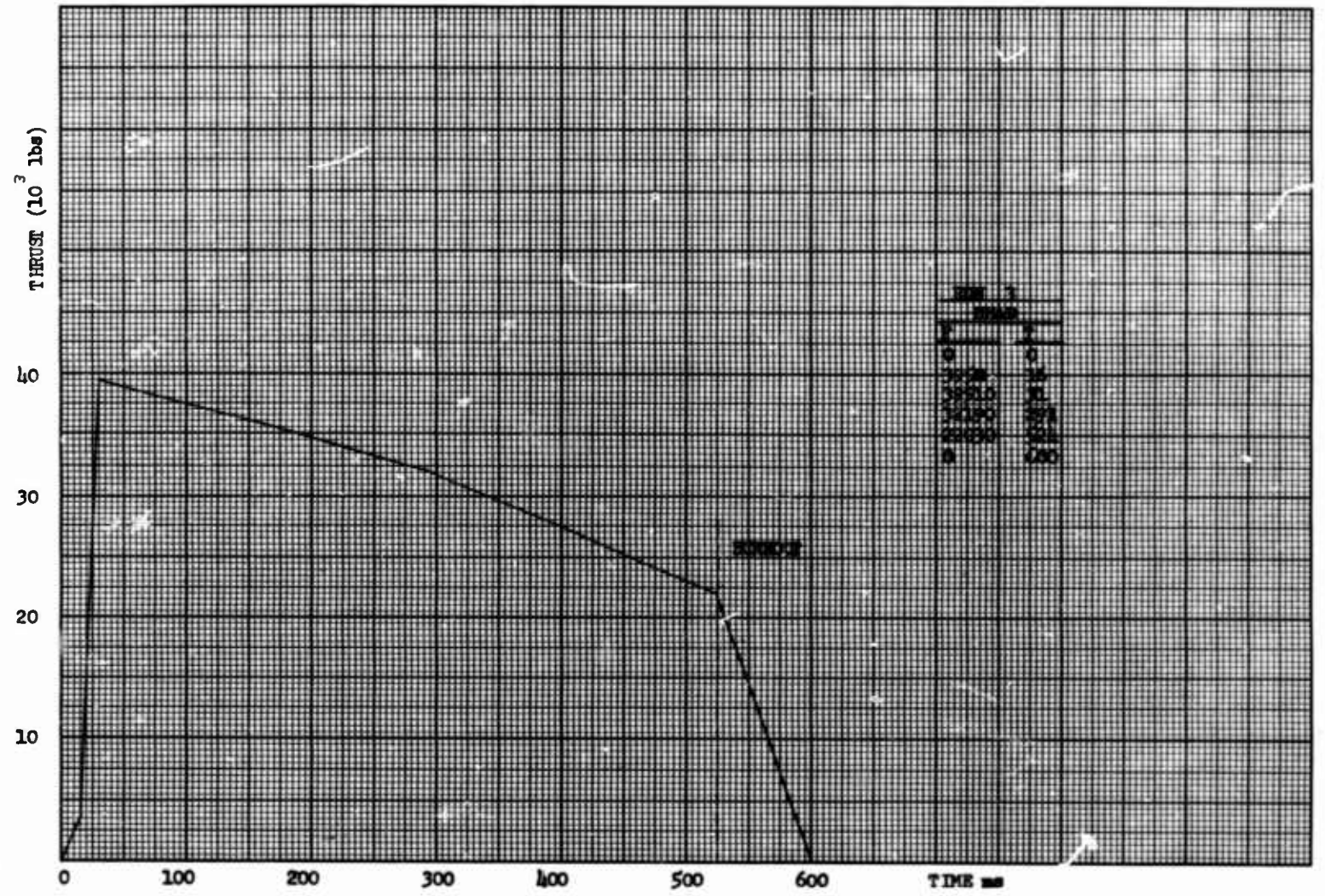

Figure 50. Estimated Thrust vs Time, Run 3

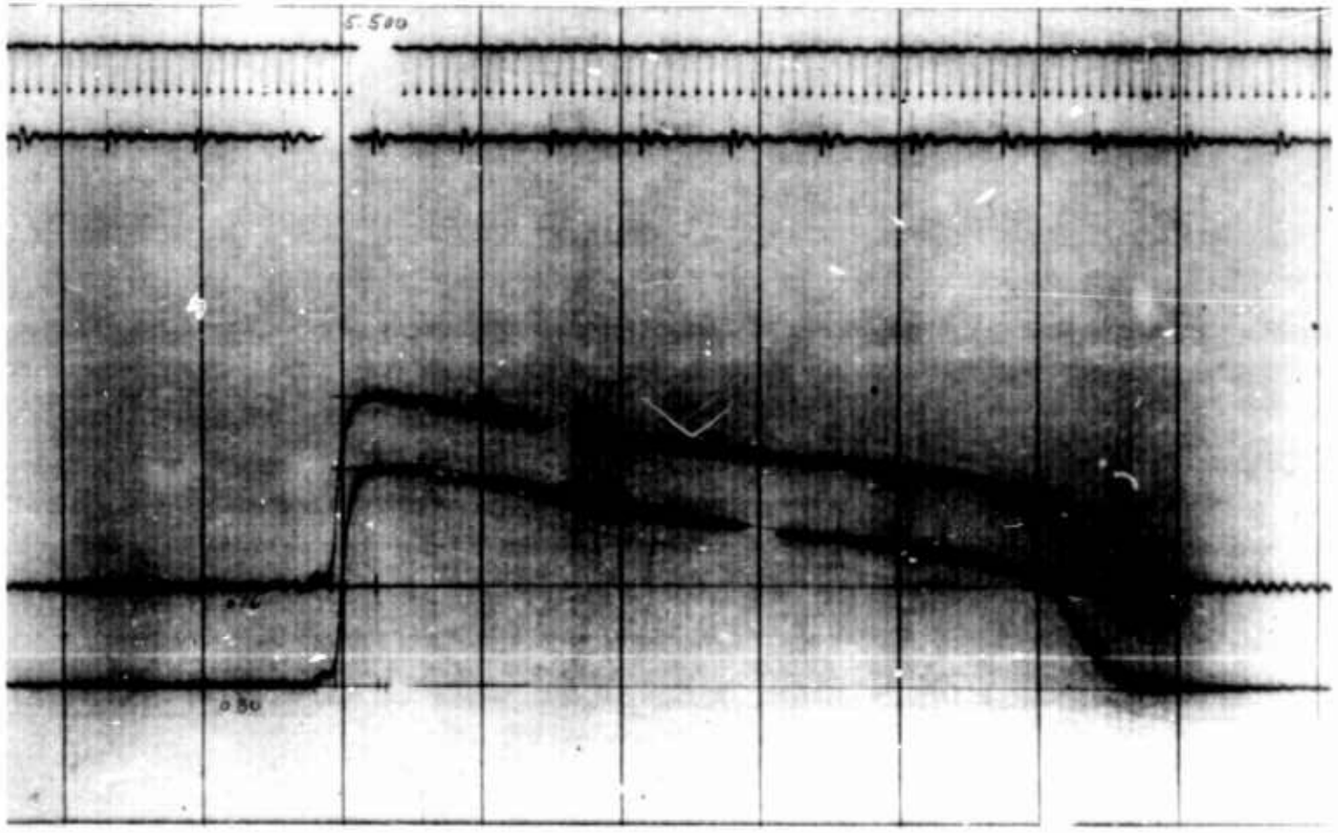

Figure 51. Oscillograph Record, Run 4

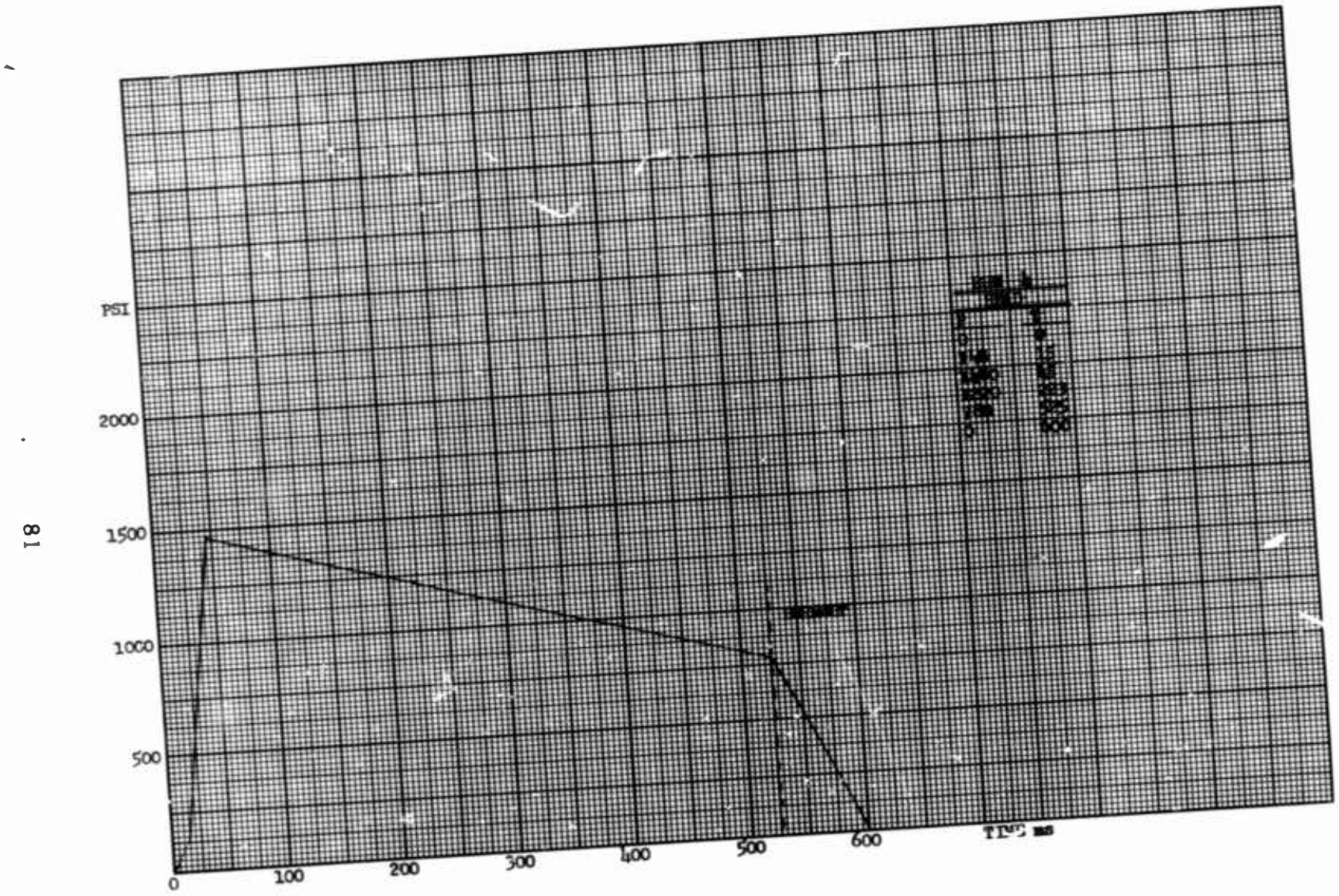

Figure 52. Linear replot, Pressure vs Time, Run 4

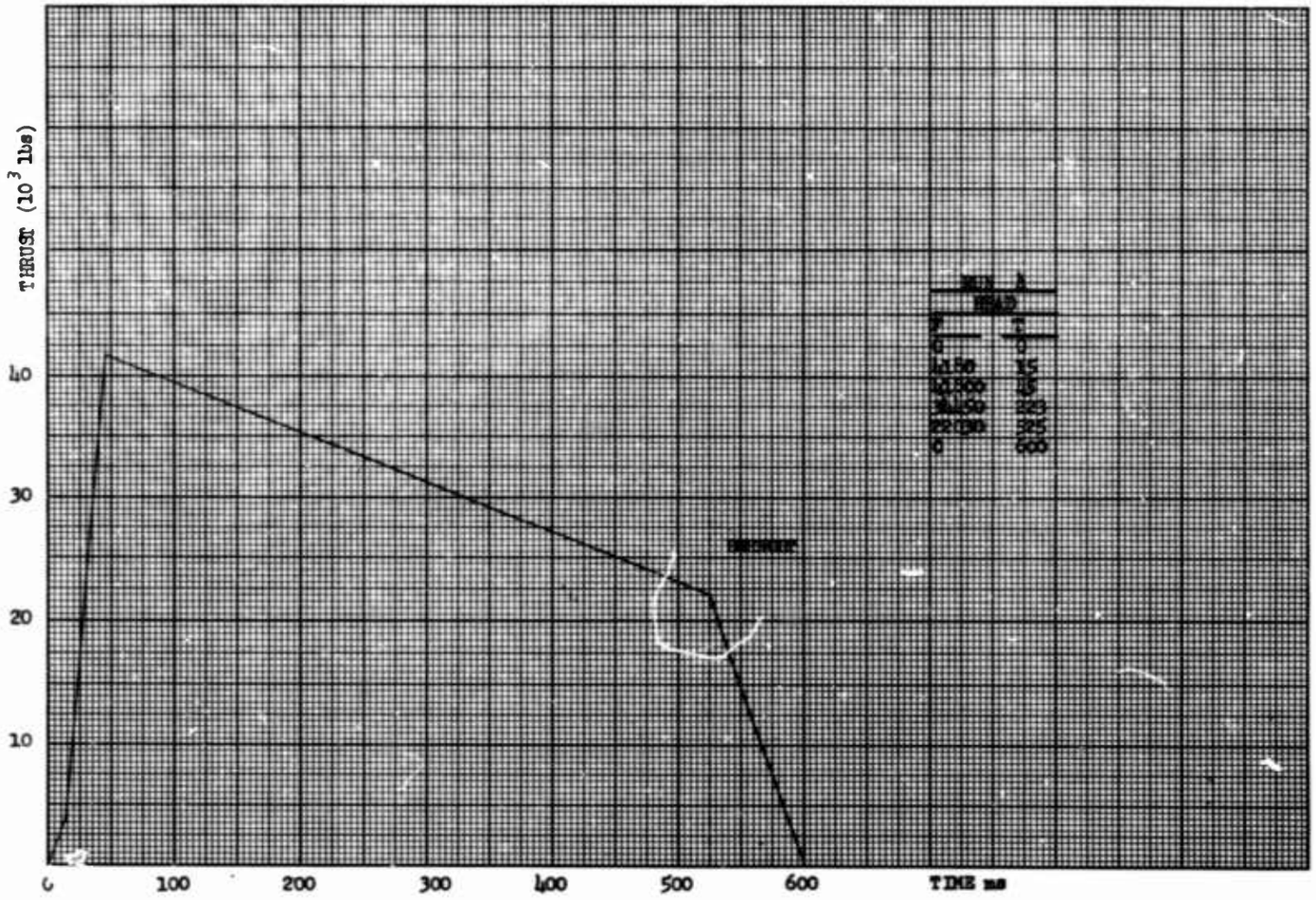

Figure 53. Estimated Thrust vs Time, Run 4

misalignment was discounted on the basis of data obtained from the multicomponent thrust stand, visual inspection of the motor for nozzle erosion after all firings, and photometrically observed exhaust pattern during free flight and static tests. Also, calculations showed that the misalignment of thrust to cause the degree of downward pitch observed would be virtually impossible because of the magnitude. Hence, the vector misalignment of the motor was absolved. Shifting of the receiver holes had occurred but on installation, the motor, acting as a jig, forced the receiver plates back into position.

Aeronautical Systems Division continued to study corrections for the aerodynamic effects. However, Frankford Arsenal decided to construct and supply an alignment guide to check the center of gravity-thrust line relationship at the next weight and balance of the capsule. The guide assembly was made of a precision-machined nozzle cover plate and a five foot long spike which attached to the center of the plate. The assembly was secured to the exit by four special clamps. When the motor was designed and constructed, the exit circle had been built concentric to the nozzle throat within several thousandths of an inch and the face of the exit was maintained parallel to the cross-sectional area of the throat within 0.001 inch. Thus, at installation, the guide spike will be coincident with the thrust line of the motor (Figure 54).

Run No. 5 (8 Nov 62) - 900 KEAS Calibration

The scheduled 900-KEAS calibration (drag) run was successfully conducted. Visual and radiographic examination of the motor, made after the run, showed no damage. No vibration transducers were in operation during the run. After visual examination, it was concluded that the XM15 rocket could be used for the 900 KEAS ejection.

Run No. 6A (11 Dec 62) - 300 KEAS Ejection (Figures 55, 56, 57)

Improvements in the XM15 mounting system were incorporated for this run. The through holes in the bulkhead provided for the mounting bolts were enlarged by the Experimental Test Branch (Edwards AFB) to reduce the installation-induced moments on the mounting bolts. Frankford Arsenal machined a radius on the 7/8 alignment pins to assist in the positioning of the motor. Full engagement diameter with the receiving holes was reduced only to the length necessary to assure final position.

Figure 54. Alignment Guide Mounted in XM15 Escape Rocket

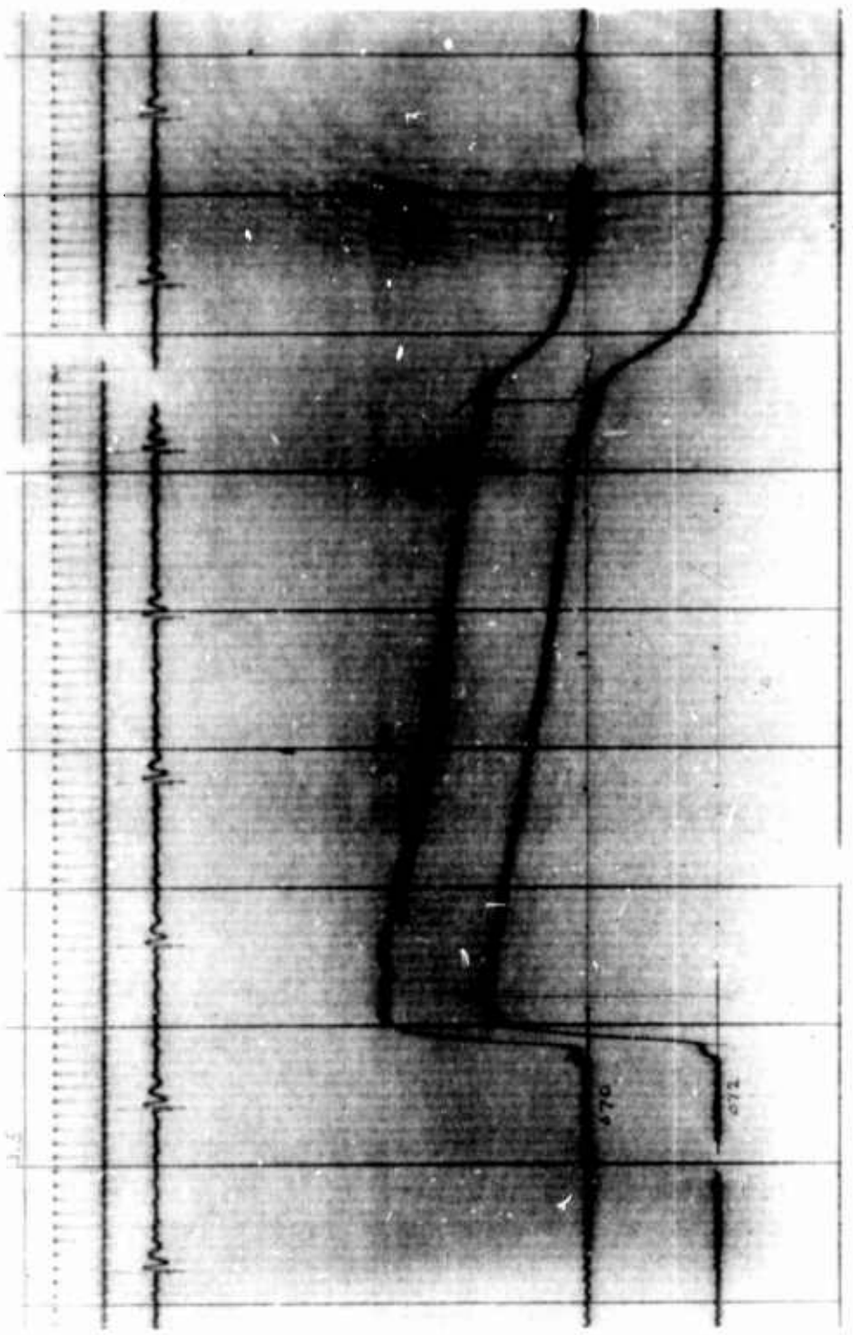

Figure 55. Oscillograph Record, Run 6A

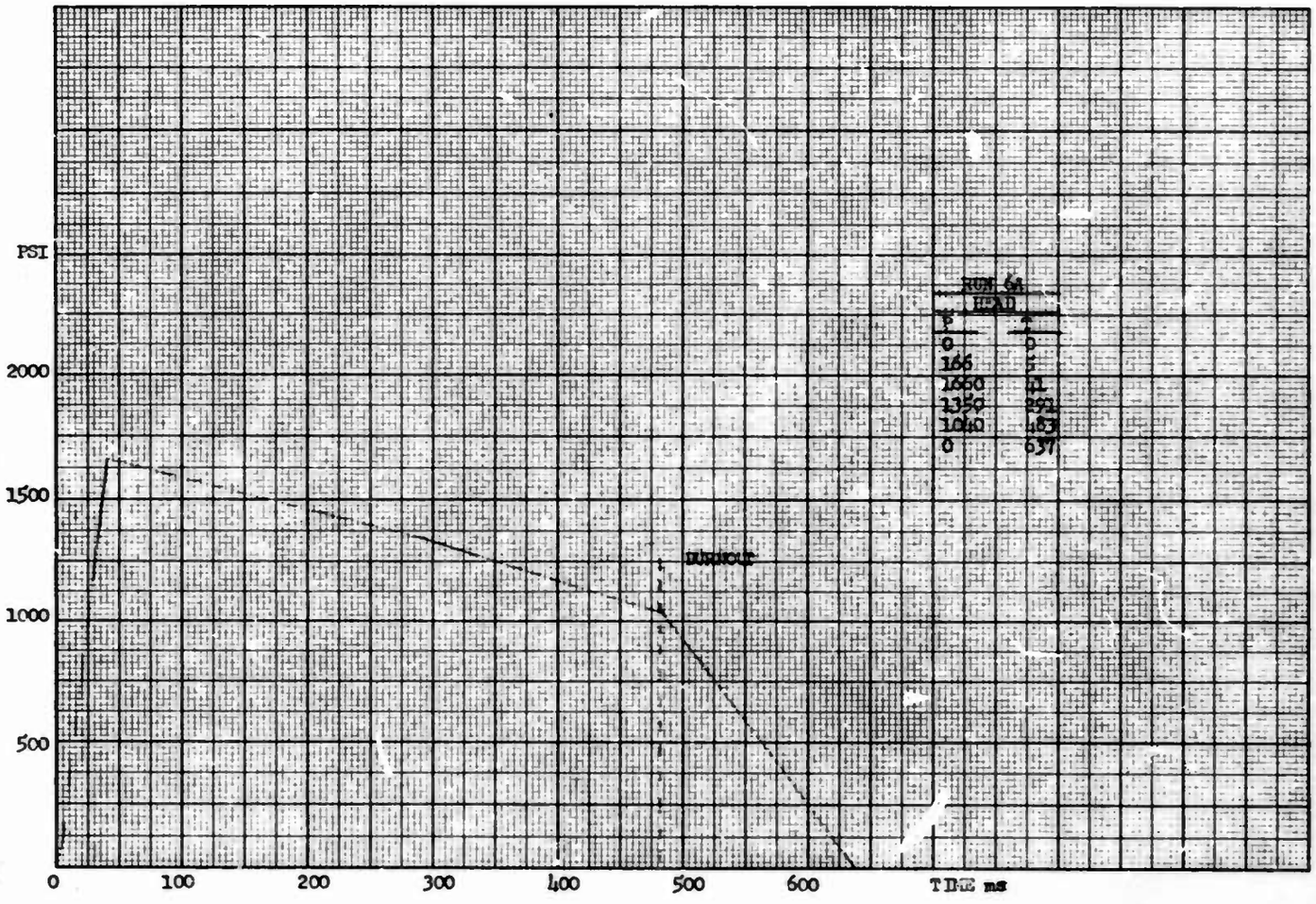

Figure 56. Linear replot, Pressure vs Time, Run 6A

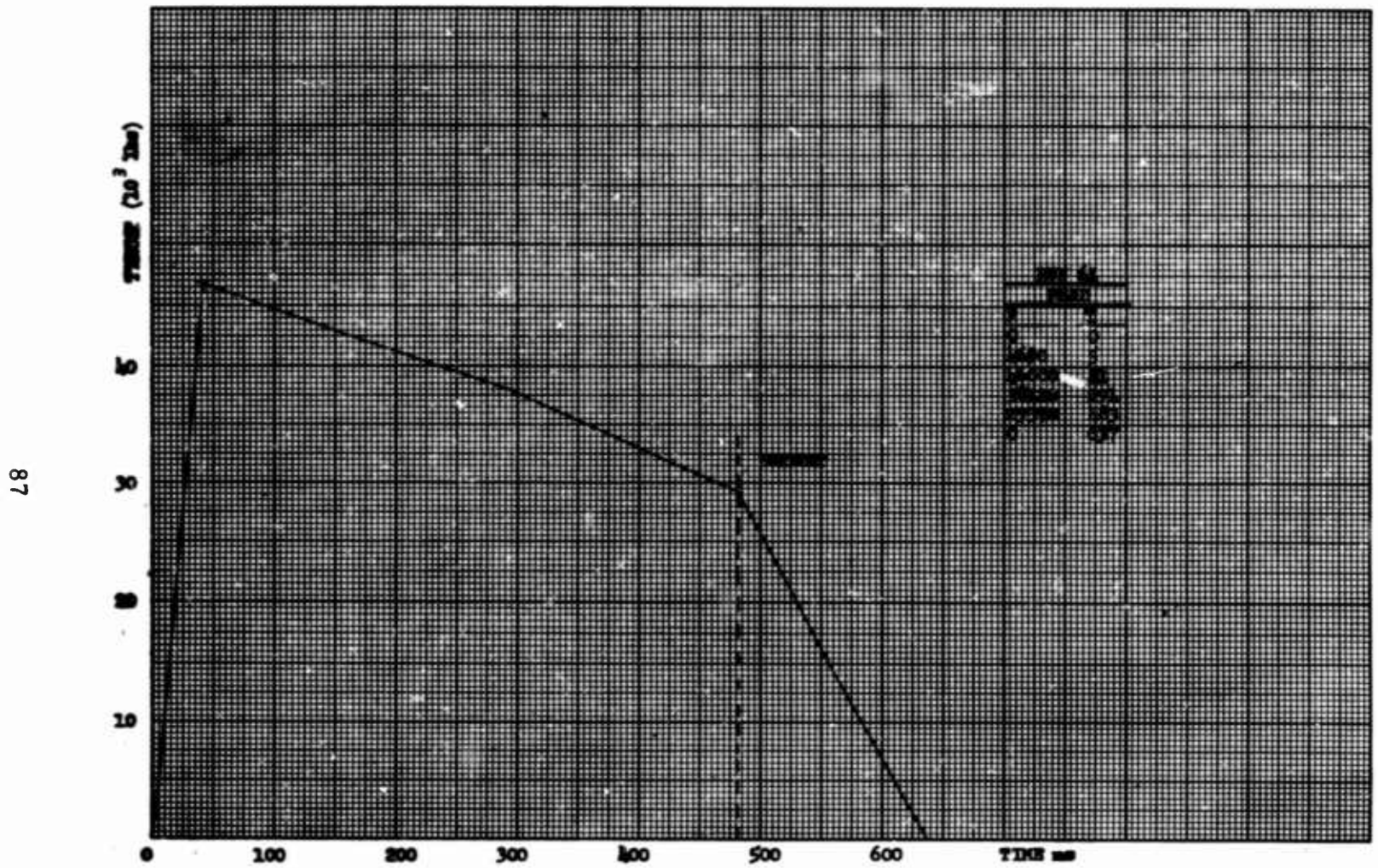

Figure 57. Estimated Thrust vs Time, Run 6A

Frankford Arsenal also provided high tensile strength (150,000 psi ultimate) 3/8-16 USS 6-line bolts to secure the motor. These were to be used to preclude bolt failures due to over-torquing. Because the tensile strength of the bolts is close to the strength of the casing, care must be taken to keep the motor in good alignment throughout the installation to avoid stripping the female threads in the motor case.

A thorough weight and balance of the unit was conducted prior to ejection. This included a horizontal and vertical balance on the knife edge balance bar and a three-point weighing. A mechanical thrust alignment check was conducted with the alignment guide. The capsule weight was 2465 pounds. The center of gravity was located three inches aft of the balance bar to provide an initial moment arm of 1.9 inches. During burning of the XM15 catapult, the center of gravity shifts forward 0.6 inch at web burnout to 2.4 inches aft of the balance bar. The average moment provided by the thrust of the XM15 caused the capsule to pitch upward. The misalignment angle of thrust line-to-center of balance bar was estimated with a transit at 17' ± 7'. Errors of measurement because of the bow in the 5-ft spike could be reduced by rotating the spike 180° from the first reading and averaging the two readings. The spike was checked on site by a precision inclinometer.

Capsule No. 3 was successfully ejected from a sled traveling at 291 KEAS (Figure 58). The capsule pitched upward during rocket thrust, the rocket moment making a correction for the forces and moments which previously caused downward pitch.

The high tensile strength bolts used in this run did not break. One of the upper bolts showed evidence of plastic deformation because of installation-induced moments. It was concluded that, as a last step in the installation procedure, the old bolts should be replaced by new ones after the motor is positioned.

Run No. 7 (11 Jan 63) - Repeat 500 KEAS (Figures 59, 60, 61)

This run is a repeat of the previous 500-KEAS ejection. The capsule was balanced the same as the 300-KEAS run with a thrust line to center of gravity initial moment arm of 1.9 inches arranged so that the thrust from the XM15 would provide a nose-up pitching moment.

Figure 58. Successful Capsule Ejection from Sled

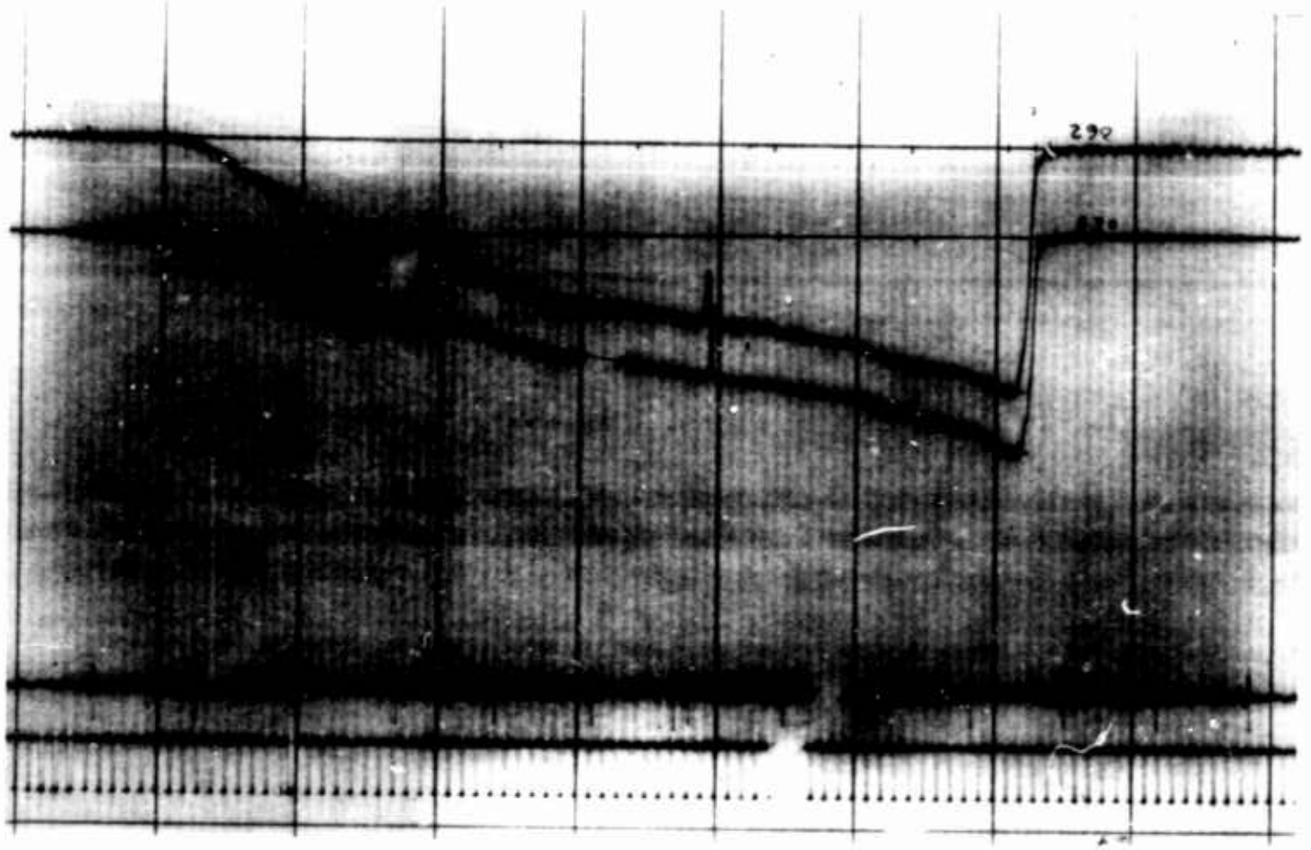

Figure 59. Oscillograph Record, Run 7

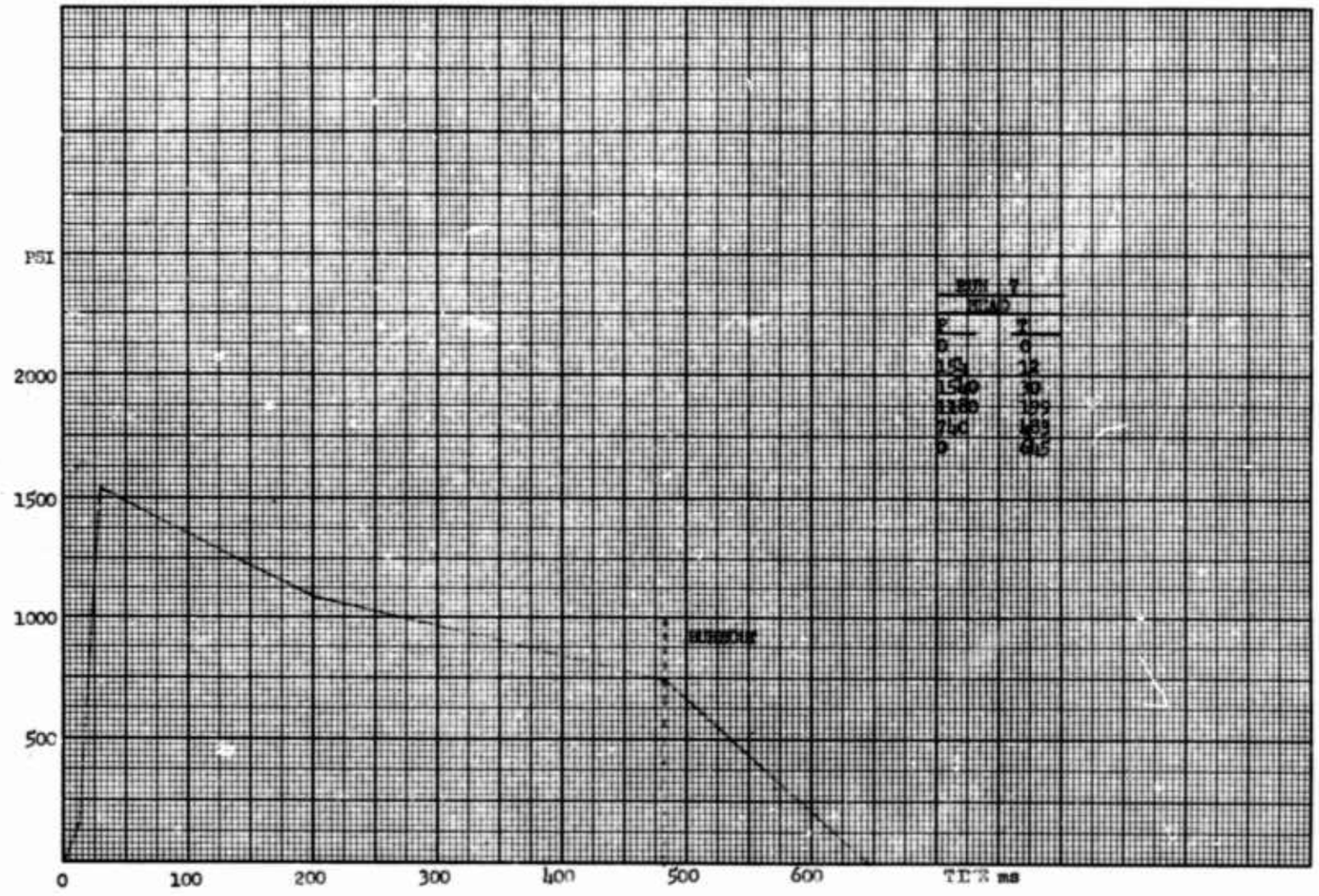

Figure 60. Linear replot, Pressure vs Time, Run 7

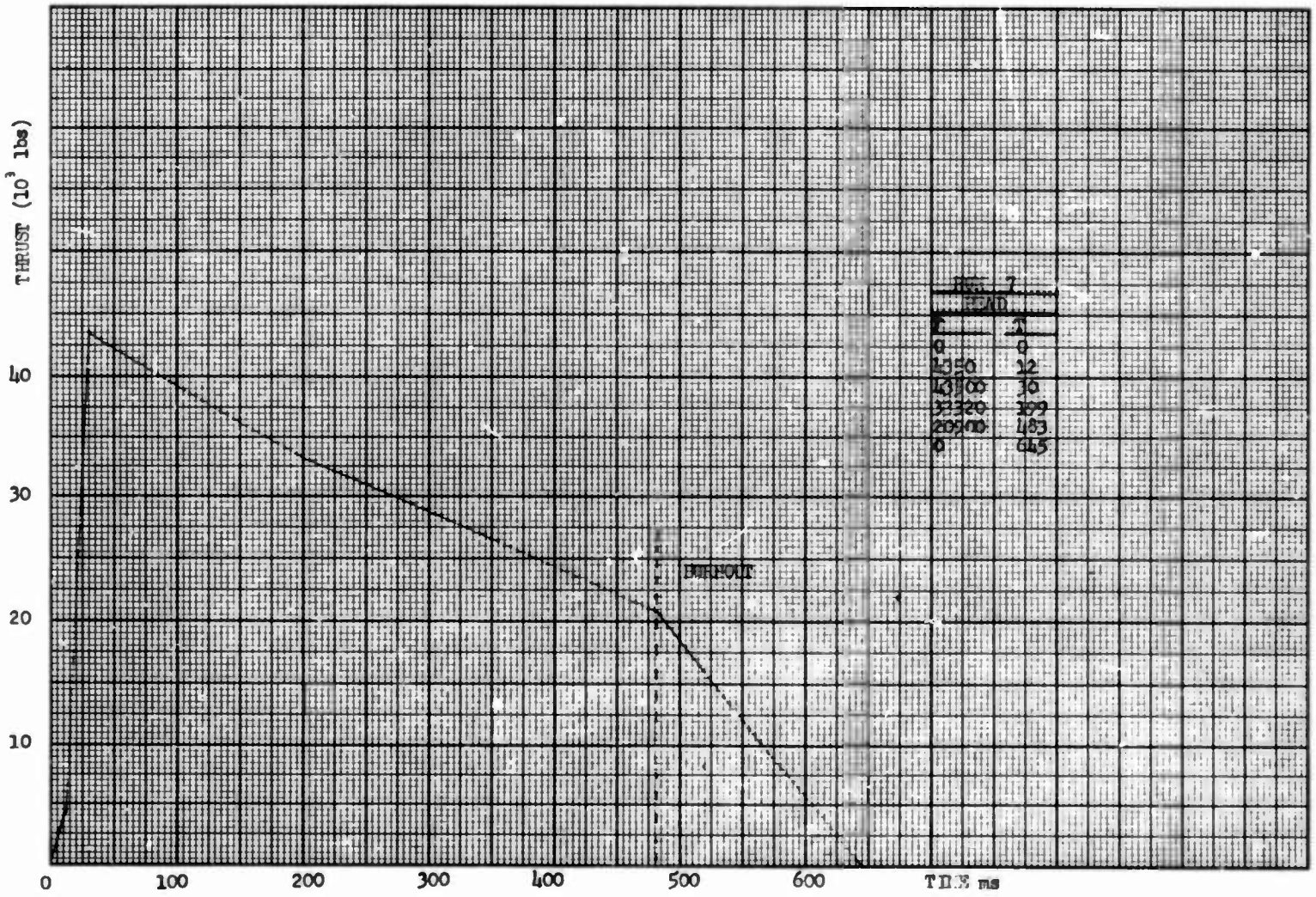

Figure 61. Estimated Thrust vs Time, Run 7

The XM15 escape rocket had a hangfire ignition of 0.400 second. This hangfire is attributed to low ambient temperatures experienced during the ready condition. It is estimated from the recorded temperatures that, at the time of the run, the rocket was approximately 30° F, the air temperature having risen from an overnight low of 20° F to 37° F at 0955 PST. In addition, several 1/4 inch long fragments of unburned rocket propellant were found in the upper wedge trough and around the sled-borne camera shield. A deep dent, discolored with orange and brown color of the unburned propellant, was observed in the sled-borne camera blast shield. The following tabulation is a record of the events of this firing which took place at an ambient temperature of approximately 37° F.

Time from Screen Box (sec)	Event	Approx Pitch Attitude (°)
0.0	Screen box	0
0.390	Rocket ignition	+10
0.403	10% max thrust	
0.410	Peak pressure	+15
0.780	Grain break-up	
0.900	Web burnout	
1.032	End of action	

The work statement called for an operating temperature of 70° ± 20° F; however, because of the abbreviated static firing program, the units had been tested at only 70° and 90° F. As a result of this run, Frankford Arsenal directed that while the capsule is on the track in the ready condition, the motor temperature be maintained between 70° and 90° F by a portable heating system.

Analysis of the grain break-up is conjectural. It may be surmised that a trap failed or that the propellant, being cold, was less able to withstand the column loading near web burnout.

Postmortem examination showed that remachined aircraft bolts had been used to secure the XM15 escape rocket. Frankford Arsenal supplied two complete sets of bolts for each remaining run, one set to be used for installation and one for permanent security. The bolts were not to be reused.

Run No. 8 (1 Feb 63) - 700 KEAS (Figures 62, 63, 64)

The weight and balance were performed with extreme care. Thrust alignment was checked using the guide and found to be well in tolerance. The thrust moment arm was maintained at 2 inches to give the capsule a nose-up attitude during rocket firing.

On Wednesday, 30 Jan 63, the capsule was placed on the track in the starting position and the heating equipment (a Nelson gasoline heater) and the thermocouple instrumentation were installed and checked out. Because of the experimental classification of the XM15 escape rocket, operation of the heater was restricted to the Frankford Arsenal engineers, the Experimental Test Branch project officer, and the Aeronautical Systems Division project engineer. Heating was applied from 0300 to 1100 hours, 31 Jan 63, but the run was postponed because of inclement weather. On 1 Feb 63, heating was applied from 0700 to 1210 hours (X - 20 minutes). Evacuation of all heating equipment was completed at X - 10 minutes in the final phase of the count down.

Estimates of XM15 motor cooling from peak temperature were made during the heating period as a function of outside temperature and wind velocity so that once the heating equipment was removed, the project officer would have go or no-go advice. Examination of the rocket P-T trace revealed that ignition and rocket operation were normal.

It was concluded that proper temperature conditioning of the rocket motor prior to future tests would help to prevent ignition delay. Because the Nelson heater was difficult to operate for this purpose, a Chromalox electric heater was mounted in a custom-made aluminum cowl for the next run.

Run No. 9 (14 Mar 63) - 900 KEAS

An XM15 escape rocket (similar to static round No. 27), with thrust increased to 48,500 pounds, was installed with high tensile bolts. A temperature of 70° F was maintained prior to the run by a Chromalox electric heater (2000 watt) mounted in a custom-fitted aluminum cowl, in lieu of the gasoline heater. This arrangement was simple, dependable, and less hazardous than the gasoline system.

Figure 62. Oscillograph Record, Run 8

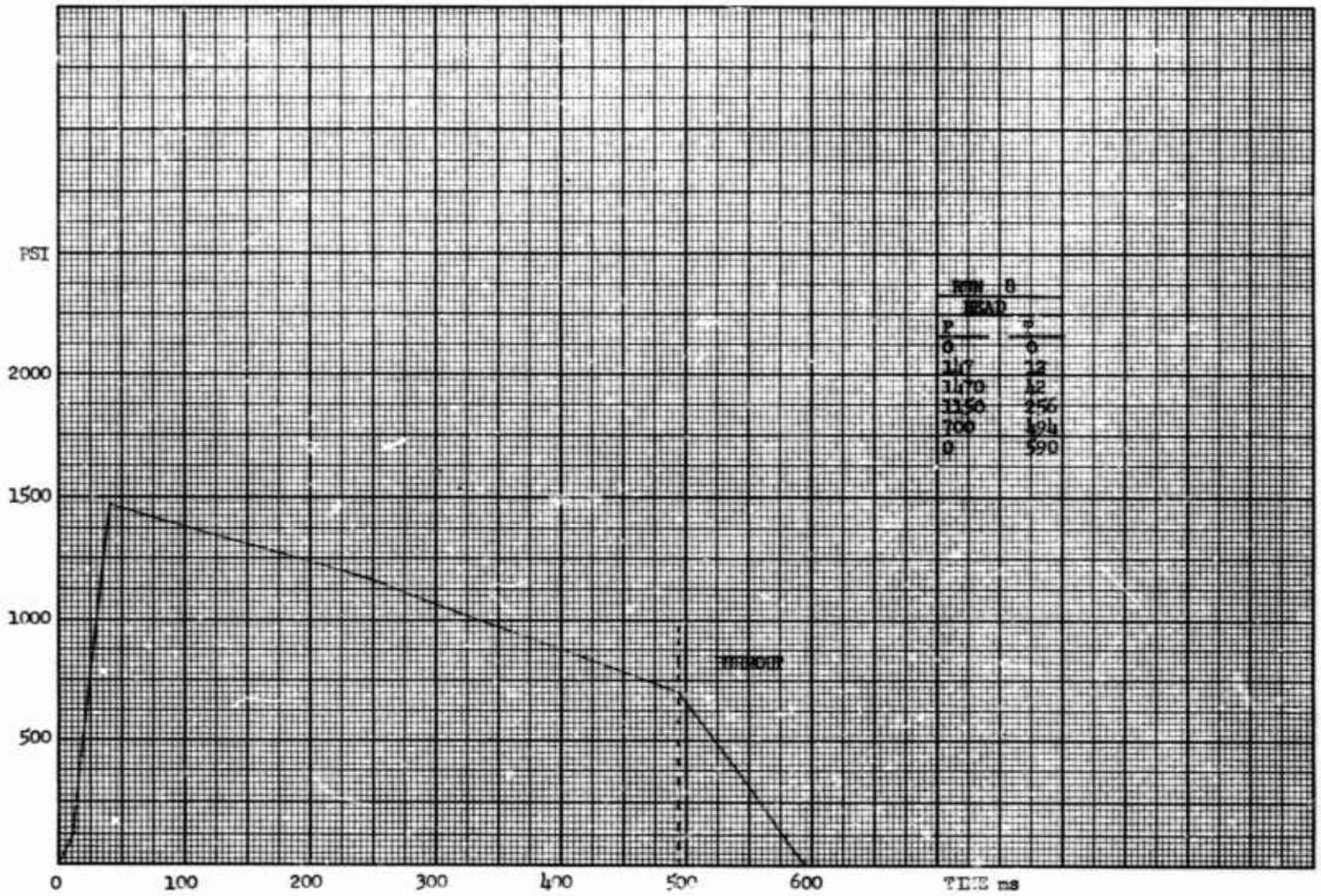

Figure 63. Linear replot, Pressure vs Time, Run 8

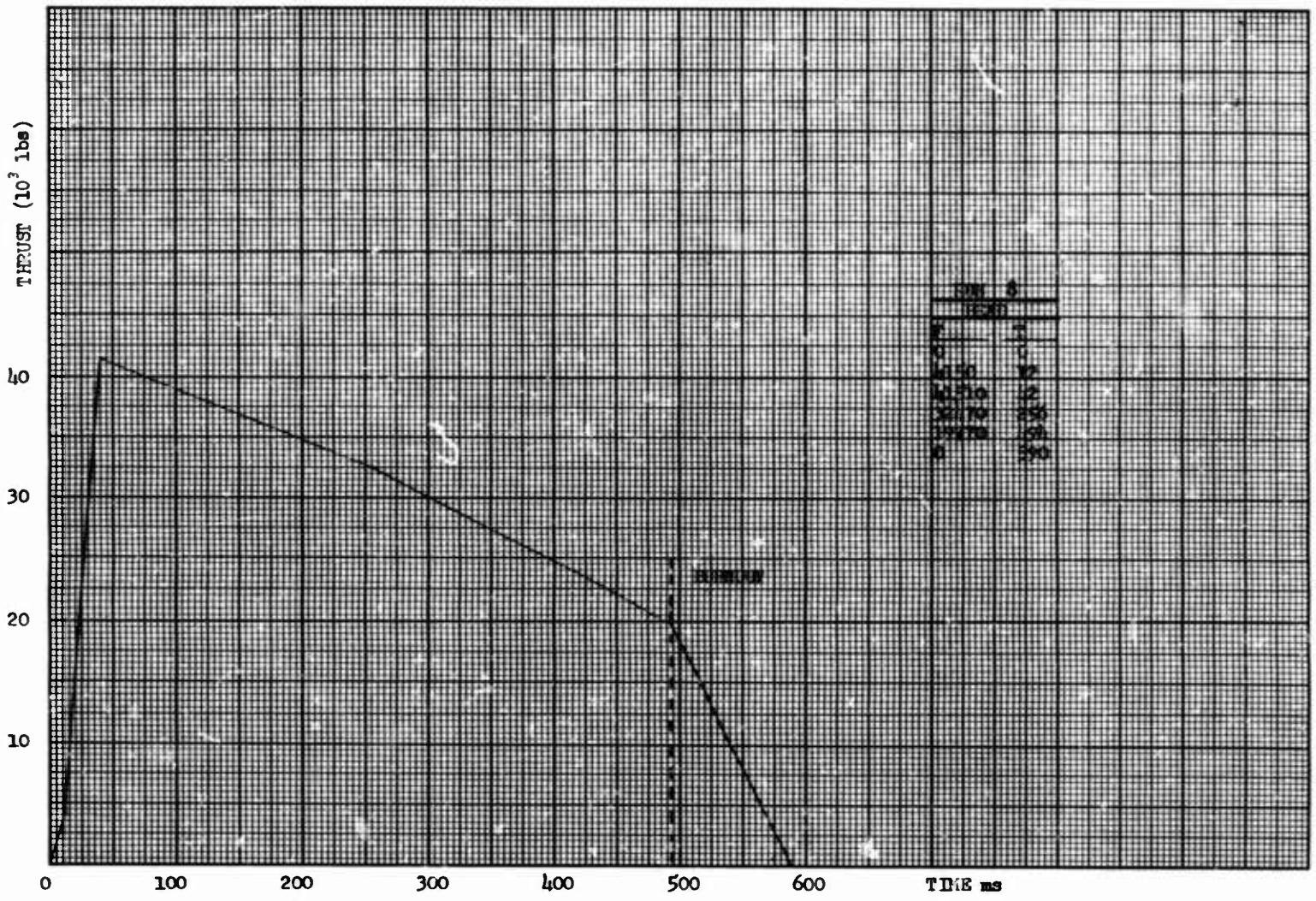

Figure 64. Estimated Thrust vs Time, Run 8

The scheduled ejection from the sled was not completed. The XM15 rocket did not fire, nor did the separating nuts, because the main cable was severed prior to engagement of the knives with the screen box. The catapult was recovered intact from the wreckage, disassembled, and returned to Picatinny Arsenal for radiographic inspection.

The case was recertified to 2000 psi for three minutes. Six grains were certified for motor installation. The other six, having suffered minor fissures at the corner of the support ring to propellant interface, were set aside. All grains could probably have survived by calling for a radius on the ring and grain instead of a sharp corner.

Run No. 10 (18 Apr 63) - Zero-Zero, Vertical (Figures 65, 66, 67)

Capsule No. 1, equipped with a normal XM15 rocket, was successfully ejected from a static mount with the water line vertical. For this test, the thrust line was through the center of gravity. The XM15 functioned normally.

The escape rocket had been temperature-conditioned by the Chromalox heater to approximately 70° F for four hours prior to the run, and the ambient temperature at the time was 54° F.

SECTION VII

CONCLUSIONS

Escape Rocket, XM15, met the criteria of a reliable source of thrust for the separable nose capsule sled test program.

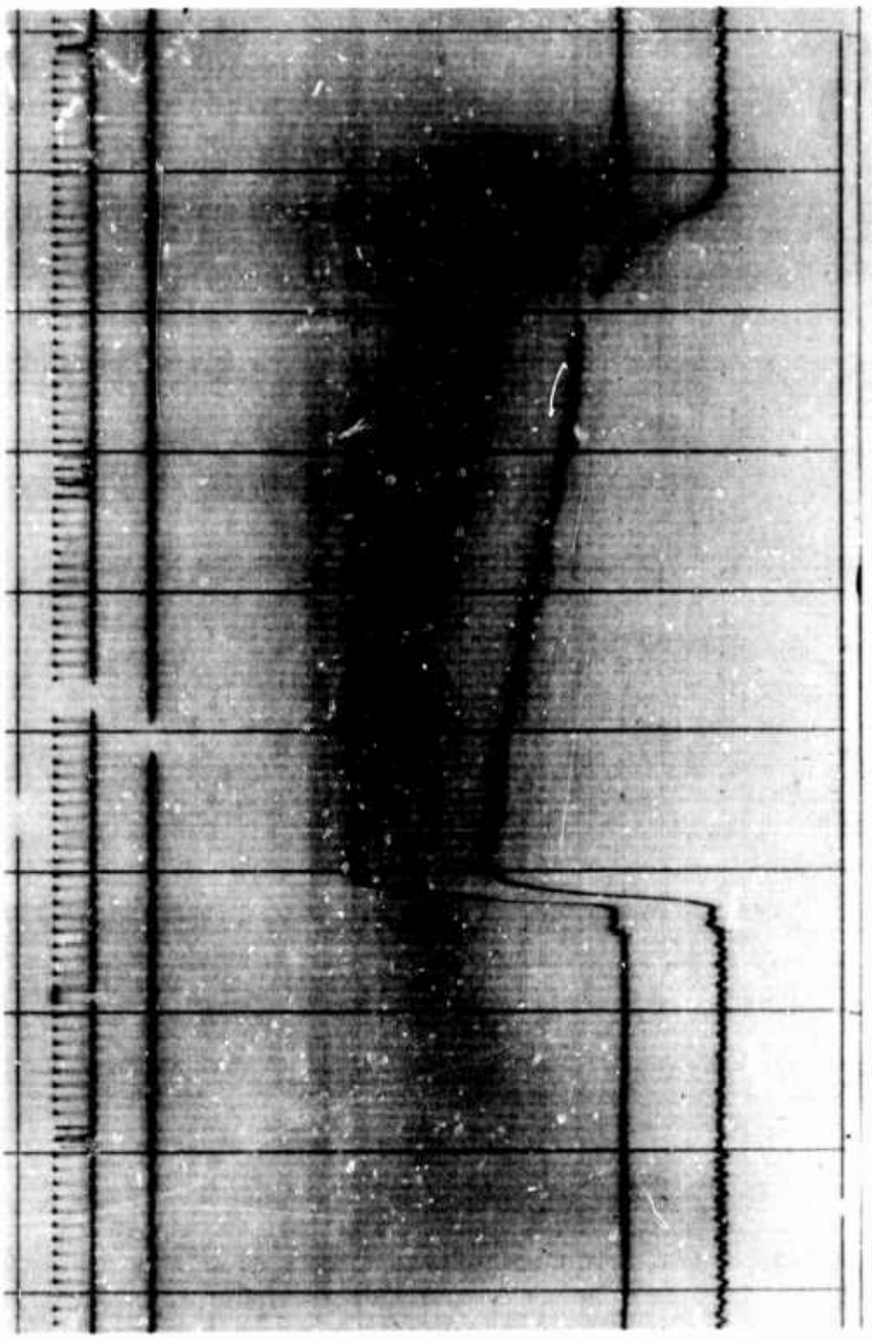

Figure 65. Oscillograph Record, Run 10

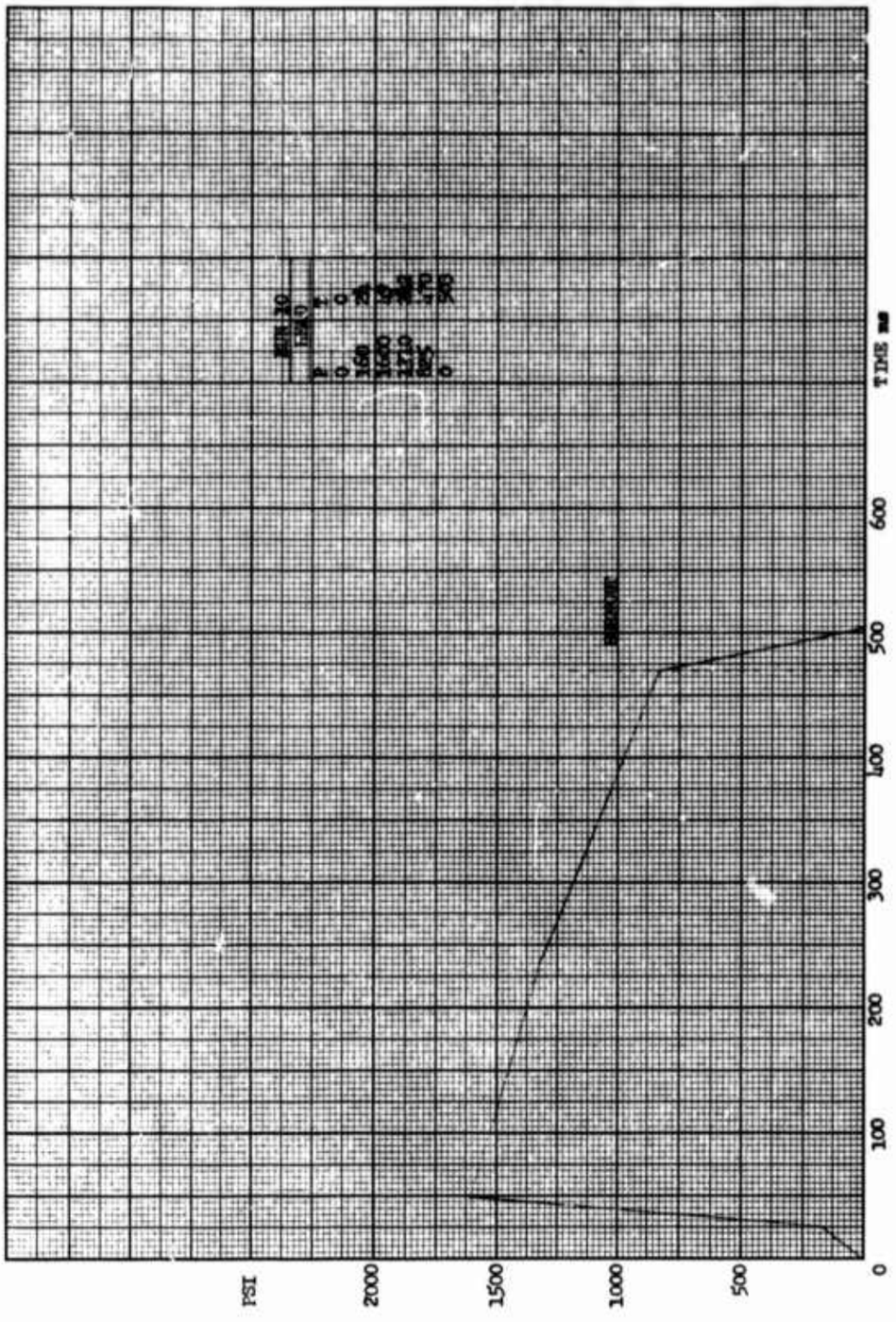

Figure 66. Linear replot, Pressure vs Time, Run 10

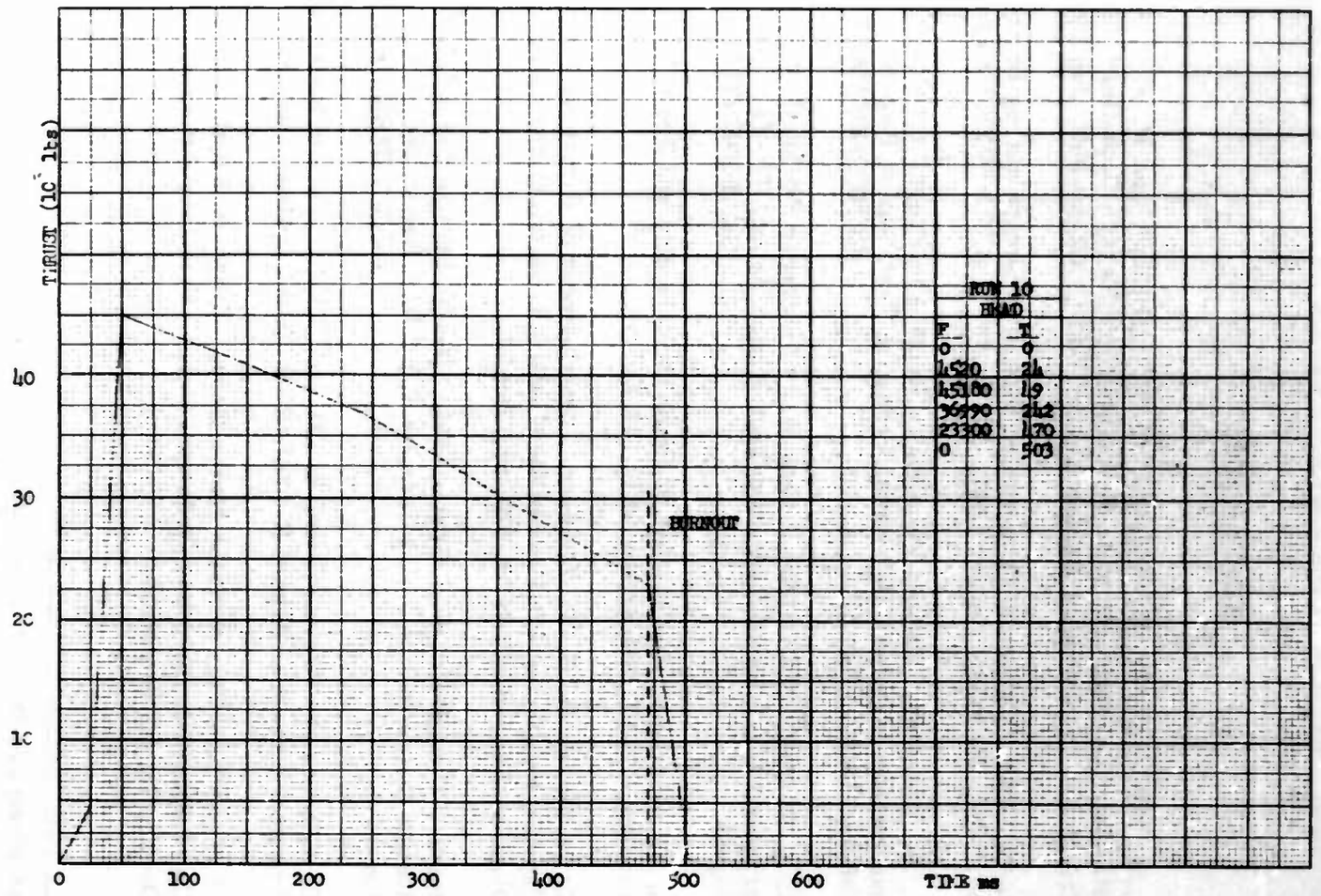

Figure 67. Estimated Thrust vs Time, Run 10

REFERENCES*

1. E. A. Newquist, M. D. Cassidy, C. W. Lindblom, and P. J. Sullivan, "Development of an Ejectable Nose Escape Capsule," Wright Air Development Center Report WADC-TR-59-493, Jun 59.

2. R. H. Olds, "Optimum Variation of Exhaust Velocity during Burning," (U), NAVORD Report 6247, 28 Oct 58 (CONFIDENTIAL)

3. C. E. Weinland, "Rocket Velocity as Related to Propellant Density and Specific Impulse (U)," Naval Ordnance Test Station Report TM No. 1000, 2 Nov 51 (CONFIDENTIAL)

4. A. J. Dierolf, "TEVROC: A New Way to Increase Rocket Performance (U)," Naval Ordnance Test Station Report TP-3220, Aug 63 (CONFIDENTIAL)

5. C. E. Weinland, "Evaluation of Propellant Density and Specific Impulse," NAVORD Report 6522, 17 Apr 59.

6. E. A. Newquist, G. F. Zimmer, "Development of Ejectable Nose Capsule Equipment for Feasibility Testing," Aeronautical Systems Division Report ASD-TDR-62-752, Jan 63.

7. Spiess, Confides, Long, Gratkowski, "Design Studies for a Solid Rocket Motor for the XM15 Catapult (U)," RDS Report No. 116, Jun 60 (CONFIDENTIAL)

8. C. S. Sterrett, "Development of XM7 and XM7E1 Escape Rockets," Frankford Arsenal Report R-1727 (RTD-TDR 63-4122), Aug 64.

9. "Fatigue Life Test of XM66 Motor Case," Emerson Electric Mfg. Co. Report No. 1292 (for Ordnance Corps, Picatinny Arsenal, Dover, N. J.) 30 Jan 62.

*Dates given are those of publication; in most instances the data were made available to this project prior to publication.

10. S. Harnett and S. Newman, "Design, Development, and Manufacture of the XM15 Catapult Rocket," Picatinny Arsenal Technical Report 3211, Nove 1964.

11. Leonard A. DeStefano, "Data Reduction of Telemetered P-T Traces of XM15 Escape Rocket," Frankford Arsenal Memorandum Report (in process).

12. G. W. Ducker, T. P. Lubinski, B. J. White, "Feasibility Testing of the Ejectable Nose Capsule Crew Escape System," Air Force Flight Dynamics Laboratory Memorandum Report ASRMDD-TM-41, Parts I through VII, Jan through Sep 1963.

BIBLIOGRAPHY

1. Bernard W. Shaffer, "Yield Strength of the Ortman Key in a Rocket Closure Assembly," New York University, College of Engineering (Research Division), Report NOrd 16497, Mar 58.

APPENDIX I

STRESS ANALYSIS OF THE XM15 ESCAPE CAPSULE ROCKET MOTOR*

*Carl W. Larson, Engineering Sciences Laboratory, Feltman Research Laboratories, Picatinny Arsenal, Technical Memorandum 1187, Oct 63.

ABSTRACT

The stresses in the XM-15 escape capsule rocket motor were determined for the maximum gas pressure forces. The design of the capsule is such that discontinuities in the geometrical configuration exist. The stresses due to these discontinuities were also analyzed.

RESULTS

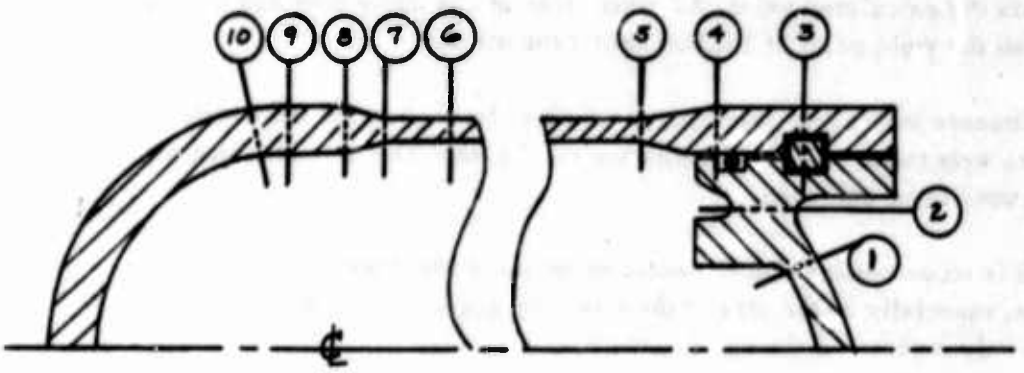

Fig 1-1. Critical sections of XM15 motor

The stresses calculated for the sections indicated in Figure 1 are tabulated below:

Section	Stresses	
	Longitudinal	Circumferential
1	+165,500	+ 82,400
2	+ 84,450	- 25,400
3	+215,800	+144,900
4	+ 54,000	- 82,050
5	+150,400	+116,000
6	+ 87,700	+175,400
7	+101,000	+151,500
8	+ 55,400	+ 92,200
9	+ 71,000	+ 68,600
10	+ 44,400	+ 34,300

CONCLUSIONS AND RECOMMENDATIONS

The design is considered to be capable of sustaining maximum loading pressures for one firing cycle without failure.

The highest stresses were found in the retainer ring notch region. This calculation is somewhat conservative since the configuration is complicated, and the actual stress should be lower in value. Also the maximum stress is above the yield point and local yielding will reduce this stress below the calculated value. All other areas of the motor body and head are below the yield point of 180,000 psi for the steel.

Stresses in the rear brackets, dowel pins, bracket welds and nozzle bolts were found to be well below the yield point. The front brackets are assumed to be unloaded.

It is recommended that the motor be subjected to a strain gage examination, especially in the area of the retaining ring notch, in order to check the values obtained through calculation.

PROCEDURE

Analysis of Loading Pattern at Head End of Shell

To analyze the head end, it is necessary to divide the actual shell into the following ideal sections; each of which can be analyzed easily to determine the discontinuity moments and shears.

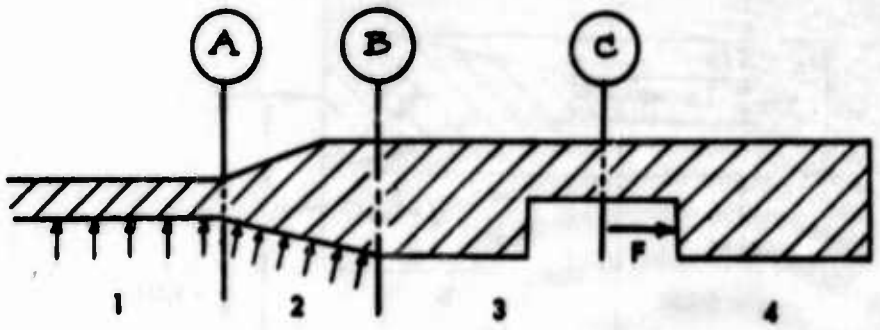

Section No. 1

Can be considered as an infinitely long cylinder since $\beta l > 5.0$ and therefore the moments and shears do not carry over from one end to the other.

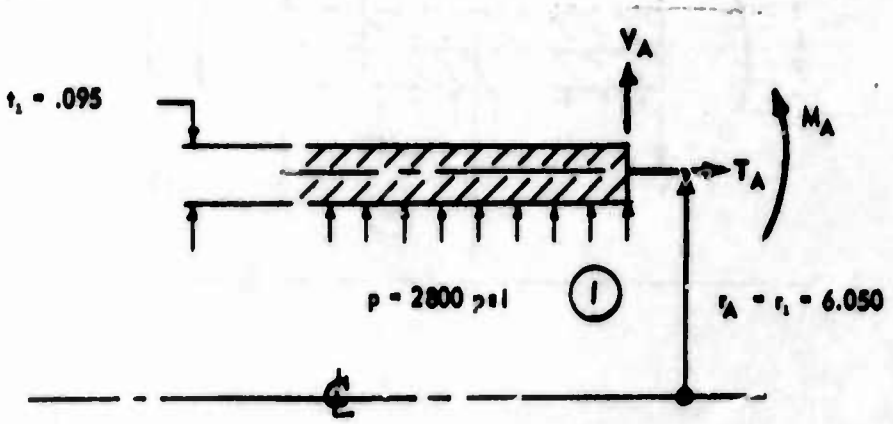

Section No. 2

Can be considered as a short cylinder since $\beta l = 0.714$

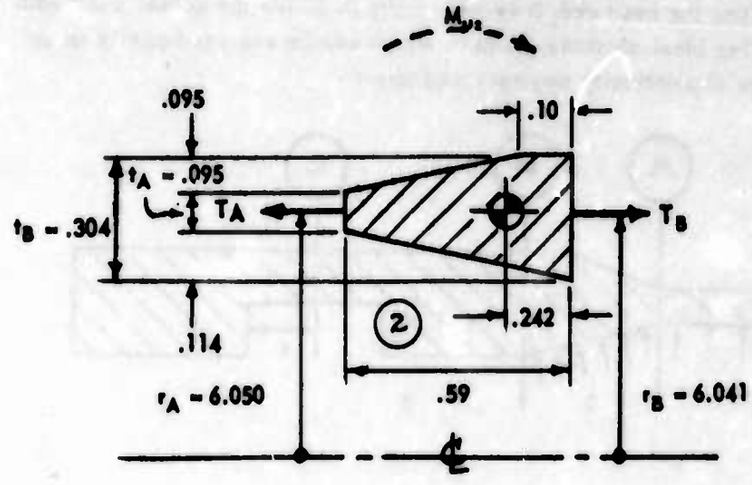

The above section can be replaced by a uniformly thick section, whose thickness is based on an equivalent moment of inertia, in order to duplicate the same sectional resistance to bending:

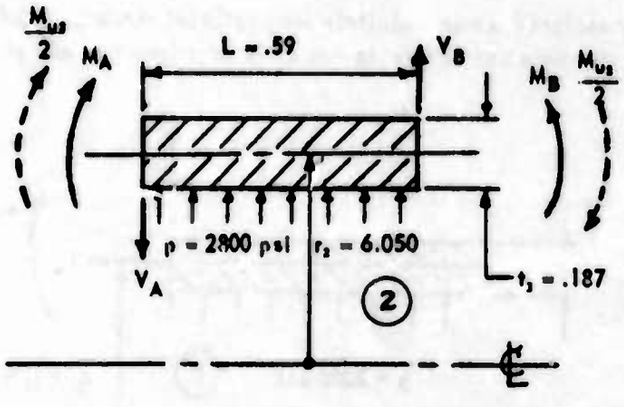

Section No. 3

Can be considered as a short cylinder, since $\beta l = 0.740$

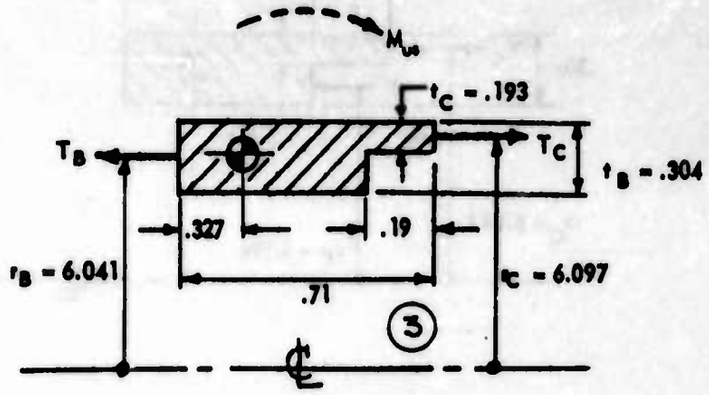

Equivalent section obtained in the same manner as Section No. 2:

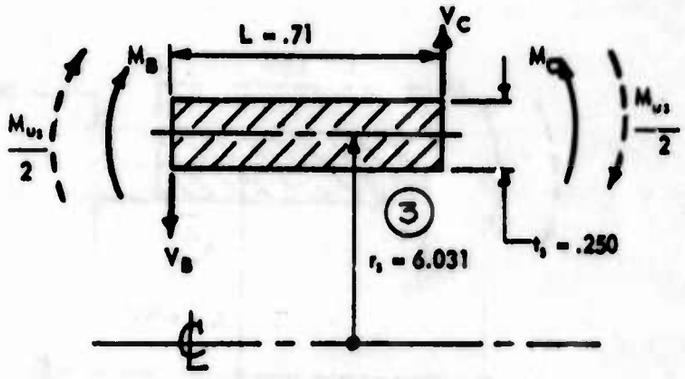

Section No. 4

Can be considered as a short cylinder since $\beta l = 1.078$

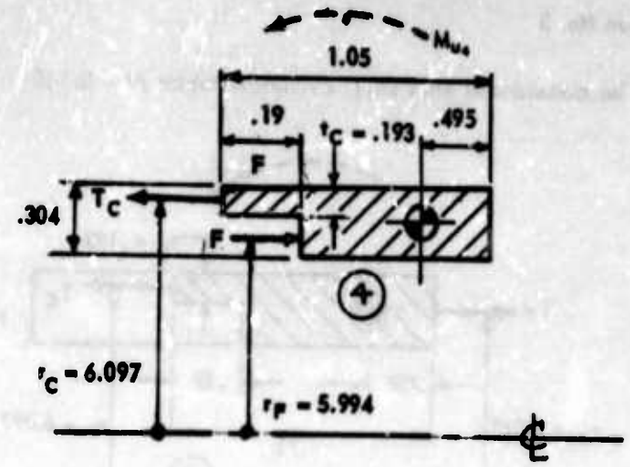

Equivalent section obtained in the same manner as Section No. 2:

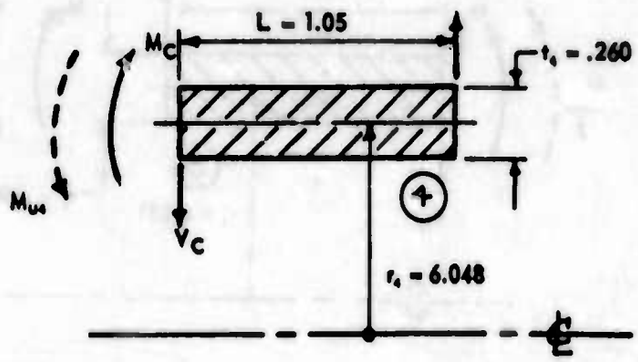

Coefficient	Section 1	Section 2	Section 3	Section 4	Section 5	Section 6	Section 7
p - Pressure (+ out)	+2800	+2800	0	0			
t - Thickness	0.095	0.187	0.250	0.260			
l - Length	∞	0.59	0.71	1.05			
r = Vertical Radius	6.050	6.050	6.051	6.048			
r_c } Radius ⊥ to	6.050	6.050	6.051	6.048			
r_c^2 } Tangent of	36.6	36.6	36.6	36.6			
r_L } Curve at	6.050	6.050	6.041	6.097			
r_R } designated pnt.	6.050	6.041	6.097	5.994			
r_h } Radius of Head	6.003	–	5.888	5.888			
r_h^2 }	36.0	–	34.7	34.7			
x_L } Dist from C.g.							
x_L^2 } of Ring to left							
x_R } and Right Axial							
x_R^2 } Load Points							
E	30×10^6	30×10^6	30×10^6	30×10^6			
$e = r_L - r_R$	0	+0.009	−0.056	+0.103			
$\phi = \sin^{-1}(r/r_c)$	90°	90°	90°	90°			
A							
I_{YY}	–	0.00319	0.00743	0.0251			
$T_L = pr_b^2/2r_L$ | $T_R = pr_h^2/2r_R$	– | 8330	8330 | 8050	8050 | 7970	7970 | 8080	|	|	|
M_U - Unbalance Body Moment (+)	0	+73.6	−449	+826			
V_U - Unbalance Body Load (+)							
$\beta = 1.285/\sqrt{r_c t}$	1.70	1.210	1.043	1.025			
β^2	2.37	1.462	1.090	1.050			
β^3	4.87	1.770	1.138	1.077			
βl	>5.0	0.714	0.740	1.078			
$1/D = 10.92/Et^3$	12750/E	1670/E	700/E	622/E			
$\sin\phi$	1	1	1	1			
$\sin^2\phi$	1	1	1	1			
$\cot\phi$							

Coefficient	Section 1	Section 2	Section 3	Section 4	Section 5	Section 6	Section 7
Y	0	16.6	15.1	4.56			
S	2	17.3	15.8	5.63			
K	0	5.89	5.51	2.53			
B	1	5.97	5.61	2.72			
V	0	1.40	1.35	0.911			
L	1	2.82	2.73	1.89			
$Y/2\beta D$	0	11450/E	2630/E	693/E			
$S/2\beta D$	7500/E	11950/E	2650/E	855/E			
$K\sin\phi/2\beta^2 D$	0	3360/E	885/E	375/E			
$B\sin\phi/2\beta^2 D$	2220/E	3400/E	900/E	402/E			
$V\sin^2\phi/2\beta^3 D$	0	660/E	207/E	132/E			
$L\sin^2\phi/2\beta^3 D$	1310/E	1330/E	420/E	274/E			
$r_c^2 X_L/EI_{YY}$							
r_c^2/EI_{YY}							
$r_c^2 X_R/EI_{YY}$							
$r_c^2 X_L^2/EI_{YY}$							
$r_c^2 X_L X_R/EI_{YY}$							
$r_c^2 X_R^2/EI_{YY}$							
r_c^2/EA							
$(S/2\beta D)M_U$							
$[(S+Y)/4\beta D]M_U$	–	+861,000/E	−1,185,000/E	+706,000/E			
$(B\sin\phi/2\beta^2 D)M_U$							
$[(B+K)\sin\phi/4\beta^2 D]M_U$	–	+249,000/E	−401,000/E	+332,000/E			
ϑ_p	0	0	0	0			
δ_p	−915,000/E	−466,000/E	0	0			
$(r_c^2 X_L/EI_{YY})M_U$							
$(r_c^2/EI_{YY})M_U$							
$(r_c^2 X_R/EI_{YY})M_U$							
$(r_c^2/EA)V_U$							

From Curves Tables or Formulas (Ref 7)

From General Equations

From the preceding tables, the following continuity equations can be obtained for equal rotations and deflections at each joint.

Rotation of Point A due to moments and shears:

$$-\frac{S_2 + Y_2}{4\beta_2 D_2} M_{u_2} = -\left(\frac{S_1}{2\beta_1 D_1} + \frac{S_2}{2\beta_2 D_2}\right) M_A + \frac{Y_2}{2\beta_2 D_2} M_B + \left(-\frac{B_1}{2\beta_1^2 D_1} + \frac{B_2}{2\beta_2^2 D_2}\right) V_A + \frac{K_2}{2\beta_2^2 D_2} V_B$$

$$-861{,}000 = -19{,}450\, M_A - 11{,}450\, M_B + 1180\, V_A + 3360\, V_B$$

Deflection at Point A due to moments, shears, and pressures:

$$\delta_{p_1} - \frac{B_2 + K_2}{4\beta_2^2 D_2} M_{u_2} - \delta_{p_2} = \left(\frac{B_1}{2\beta_1^2 D_1} - \frac{B_2}{2\beta_2^2 D_2}\right) M_A + \frac{K_2}{2\beta_2^2 D_2} M_B + \left(\frac{L_1}{2\beta_1^2 D_1} + \frac{L_2}{2\beta_2^2 D_2}\right) V_A + \frac{V_2}{2\beta_2^2 D_2} V_B$$

$$-698{,}000 = -1180\, M_A + 3360\, M_B + 2640\, V_A + 660\, V_B$$

Rotation of Point B due to moments and shears:

$$\frac{S_2 + Y_2}{4\beta_2 D_2} M_{u_2} - \frac{S_3 + Y_3}{2\beta_3 D_3} M_{u_3} = \frac{Y_2}{2\beta_2 D_2} M_A - \left(\frac{S_2}{2\beta_2 D_2} + \frac{S_3}{2\beta_3 D_3}\right) M_B + \frac{Y_3}{2\beta_3 D_3} M_C - \frac{K_2}{2\beta_2^2 D_2} V_A + \left(-\frac{B_2}{2\beta_2^2 D_2} + \frac{B_3}{2\beta_3^2 D_3}\right) V_B + \frac{K_3}{2\beta_3^2 D_3} V_C$$

$$2{,}046{,}000 = 11450\, M_A - 14{,}600\, M_B + 2630\, M_C - 3360\, V_A - 2500\, V_B + 885\, V_C$$

Deflection at Point B due to moments, shears, and pressure:

$$-\frac{B_2+K_2}{4\beta_2^3 D_2} M_{us} + \delta_{P_2} - \frac{B_3+K_3}{2\beta_3^3 D_3} M_{us} = -\frac{K_2}{2\beta_2^3 D_2} M_A + \left(\frac{B_2}{2\beta_2^3 D_2} - \frac{B_3}{2\beta_3^3 D_3}\right) M_B$$

$$+\frac{K_3}{2\beta_3^3 D_3} M_C + \frac{V_2}{2\beta_2^3 D_2} V_A + \left(\frac{L_2}{2\beta_2^3 D_2} + \frac{L_3}{2\beta_3^3 D_3}\right) V_B + \frac{V_3}{2\beta_3^3 D_3} V_C$$

$$-314{,}000 = -3360\, M_A + 2500\, M_B + 885\, M_C + 660\, V_A + 1750\, V_B + 207\, V_C$$

Rotation of Point C due to moments and shears:

$$\frac{S_3+Y_3}{2\beta_3 D_3} M_{us} - \frac{S_4}{2\beta_4 D_4} M_{us} - \frac{Y_3}{2\beta_3 D_3} M_B - \left(\frac{S_3}{2\beta_3 D_3} + \frac{S_4}{2\beta_4 D_4}\right) M_C$$

$$-\frac{K_3}{2\beta_3^2 D_3} V_B + \left(-\frac{B_3}{2\beta_3^2 D_3} + \frac{B_4}{2\beta_4^2 D_4}\right) V_C$$

$$-1{,}891{,}000 = 2630\, M_B - 3505\, M_C - 885\, V_B - 498\, V_C$$

Deflection at Point C due to moments and shears:

$$-\frac{B_3+K_3}{2\beta_3^3 D_3} M_{us} - \frac{B_4}{2\beta_4^3 D_4} M_{us} = -\frac{K_3}{2\beta_3^3 D_3} M_B + \left(\frac{B_3}{2\beta_3^3 D_3} - \frac{B_4}{2\beta_4^3 D_4}\right) M_C$$

$$+\frac{V_3}{2\beta_3^3 D_3} V_B + \left(\frac{L_3}{2\beta_3^3 D_3} + \frac{L_4}{2\beta_4^3 D_4}\right) V_C$$

$$+69{,}000 = -885\, M_B + 498\, M_C + 207\, V_B + 694\, V_C$$

Solving the preceding equations simultaneously, we obtain the following values for the moments and shears at each section:

M_A = 94.2 in.-lb/in.	V_A = −519 lb/in.	T_A = 8330 lb/in.
M_B = 424 in.-lb/in.	V_B = −974 lb/in.	T_B = 8050 lb/in.
M_C = 1082 in.-lb/in.	V_C = +154.6 lb/in.	T_C = 7970 lb/in.

The maximum stresses at each section will be as follows:

Section A

Longitudinal stress

$$S_t = \frac{T_A}{t_A} \pm \frac{6M_A}{t_A^2} = \frac{8330}{0.095} + \frac{(6)(94.2)}{(0.095)^2}$$

$$S_t = 87{,}800 + 62{,}600 = 150{,}400 \text{ psi}$$

Circumferential stress

$$S_h = \frac{2}{t_A}[T_A + \beta_1 r_1 V_A + \beta_1^2 r_1 M_A] \pm \nu \frac{6M_A}{t_A^2}$$

$$S_h = \frac{2}{0.095}[8330 + (1.70)(6.050)(-519) + (2.87)(6.050)(94.2) + (0.3)(62{,}600)$$

$$S_h = 97{,}200 + 18{,}800 = 116{,}000 \text{ psi}$$

Section B

Longitudinal stress

$$S_t = \frac{T_B}{t_B} \pm \frac{6M_B}{t_B^2} = \frac{8050}{0.304} + \frac{(6)(424)}{(0.304)^2}$$

$$S_t = 26{,}500 + 27{,}500 = 54{,}000 \text{ psi}$$

Circumferential stress

$$\delta_{B_2} = -\frac{B_2}{2\beta_2^3 D_2} M_B^1 + \frac{K_2}{2\beta_2^2 D_2} M_A^1 - \frac{L_2}{2\beta_2^3 D_2} V_B - \frac{V_2}{2\beta_2^3 D_2} V_A$$

$$E\delta_{B_2} = -(3400)(387) + (3360)(133) - (1330)(-974) - (660)(-519)$$

$$E\delta_{B_2} = 770{,}000$$

$$S_h = 2\frac{T_B}{t_B} - \frac{\delta_{B_2}}{r_2} \pm \nu \frac{6M_B}{t_B^2}$$

$$S_h = (2)(26{,}500) - \frac{770{,}000}{6.063} + (0.3)(27{,}500)$$

$$S_h = -73{,}800 - 8250 = -82{,}050 \text{ psi}$$

Section C

Longitudinal stress

$$S_C = \frac{T_C}{t_C} \pm \frac{6M_C}{t_C^2} = \frac{7970}{0.193} + \frac{(6)(1082)}{(0.193)^2}$$

$$S_t = 41{,}300 + 174{,}400 = 215{,}800 \text{ psi}$$

Circumferential stress

$$\delta_{C_4} = -\frac{B_4}{2\beta_4^3 D_4} M_C^1 + \frac{L_4}{2\beta_4^2 D_4} V_C$$

$$E\delta_{C_4} = -(402)(256) + (274)(154.6) = -392{,}600$$

$$S_h = 2\frac{T_C}{t_C} - \frac{\delta_{C_4}}{r_4} \pm \nu \frac{6M_C}{t_C^2}$$

$$S_h = (2)(41.300) + \frac{60,700}{6.048} + (0.3)(174,400)$$

$$S_h = 92,600 + 52,300 = 144,900 \text{ psi}$$

Analysis of Loading Pattern at Junction of Rear Spherical Head and Shell

In determining the discontinuity moments and shears, it is necessary to divide the actual shell into the following idealized sections, each of which can be analyzed easily.

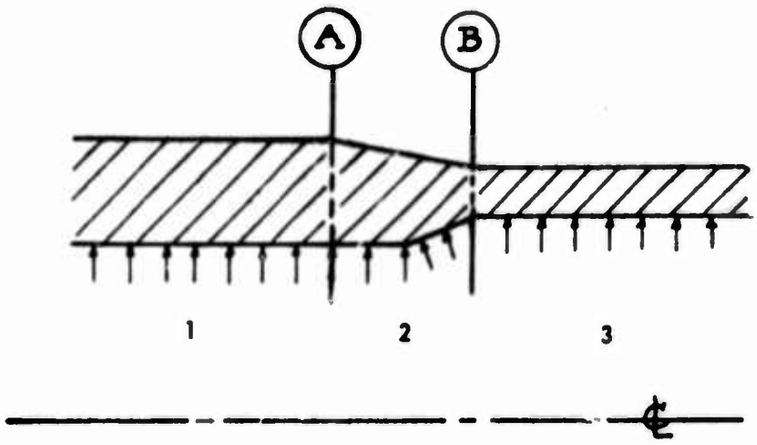

Section No. 1

Can be considered as an infinitely long cylinder since $\beta l > 5.0$ and therefore the moments and shears do not carry over from one end to the other.

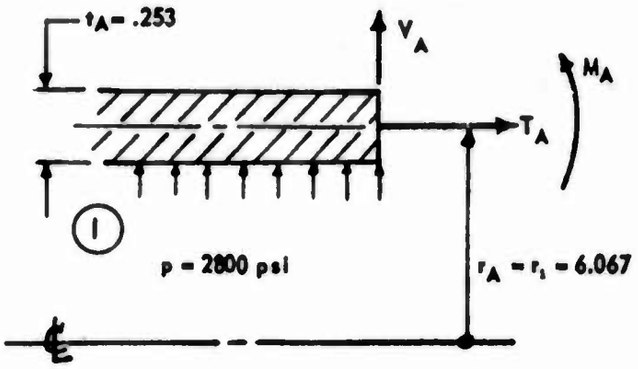

Section No. 2

Can be considered as a short section since $\beta l = 0.691$

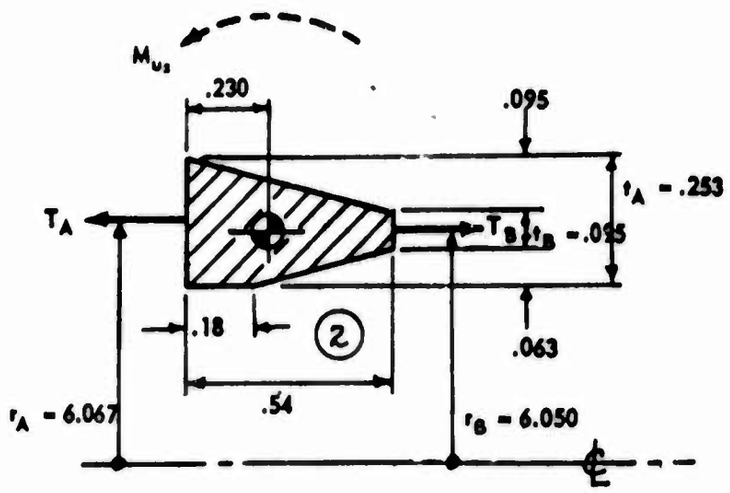

The above section can be replaced by a uniformly thick section, whose thickness is based on an equivalent moment of inertia, in order to duplicate the same sectional resistance to bending.

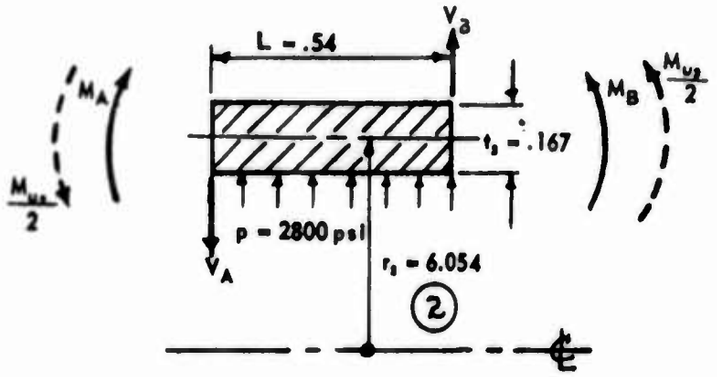

Section No. 3

Can be considered as an infinitely long cylinder since $\beta l > 5.0$ and therefore the moments and shears do not carry over from one end to the other.

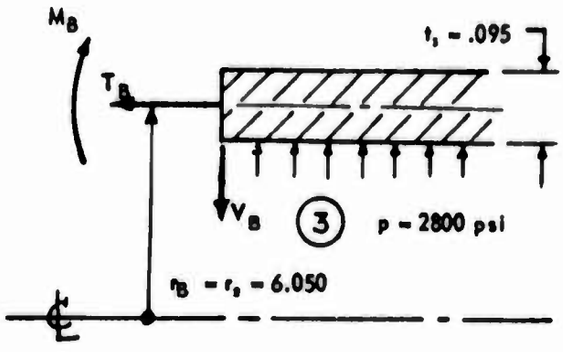

Coefficient	Section 1	Section 2	Section 3	Section 4	Section 5	Section 6	Section 7
p - Pressure (+ out)	+2800	+2800	+2800				
t - Thickness	0.253	0.167	0.095				
l - Length	∞	0.54	∞				
r = Vertical Radius	6.067	6.054	6.050				
r_c Radius ⊥ to	6.067	6.054	6.050				
r_c^2 Tangent of	36.8	36.7	36.6				
r_L Curve at	6.067	6.067	6.050				
r_R designated pnt.	6.067	6.050	6.050				
r_h Radius of Head	5.940	–	6.003				
r_h^2 Radius of Head	35.3	–	36.0				
x_L Dist From C.g.							
x_L^2 of Ring to left							
x_R and Right Axial							
x_R^2 Load Points							
E	30×10^6	30×10^6	30×10^6				
$e = r_L - r_R$	0	+0.017	0				
$\phi = \sin^{-1}(r/r_c)$	90°	90°	90°				
A							
I_{YY}	–	0.00219	–				
$T_L = pr_h^2/2r_L$ | $T_R = pr_h^2/2r_R$	– | 8130	8130 | 8330	8330 | –				
M_U - Unbalance Body Mom. (+)	0	+140	0				
V_U - Unbalance Body Load (+)							
$\beta = 1.285/\sqrt{r_c t}$	1.037	1.280	1.70				
β^2	1.073	1.635	2.87				
β^3	1.112	2.09	4.87				
βl	>5.0	0.691	>5.0				
$1/D = 10.92/Et^3$	675/E	2345/E	12750/E				
$\sin\phi$	1	1	1				
$\sin^2\phi$	1	1	1				
$\cot\phi$							

Coefficient	Section 1	Section 2	Section 3	Section 4	Section 5	Section 6	Section 7
Y	0	18.3	0				
S	2	19.0	2				
K	0	6.29	0				
B	1	6.37	1				
V	0	1.45	0				
L	1	2.91	1				
$Y/2\beta D$	0	16800/E	0				
$S/2\beta D$	650/E	17400/E	7500/E				
$K\sin\phi/2\beta^2 D$	0	4510/E	0				
$B\sin\phi/2\beta^2 D$	314/E	4570/E	2220/E				
$V\sin^2\phi/2\beta^3 D$	0	815/E	0				
$L\sin^2\phi/2\beta^3 D$	303/E	1630/E	1310/E				
$r_c^2 X_L/EI_{YY}$							
r_c^2/EI_{YY}							
$r_c^2 X_R/EI_{YY}$							
$r_c^2 X_L^2/EI_{YY}$							
$r_c^2 X_L X_R/EI_{YY}$							
$r_c^2 X_R^2/EI_{YY}$							
r_c^2/EA							
$(S/2\beta D)M_U$							
$[(S+Y)/4\beta D]M_U$	–	+2,390,000/E	–				
$(B\sin\phi/2\beta^2 D)M_U$							
$[(B+K)\sin\phi/4\beta^2 D]M_U$	–	+635,000/E	–				
θ_p From General Equations	0	0	0				
δ_p From General Equations	-346,000/E	-522,000/E	-915,000/E				
$(r_c^2 X_L/EI_{YY})M_U$							
$(r_c^2/EI_{YY})M_U$							
$(r_c^2 X_R/EI_{YY})M_U$							
$(E^2/EA)V_U$							

From the preceding tables, the following continuity equations can be obtained for equal rotations and deflections at each joint.

Rotation of Point A due to moments and shears:

$$-\frac{S_2+Y_2}{4\beta_2 D_2} M_{u_2} = -\left(\frac{S_1}{2\beta_1 D_1} + \frac{S_2}{2\beta_2 D_2}\right) M_A + \frac{Y_2}{2\beta_2 D_2} M_B + \left(-\frac{B_1}{2\beta_1^1 D_1} + \frac{B_2}{2\beta_2^1 D_2}\right) V_A + \frac{K_2}{2\beta_2^1 D_2} V_B$$

$$-2{,}390{,}000 = -18{,}050\, M_A + 16{,}800\, M_B + 4255\, V_A + 4510\, V_B$$

Deflection at Point A due to moments, shears and pressure:

$$\delta_{p_1} - \frac{B_2+K_2}{4\beta_2^1 D_2} M_{u_2} - \delta_{p_2} = \left(\frac{B_1}{2\beta_1^1 D_1} - \frac{B_2}{2\beta_2^1 D_2}\right) M_A + \frac{K_2}{2\beta_2^1 D_2} M_B + \left(\frac{L_1}{2\beta_1^1 D_1} + \frac{L_2}{2\beta_2^1 D_2}\right) V_A + \frac{V_2}{2\beta_2^1 D_2} V_B$$

$$-459{,}000 = -4255\, M_A + 4510\, M_B + 1933\, V_A + 815\, V_B$$

Rotation of Point B due to moments and shears:

$$\frac{S_2+Y_2}{4\beta_2 D_2} M_{u_2} = \frac{Y_2}{2\beta_2 D_2} M_A - \left(\frac{S_2}{2\beta_2 D_2} + \frac{S_3}{2\beta_3 D_3}\right) M_B - \frac{K_2}{2\beta_2^1 D_2} V_A + \left(-\frac{B_2}{2\beta_2^1 D_2} + \frac{B_3}{2\beta_3^1 D_3}\right) V_B$$

$$2{,}390{,}000 = 16{,}800\, M_A - 24{,}900\, M_B - 4510\, V_A - 2350\, V_B$$

Deflection at Point B due to moments, shears, and pressure:

$$-\frac{B_2 + K_2}{4\beta_2^3 D_2} M_{u2} + \delta_{p2} - \delta_{p1} = -\frac{K_2}{2\beta_2^3 D_2} M_A + \left(\frac{B_2}{2\beta_2^3 D_2} - \frac{B_1}{2\beta_1^3 D_1}\right) M_B + \frac{V_2}{2\beta_2^3 D_2} V_A$$

$$+ \left(\frac{L_2}{2\beta_2^3 D_2} + \frac{L_1}{2\beta_1^3 D_1}\right) V_B$$

$$-242{,}000 = -4510\, M_A + 2350\, M_B + 815\, V_A + 2940\, V_B$$

Solving the preceding equations simultaneously, we obtain the following values for the shears and moments at each section:

$M_A = 249$ in.-lb/in. $\quad V_A = 164.2$ lb/in. $\quad T_A = 8130$ lb/in.

$M_B = 20.0$ in.-lb/in. $\quad V_B = 239$ lb/in. $\quad T_B = 8330$ lb/in.

The maximum stresses at each section will be:

Section A

Longitudinal stress

$$S_t = \frac{T_A}{t_A} \pm \frac{6M_A}{t_A^2} = \frac{8130}{0.254} + \frac{(6)(249)}{(0.253)^2}$$

$$S_t = 32{,}000 + 23{,}400 = 55{,}400 \text{ psi}$$

Circumferential stress

$$S_h = 2\frac{T_A}{t_A} + \frac{2\beta_1 r_1}{t_A} V_A + \frac{2\beta_1^2 r_1}{t_A} M_A \pm \nu \frac{6M_A}{t_A^2}$$

$$S_h = \frac{2}{0.253}[8130 + (1.037)(6.065)(164.2) + (1.073)(6.065)(249)]$$

$$+ (0.3)(23{,}400)$$

$$S_h = 85{,}200 + 7000 = 92{,}200 \text{ psi}$$

Section B

Longitudinal stress

$$S_t = \frac{T_B}{t_B} \pm \frac{6M_B}{t_B^2} = \frac{8330}{0.095} + \frac{(6)(20.0)}{(0.095)^2}$$

$$S_t = 87{,}700 + 13{,}300 = 101{,}000 \text{ psi}$$

Circumferential stress

$$S_h = 2\frac{T_B}{t_B} - 2\frac{\beta_s r_s}{t_B} V_B + 2\frac{\beta_s^2 r_s}{t_B} M_B \pm \nu \frac{6M_B}{t_B^2}$$

$$S_h = \frac{2}{0.095}[8330 - (1.70)(6.042)(164.2) + (2.87)(6.042)(20.0)] + (0.3)(13{,}300)$$

$$S_h = 147{,}500 + 4000 = 151{,}500 \text{ psi}$$

Analysis of Front Spherical Head

In order to determine the discontinuity moments and shears, it is necessary to divide the spherical head into the following idealized sections which can be easily analyzed.

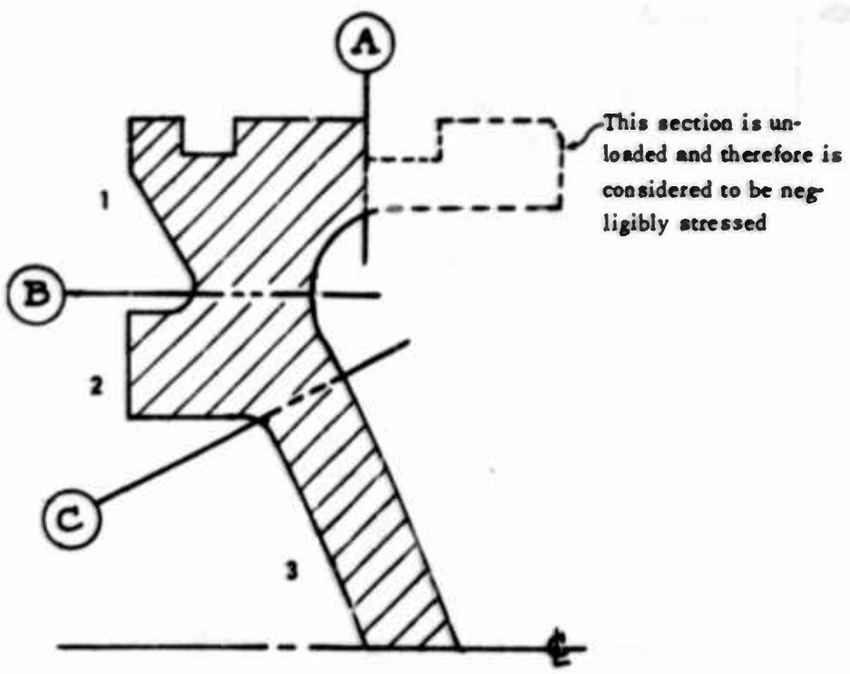

Section No. 1

Can be considered to be a ring since $\beta l < 0.5$

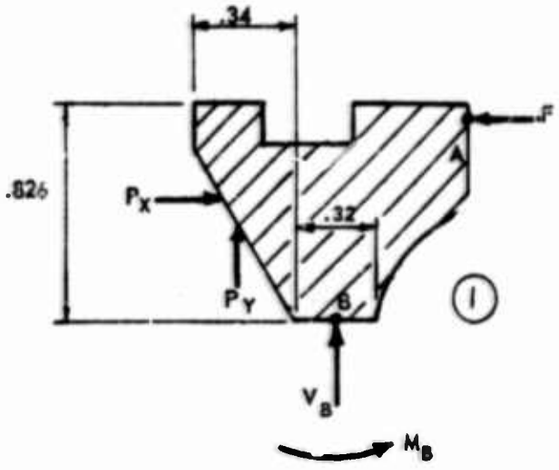

F = 8200 lb/in.*

P_X = 2310 lb/in.

P_Y = 950 lb/in.

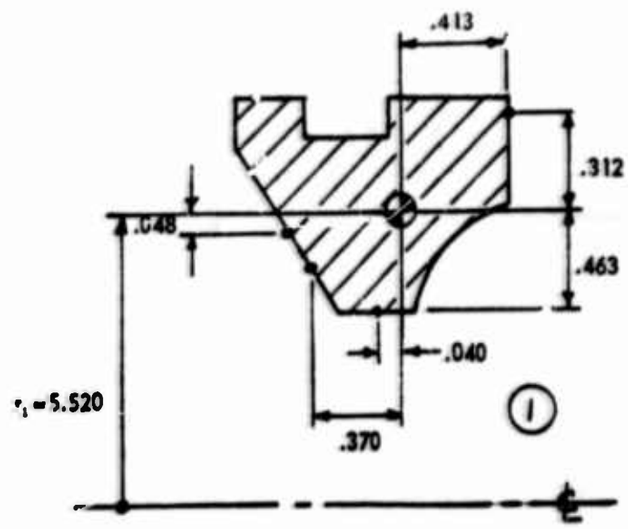

*$F = \frac{(2800)(5.89)^2}{(2)(5.83)} = 8200$ lb/in.

$M_u = -(950)(0.370) + (2310)(.048) + (8200)(0.312) = +2317$ in. lb/in.

$V_u = -950$ lb/in.

Section No. 2

Can be considered to be a ring since $\beta l < 0.5$

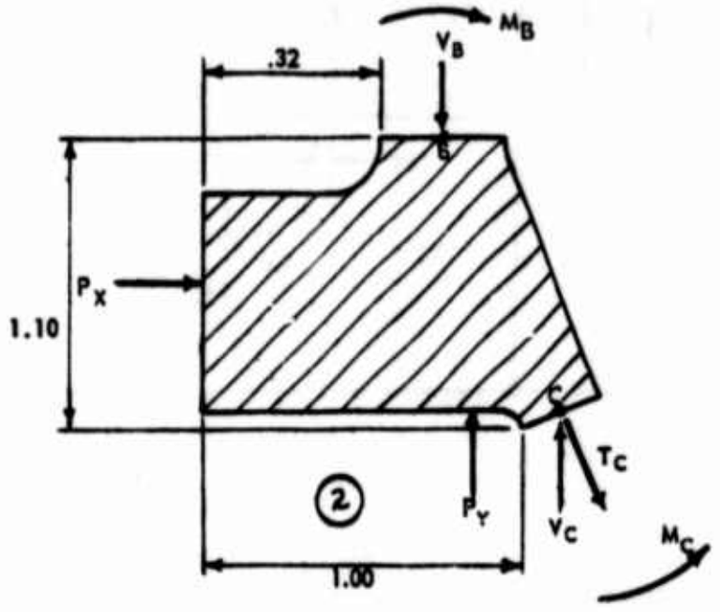

$P_X = 3080$ lb/in.

$P_Y = 1900$ lb/in.

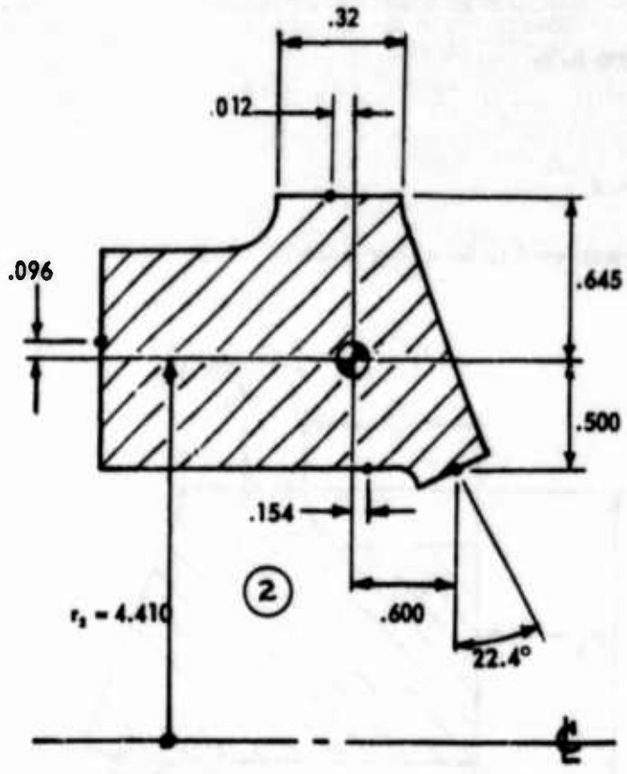

$M_u = (1900)(0.154) - (3080)(0.096) - (14350)(0.368) = -5285$ in.-lb/in.

$V_u = -1900 + (14350)(\cos 22.4°) + 11{,}370$ lb/in.

Section No. 3

Can be considered to be a long spherical sector since $\beta l > 5.0$

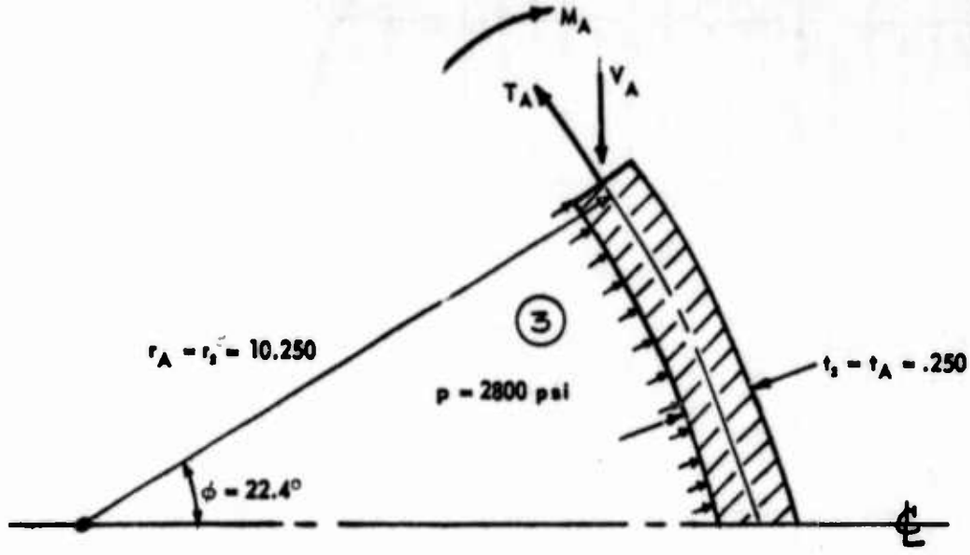

Coefficient	Section 1	Section 2	Section 3	Section 4	Section 5	Section 6	Section 7
p - Pressure (+ out)	2800	2800	+2800				
t - Thickness	–	–	0.250				
l - Length	–	–	∞				
r = Vertical Radius	–	–	3.900				
r_c Radius ⊥ to	5.520	4.410	10.250				
r_c^2 Tangent of	30.5	19.45	105.1				
r_L Curve at							
r_R Designated pnt.							
r_h Radius of Head							
r_h^2							
X_L Dist From C.g.	0.040	0.012	–				
X_L^2 of Ring to left	0.0016	0.000144	–				
X_R and Right Axial	0.413	0.600	–				
X_R^2 Load Points	0.1706	0.360	–				
E	30×10^6	30×10^6	30×10^6				
$e = r_L - r_R$							
$\phi = \sin^{-1}(r/r_c)$	–	–	22.4°				
A	0.483	0.979	–				
I_{YY}	0.0245	0.0849	–				
$T_L = pr_h^2/2r_L$ | $T_R = pr_h^2/2r_R$	0 | 0	0 | 14350	14350 | –				
M_U - Unbalance Body Mom. (+)	+2317	−5285	–				
V_U - Unbalance Body Load (+)	−950	+11,370	–				
$\beta = 1.285/\sqrt{r_c t}$	–	–	0.805				
β^2	–	–	0.648				
β^3	–	–	0.522				
βl	–	–	>5.0				
$1/D = 10.92/Et^3$	–	–	700/E				
$\sin\phi$	–	–	0.381				
$\sin^2\phi$	–	–	0.145				
$\cot\phi$							

Coefficient	Section 1	Section 2	Section 3	Section 4	Section 5	Section 6	Section 7
Y	–	–	0				
S	–	–	2				
K	–	–	0				
B	–	–	1				
V	–	–	0				
L	–	–	1				
$Y/2\beta D$	–	–	0				
$S/2\beta D$	–	–	870/E				
$K\sin\phi/2\beta^2 D$	–	–	0				
$B\sin\phi/2\beta^2 D$	–	–	203/E				
$V\sin^2\phi/2\beta^3 D$	–	–	0				
$L\sin^2\phi/2\beta^3 D$	–	–	97.0/E				
$r_c^2 X_L/EI_{YY}$	49.8/E	2.75/E	–				
r_c^2/EI_{YY}	1245/E	229/E	–				
$r_c^2 X_R/EI_{YY}$	514/E	137.4/E	–				
$r_c^2 X_L^2/EI_{YY}$	1.992/E	0.0330/E	–				
$r_c^2 X_L X_R/EI_{YY}$	20.6/E	1.65/E	–				
$r_c^2 X_R^2/EI_{YY}$	212/E	82.4/E	–				
r_c^2/EA	63.1/E	19.87/E	–				
$(S/2\beta D)M_U$							
$[(S+Y)/4\beta D]M_U$							
$(B\sin\phi/2\beta^2 D)M_U$							
$[(B+K)\sin\phi/4\beta^2 D]M_U$							
θ_p From General Equations	–	–	0				
δ_p From General Equations	–	–	-157,000/E				
$(r_c^2 X_L/EI_{YY})M_U$	+115,400/E	-14,350/E	–				
$(r_c^2/EI_{YY})M_U$	+2,885,000/E	-1,210,000/E	–				
$(r_c^2 X_R/EI_{YY})M_U$	+1,191,000/E	-726,000/E	–				
$(r_c^2/EA)V_U$	-59,950/E	+226,000/E	–				

From the preceding tables, the following continuity equations can be obtained for equal rotations and deflections at each joint.

Rotation of Point B due to moments, shears, and pressure:

$$\left(\frac{r_C^2}{EI_{YY}}\right)_1 M_{u_1} - \left(\frac{r_C^2}{EI_{YY}}\right)_2 M_{u_2} = -\left[\left(\frac{r_C^2}{EI_{YY}}\right)_1 + \left(\frac{r_C^2}{EI_{YY}}\right)_2\right] M_B + \left(\frac{r_C}{EI_{YY}}\right)_2 M_C$$

$$+ \left[-\left(\frac{r_C^2 X_R}{EI_{YY}}\right)_1 + \left(\frac{r_C^2 X_L}{EI_{YY}}\right)_2\right] V_B + \left(\frac{r_C^2 X_R}{EI_{YY}}\right)_2 V_C$$

$$4{,}095{,}000 = -1474\, M_B + 229\, M_C - 511\, V_B + 137.4\, V_C$$

Deflection at Point B due to moments, shears and pressure:

$$-\left(\frac{r_C^2 X_R}{EI_{YY}}\right)_1 M_{u_1} + \left(\frac{r_C^2}{EA}\right)_1 V_{u_1} - \left(\frac{r_C^2 X_L}{EI_{YY}}\right)_2 M_{u_2} - \left(\frac{r_C^2}{EA}\right)_2 V_{u_2} = \left[\left(\frac{r_C^2 X_R}{EI_{YY}}\right)_1\right.$$

$$\left. - \left(\frac{r_C^2 X_L}{EI_{YY}}\right)_2\right] M_B + \left(\frac{r_C^2 X_L}{EI_{YY}}\right)_2 M_C + \left[\left(\frac{r_C^2}{EA}\right)_1 + \left(\frac{r_C^2 X_R^2}{EI_{YY}}\right)_1\right.$$

$$\left. + \left(\frac{r_C^2}{EA}\right)_2 + \left(\frac{r_C^2 X_L^2}{EI_{YY}}\right)_2\right] V_B + \left[\left(\frac{r_C^2 X_L X_R}{EI_{YY}}\right)_2 - \left(\frac{r_C^2}{EA}\right)_2\right] V_C$$

$$-1{,}462{,}500 = +511\, M_B + 2{,}75\, M_C + 295\, V_B - 18.22\, V_C$$

Rotation of Point C due to moments, shears, and pressure:

$$\left(\frac{r_C^2}{EI_{YY}}\right)_2 M_{u_2} = \left(\frac{r_C^2}{EI_{YY}}\right)_2 M_B - \left[\left(\frac{r_C^2}{EI_{YY}}\right)_2 + \left(\frac{S}{2\beta D}\right)_2\right] M_C - \left(\frac{r_C^2 X_L}{EI_{YY}}\right)_2 V_B$$

$$+ \left[-\left(\frac{r_C^2 X_R}{EI_{YY}}\right)_2 + \left(\frac{B \sin \phi}{2\beta^2 D}\right)_2\right] V_C$$

$$-1{,}210{,}000 = 229\, M_B - 1099\, M_C - 2.75\, V_B + 65.6\, V_C$$

Deflection at Point C due to moments, shears, and pressure:

$$-\left(\frac{r_C^2 X_R}{E I_{YY}}\right)_2 M_{us} + \left(\frac{r_C^2}{EA}\right)_2 V_{us} - \delta_{ps} = -\left(\frac{r_C^2 X_R}{E I_{YY}}\right)_2 M_B + \left[\left(\frac{r_C^2 X_R}{E I_{YY}}\right)_2 - \left(\frac{B \sin\phi}{2\beta^3 D}\right)_1\right] M_C$$

$$+\left[\left(\frac{r_C^2 X_L X_R}{E I_{YY}}\right)_2 - \left(\frac{r_C^2}{EA}\right)_2\right] V_B + \left[\left(\frac{r_C^2}{EA}\right)_2 + \left(\frac{r_C^2 X_R^2}{E I_{YY}}\right)_2 + \left(\frac{L \sin^3\phi}{2\beta^3 D}\right)_1\right] V_C$$

$$1{,}109{,}000 = -137.4\, M_B - 65.6\, M_C - 18.22\, V_B + 199.3\, V_C$$

Solving the preceding equations simultaneously, we obtain the following values for the shears and moments at each section:

$M_A = 0$ in.-lb/in.	$V_A = 0$ lb/in.	$T_A = 0$ lb/in.
$M_B = -1313$ in.-lb/in.	$V_B = -2385$ lb/in.	$T_B = 2385$ lb/in.
$M_C = 1130$ in.-lb/in.	$V_C = 4962$ lb/in.	$T_C = 14{,}350$ lb/in.

The maximum stresses at each section will be:

Section B

Joint tensile stress

$$S_t = \frac{T_B}{t_B} \pm \frac{6 M_B}{t_B^2} = \frac{2385}{0.32} + \frac{(6)(1313)}{(0.32)^2}$$

$$S_t = 7450 + 77{,}000 = 84{,}450 \text{ psi}$$

Hoop stress

$$S_h = -\frac{V_{net}\, r_1}{A} - X_L \frac{M_{net}\, r_1}{I_{YY}}$$

$$S_h = -\frac{(1435)(5.52)}{0.483} - 0.040\, \frac{(1004)(5.52)}{0.0245}$$

$$S_h = -25{,}400 \text{ psi}$$

Section C

Longitudinal stress

$$S_t = \frac{T_C}{t_C} \pm \frac{6M_C}{t^2_C} = \frac{14350}{0.250} + \frac{(6)(1130)}{(0.25)^2}$$

$$S_t = 57{,}500 + 108{,}000 = 165{,}500 \text{ psi}$$

Hoop stress

$$S_h = \frac{2}{t_C}[T_C - \beta_1 r_1 \sin\phi\, V_C + \beta^2 r_1 M_C] \pm \nu \frac{6M_C}{t_C}$$

$$S_h = \frac{2}{0.250}[14{,}350 - (0.805)(10.25)(0.381)(4962) + (0.648)(10.25)(1130)] + (0.3)(108{,}000)$$

$$S_h = 50000 + 32400 = 82{,}400 \text{ psi}$$

Junction of Rear Spherical Head and Cylindrical Shell

Radius of head and shell, $r = 6.125$ in.

Thickness of head and shell, $t = 0.250$ in.

Maximum pressure, $p = 2800$ psi

Maximum hoop stress in spherical head due to discontinuity shears is (see Ref 1, p 409):

$$S_h = 0.647 \frac{pr}{t} = 0.647 \frac{(2800)(6.125)}{0.250}$$

$$S_h = 44{,}400 \text{ psi}$$

Maximum hoop stress in cylindrical shell due to discontinuity shears is (see Ref 1, p 409):

$$S_h = 1.032 \frac{pr}{t} = 1.032 \frac{(2800)(6.125)}{0.250}$$

$$S_h = 71{,}000 \text{ psi}$$

Analysis of Brackets

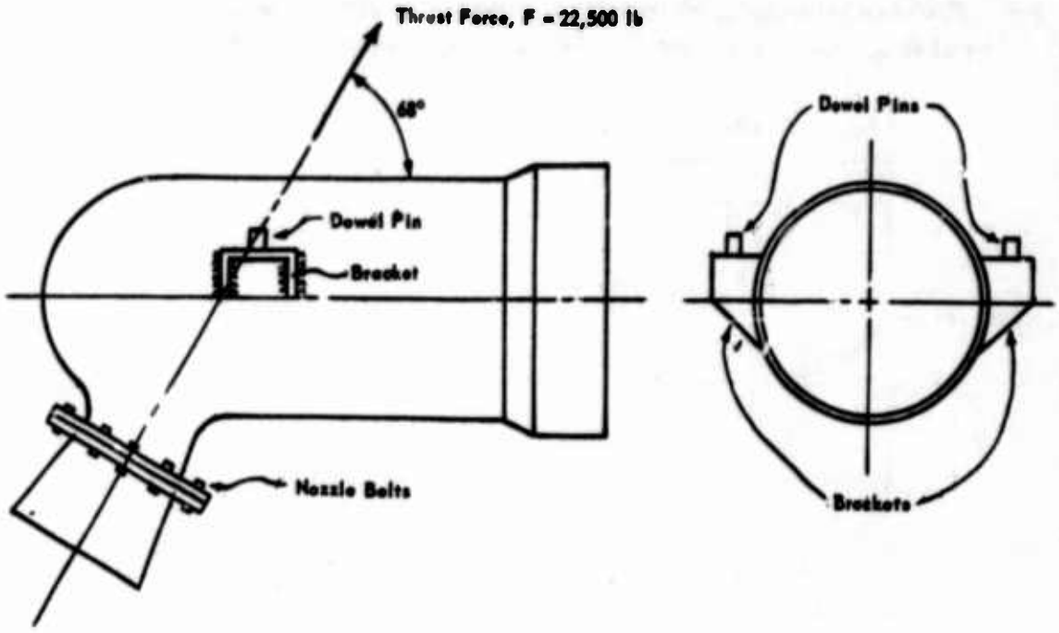

Dowel Pins

The dowel pins resist shear load only, and the shear load on each pin is equal to one-half the horizontal component of the thrust load.

Pin diameter, d = 0.625 in.

$$S_S = \frac{F \cos 68^\circ}{0.785\, d^2} = \frac{(22{,}500)(0.375)}{(0.785)(0.625)^2}$$

$$S_S = 27{,}500 \text{ psi}$$

Brackets

Each bracket is assumed to be a cantilever beam with the bending loads equal to one-half the horizontal and vertical components of the thrust load.

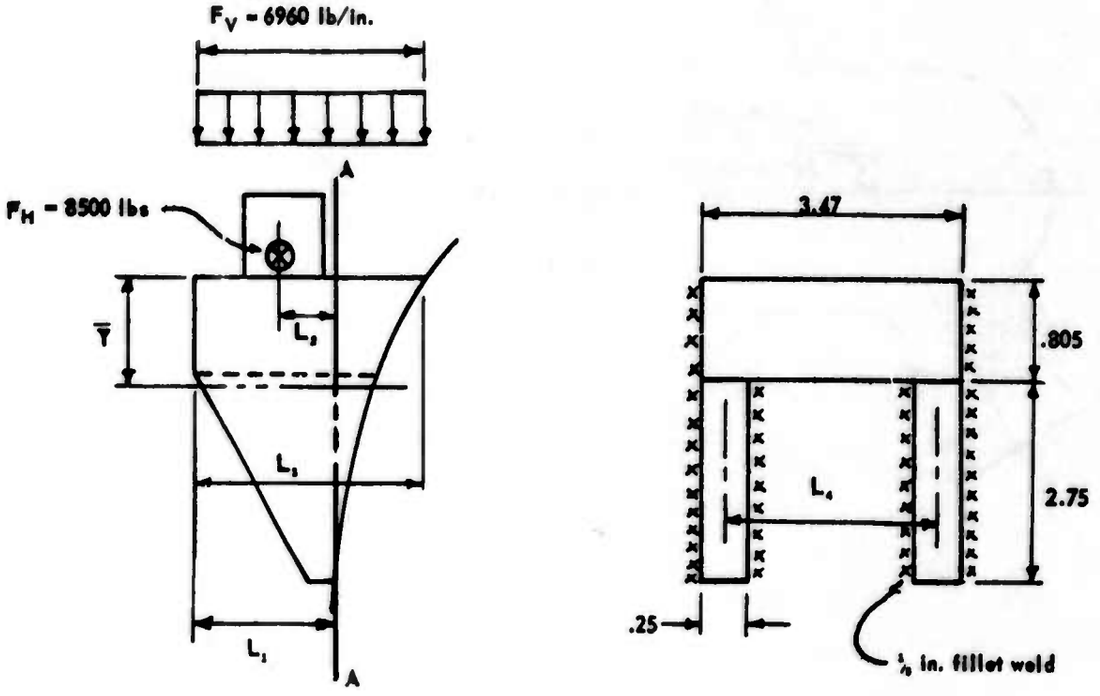

$L_1 = 2.18$ in.

$L_2 = 1.35$ in.

$L_3 = 3.80$ in.

$L_4 = 3.22$ in.

Determination of bending stress in Section A-A:

Location of the horizontal center of gravity axis:

$$\bar{Y} = \frac{(3.47)(0.805)(0.402) + (2)(2.75)(0.25)(2.18)}{(3.47)(0.805) + (2)(2.75)(0.25)} = 0.986 \text{ in.}$$

The moment of inertia about the horizontal c. g. axis is:

$$I = \frac{(3.47)(0.805)^3}{12} + \frac{(0.50)(2.75)^3}{12} + (2.80)(0.584)^2 + (1.375)(1.194)^2$$

$$I = 3.93 \text{ in.}^4$$

Bending stress due to vertical component of the thrust force is:

$$S_b = \frac{F_V L_1^2 C}{I} = \frac{(6960)(2.18)^2(2.569)}{(2)(3.93)}$$

$$S_b = 10{,}800 \text{ psi}$$

Moment of inertia about the vertical c.g. axis is:

$$I = \frac{(0.805)(3.47)^3}{12} + \frac{(2)(2.75)(0.25)^3}{12} + (1.375)(1.61)^2$$

$$I = 6.36 \text{ in.}^4$$

Bending stress due to horizontal component of the thrust force is:

$$S_b = \frac{F_H L_2 C}{I} = \frac{(8500)(1.35)(1.735)}{6.36}$$

$$S_b = 3100 \text{ psi}$$

Maximum compressive stress at Section A-A is:

$$S_C = 10{,}800 + 3100 = 13{,}900 \text{ psi}$$

Maximum shear stress due to twisting is:

$$S_S = \frac{3 F_H \bar{Y} t_1}{b_1 t_1^3 + 2 b_2 C_2^3} = \frac{(3)(8500)(0.986)(0.805)}{(3.47)(0.805)^3 + (2)(2.75)(0.25)^3}$$

$$S_S = 10,700 \text{ psi}$$

Bracket weld stresses =

All welds are ⅛-inch fillet type (b = ⅛-in.).

Maximum tensile stress, based on Figure 22 (p 31), is (see Ref 6, p 451):

$$S_t = \frac{4.24 F_V L_3^2}{4 b h^2} + \frac{0.707 F_H L_2}{L_4 b h}$$

$$S_t = \frac{(4.24)(6960)(3.00)^2}{(4)(0.125)(2.75)^2} + \frac{(0.707)(8500)(1.35)}{(3.22)(0.125)(2.75)}$$

$$S_t = 70,000 + 7350 = 77,350 \text{ psi}$$

Maximum shear stress, based on Figure 22, is (see Ref 6, p 451):

$$S_S = \frac{0.707 F_H \bar{Y}}{L_4 b h} = \frac{(0.707)(8500)(0.986)}{(3.22)(0.125)(2.75)}$$

$$S_S = 5350 \text{ psi}$$

Nozzle Bolts

Type of bolt – ⅛ in. 16UNC-2B

No. of bolts, n = 12

Bolt tensile area, A_t = 0.0775 in.^{2}

Venturi largest diameter, D = 6.50 in.

Venturi throat diameter, d = 4.74 in.

Total force on bolts due to a pressure of 2800 psi on the nozzle Venturi:

$$F = p A_N = (2800)(0.785)(6.30^2 - 4.74^2)$$

$$F = 43{,}300 \text{ lb}$$

Maximum tensile stress in each bolt is:

$$S_t = \frac{F}{n A_t} = \frac{43{,}300}{(12)(0.0775)}$$

$$S_t = 46{,}500 \text{ psi}$$

REFERENCES

1. S. Timoshenko, *Theory of Plates and Shells*, McGraw-Hill, New York, 1940

2. Raymond J. Roark, *Formulas for Stress and Strain*, McGraw-Hill, New York, 1940

3. S. Timoshenko, *Strength of Materials, Part II, Advanced Theory and Problems*, 2nd Ed., D. Van Nostrand, New York, 1952

4. V. L. Maleev and J. B. Hartmann, *Machine Design*, International Textbook Co., Scranton, Pa., 1955

5. R. G. Salamon and C. W. Larson, *Stress Analysis of a Solid Propellant Sustainer Motor for a Free Flight Missile A Rocket*, Technical Memorandum FRL-TM-19, Picatinny Arsenal, August 1962

6. V. M. Faires, *Design of Machine Elements*, The MacMillan Co., New York, 949

7. S. M. Breslan and S. R. Sadin, *Development of Stress Analysis Form Sheets*, M. W. Kellogg Co., SPD Report 340, 31 Oct 1952

GLOSSARY

A	=	Area
D	=	Diameter
E	=	Modulus of elasticity
F	=	Force per linear inch
I	=	Moment of inertia
I_{yy}	=	Moment of inertia about y axis
K	=	Coefficient
L, l	=	Length
M	=	Bending Moment
M_u	=	Unbalanced body moment +
P	=	Force per linear inch
p	=	Pressure
r	=	Radius, radius of curvature
S	=	Stress
T	=	Tensile force
t	=	Thickness
V	=	Shearing force
V_u	=	Unbalanced body load +
x	=	Distance
X,Y,Z	=	Axial forces in bars, unknown reactions
β	=	Numerical coefficient
δ	=	Total elongation, total deflection, distance
θ	=	Angle

ν = Poisson's ratio

φ = Angle

Subscripts

1 - 10 = Sections, area

A,B,C = Ideal sections, area

H = Horizontal

h = Circumferential

L = Longitudinal

N = Nozzle

R = Radial

S = Shear

t = Longitudinal, tensile

X,y = Components

APPENDIX II

STATIC TEST EQUIPMENT AND INSTRUMENTATION*

Stand Construction

The stand is made up of a frame, cradle, and six struts. Heavy welded steel construction is used on the frame and cradle to minimize deflections under load. Thin-plate type commercial flexures are used in each of the six struts to provide six component thrust measuring capabilities. Three double bridge gages and three dummy gages are used when measuring only three components. The dummy gages allow less deflection in the side direction than the actual gages when thrust measurements in this direction are not needed. Right and left hand thread commercial turnbuckle adjustments are provided in five of the struts so that stand alignment may be obtained by optical means rather than expensive precision machining. One side of the turnbuckle in the three side struts is left unlocked to allow for rotation of the cradle.

After assembly, the stand consists of a single unit capable of being moved between the test bay and the storage area without the need for realignment of the stand. The stand is designed to mate with the normal mounting surface of the rocket motor, and this mating surface is adjusted to be 68 degrees relative to the main thrust gage. No attempt is made to align the rocket motor itself with the stand. Angle measurements will, therefore, include any error in the manufacture of the motor body.

An inherent error is found in all stands of this type due largely to deflections in the gages and flexures under load. These errors are commonly reduced by using in-place calibration, which consists of applying a known load to the stand in a known direction and reading the gage outputs. Because of the required precision in applying this load, this method is expensive and is not used on this stand. Instead, the inherent errors are compensated for by mathematical means.

---

*Extracted from Picatinny Arsenal Technical Memorandum 1344, "Static Testing of the XM-15 Catapult Rocket," Frank C. Femia and Henry A. Pontious (Ammunition Engineering Directorate), Dec 1963.

Simplified Stand Operation

A schematic of the test setup is shown in Figure II-1. The rocket motor is mounted with its nozzle center line horizontal and directly in line with the main gage, R_1. Gage R_2 is also horizontal and gage R_3 is vertical. α is the nozzle cant angle, a is the distance between gages R_1 and R_2, b is the distance from the nozzle throat to the intersection o, s is the vertical displacement of the thrust vector at the nozzle throat, and θ is the angle which the thrust vector makes with the horizontal. A simplified schematic is shown in Figure II-2.

From this figure, the following relationships are found:

$$T \sin \theta = R_3$$

$$T \cos \theta = R_1 + R_2$$

$$s\ T \cos \theta = a\ R_2 + b\ T \sin \theta$$

From these equations, the thrust magnitude, T, direction θ, and position s may be found for any value of R_1, R_2, and R_3. A number of factors are neglected in these equations, however, and these must be accounted for if meaningful results are to be obtained.

Complete Stand Analysis

The use of a strain type thrust gage to measure the rocket thrust introduces, of necessity, a certain amount of deflection in the stand. If gage R_1 is to measure the thrust accurately, the rocket must be free to move forward by the amount of the deflection in gage R_1. This movement must not be restricted by strut 3. Similarly, vertical movement of the rocket must not be restricted by struts 1 and 2 if the vertical component of the thrust is to be measured by gage R_3. Thin plate type flexures are used in all struts (including 4, 5, and 6, which are not shown) to allow these struts to bend easily under a side load but maintain relative rigidity in the axial direction. Use of these flexures does, however, add to the amount of deflection in each of the struts.

A schematic of the stand deflecting under load is shown in Figure II-3. The struts deflect by amounts δ_1, δ_2, and δ_3, and bend through angles β_1, β_2, and β_3. The vertical axis rotates through an angle ϵ.

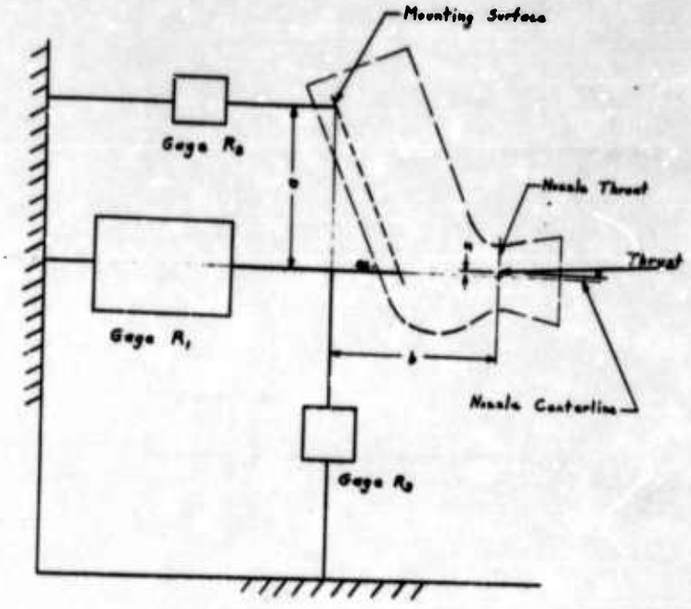

Figure II-1. Schematic of the Test Setup

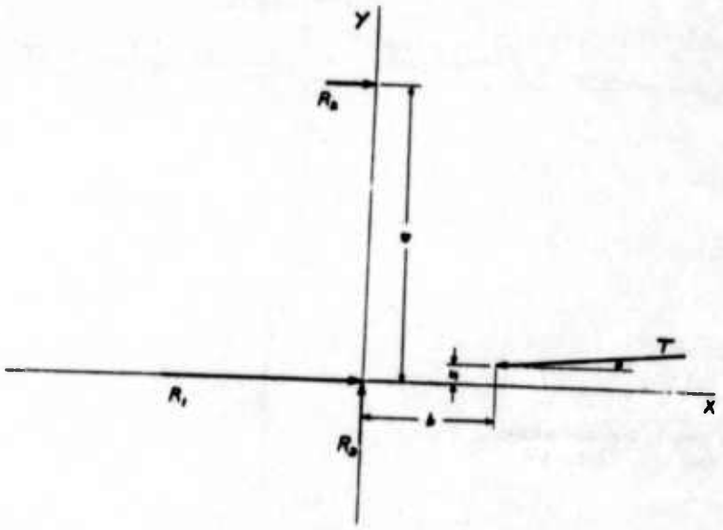

Figure II-2. Simplified Schematic

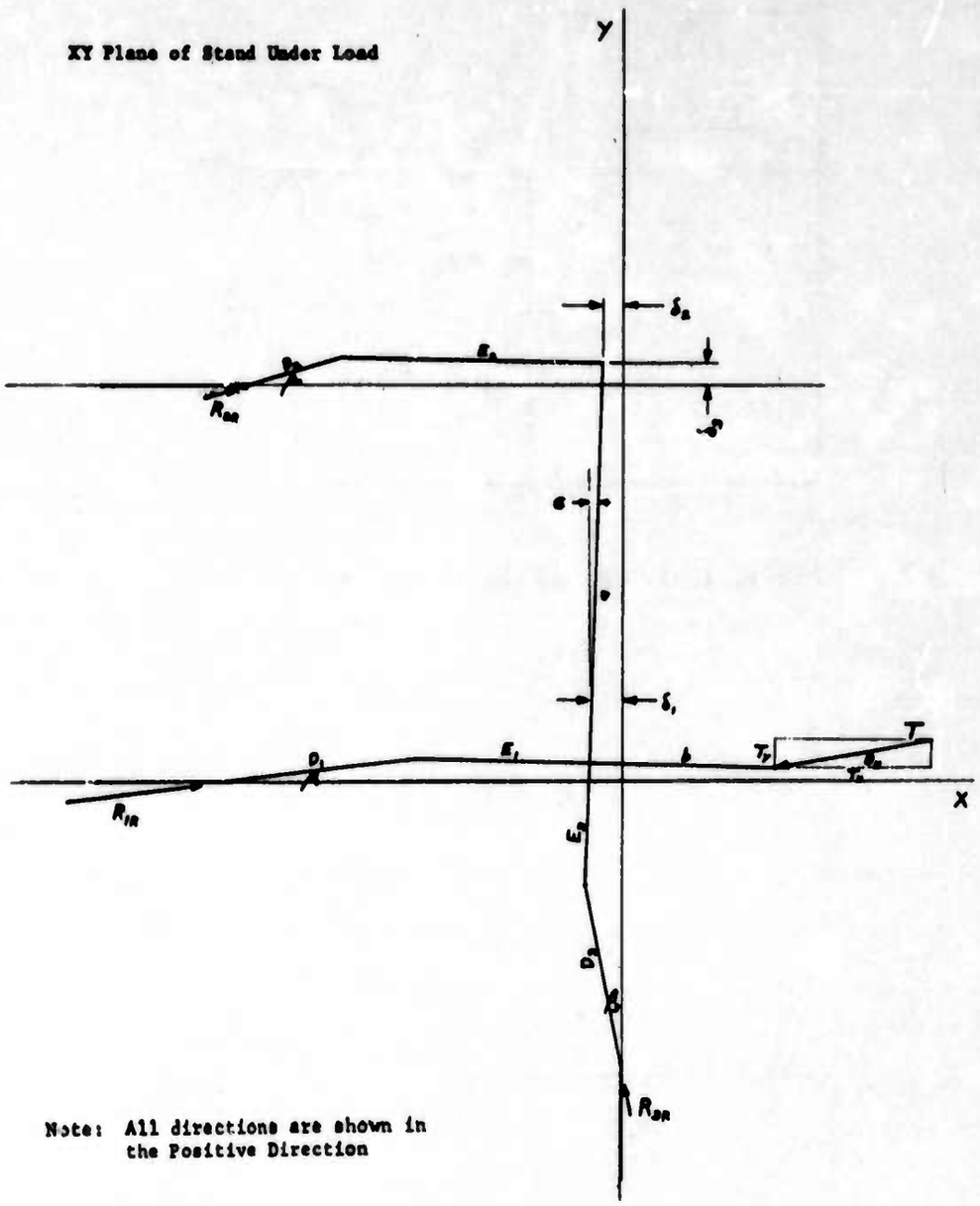

Figure II-3. Schematic of the Stand Deflecting under Load

R_{1R}, R_{2R}, and R_{3R} are the gage readouts for gages R_1, R_2, and R_3, respectively, and T_x and T_y are the x and y components of the thrust. D_1, D_2, and D_3 are the distances between pivot centers of the flexures. F_{RV} is the vertical resistance of flexures in struts 1, 2, 4, 5, and 6 to deflection δ_3 and F_{RH} is the horizontal resistance of flexures in struts 3, 4, 5, and 6 to deflection δ_1. Since the thrust position is not required in these tests, this analysis is simplified by considering only the thrust magnitude and direction. From Figure II-3:

$$\Sigma F_x = 0$$

$$R_{1R} \cos \beta_1 + R_{2R} \cos \beta_2 - R_{3R} \sin \beta_3 + F_{RH} = T_x$$

$$\Sigma F_y = 0$$

$$R_{1R} \sin \beta_1 + R_{2R} \sin \beta_2 + R_{3R} \cos \beta_3 + F_{RV} = T_y$$

By geometry

$$\sin \beta_1 = (\delta_3 + E_1 \sin \epsilon)/D_1$$

$$\sin \beta_2 = (\delta_3 + E_2 \sin \epsilon - a + a \cos \epsilon)/D_2$$

$$\sin \beta_3 = (\delta_1 + E_3 \sin \epsilon)/D_3$$

$$\sin \epsilon = (\delta_1 - \delta_2)/a$$

The values of β_1, β_2, β_3, and ϵ are always small (see example) for this stand, and the cosines of these angles may be set at unity with negligible error.

The significance of reducing all cosine values to unit may be shown as follows. The largest angles involved here will be on the order of 12 to 24 minutes, and most angles will be considerably less than this. Since cos 24' = 0.99998, the error introduced will be 1.00000 - 0.99998 = 0.00002. The percentage error may be found by

$$\text{error} = \frac{0.00002}{0.99998} = .00002$$

$$= .002\%$$

The values of F_{RH} and F_{RV} may be determined from manufacturers specifications. For the expected angular values (see example), the resistance values in the struts will be on the order of:

$$\beta_1 = 4' \qquad F_{1V} = \frac{50 \text{ in. lb}}{22.75 \text{ in.}} = 2.2 \text{ lb}$$

$$\beta_2 = 8' \qquad F_{2V} = \frac{3 \text{ in. lb}}{23.69 \text{ in.}} = .13 \text{ lb}$$

$$\beta_3 = 20' \qquad F_{3H} = \frac{8 \text{ in. lb}}{17.94 \text{ in.}} = .45 \text{ lb}$$

F_{4V}, F_{5V}, F_{6V}, F_{4H}, F_{5H}, and F_{6H} will be on the same order as F_{2V} and F_{3H}. From inspection of the stand:

$$F_{RV} = F_{1V} + F_{2V} + F_{4V} + F_{5V} = F_{6V}$$

$$F_{RH} = F_{3H} + F_{4H} = F_{5H} = F_{6H}$$

It is seen that F_{RV} and F_{RH} are negligible compared to R_{1R} and R_{3R}.

The bending in the flexures will also produce some torque in the system. This will result in equal and opposite forces in R_1, and R_2. These forces are also small and may be neglected.

The previous equations may now be combined and simplified to

$$T_x = R_{1R} + R_{2R} - \frac{\delta_1 + K E_3}{D_3} R_{3R}$$

$$T_y = \frac{\delta_3 + K E_1}{D_1} R_{1R} + \frac{\delta_3 + K E_2}{D_2} R_{2R} + R_{3R}$$

where

$$K = \frac{\delta_1 - \delta_2}{a}$$

Before stand assembly, each complete strut was statically loaded and its deflection measured to determine its elasticity with the following results:

$$\delta_1 = 18 \times 10^{-7} R_{1R}$$

$$\delta_2 = 120 \times 10^{-7} R_{2R}$$

$$\delta_3 = 70 \times 10^{-7} R_{3R}$$

These values were determined with no bending in the flexures, so under stand conditions the elasticity would contain cosine terms which, however, may be neglected as before.

Geometric constants for the stand are:

$a = 21.79$ in.	$D_1 = 16.00$ in.	$E_1 = 6.75$ in.
$b = 10.91$ in.	$D_2 = 12.75$ in.	$E_2 = 10.94$ in.
	$D_3 = 12.50$ in.	$E_3 = 5.44$ in.

Thus:

$$T_x = R_{1R} + R_{2R} - R_{3R} (1.80 R_{1R} - 2.40 R_{2R}) 10^{-7}$$

$$T_y = R_{1R} (.349 R_{1R} - 2.32 R_{2R} + 4.38 R_{3R}) 10^{-7}$$

$$+ R_{2R} (.710 R_{1R} - 4.72 R_{2R} + 5.49 R_{3R}) 10^{-7} + R_{3R}$$

On investigation of the stand geometry and Figure II-3 it is seen that the gage loads due to the weight of the stand and motor will affect some of the terms of these equations. Using approximate average values (the motor weight changes during firing) of these loads, the equations become:

$$T_x = R_{1R} + R_{2R} - (R_{3R} + 500) (1.80 R_{1R} - 2.40 R_{2R}) 10^{-7}$$

$$T_y = (R_{1R} + 80) (.349 R_{1R} - 2.32 R_{2R} + 4.38 R_{3R}) 10^{-7}$$

$$+ (R_{2R} - 80) (.710 R_{1R} - 4.72 R_{2R} + 5.49 R_{3R}) 10^{-7} + R_{3R}$$

The angle of thrust relative to the horizontal is then:

$$\theta_H = \tan^{-1} (T_y/T_x)$$

The angle of thrust relative to the centerline of the nozzle is:

$$\theta = \theta_H + \epsilon$$

The magnitude of the thrust is:

$$T = T_x/\cos \theta_H$$

EXAMPLE

Round 22 using Action Time Avg. Thrust Values

$$R_{1R} = 32160 \text{ lb} \qquad R_{2R} = 22 \text{ lb} \qquad R_{3R} = -106 \text{ lb}$$

$$T_x = R_{1R} + R_{2R} - (R_{3R} + 500)(1.80\, R_{1R} - 2.40\, R_{2R})\, 10^{-7}$$

$$= 32160 + 22 - 2$$

$$= 32180 \text{ lb}$$

$$T_y = (R_{1R} + 80)(.349\, R_{1R} - 2.32\, R_{2R} + 4.38\, R_{3R})\, 10^{-7}$$

$$+ (R_{2R} - 80)(.710\, R_{1R} - 4.72\, R_{2R} + 5.49\, R_{3R})\, 10^{-7} + R_{3R}$$

$$= 35 - 0 - 106$$

$$= -70 \text{ lb}$$

$$\theta_H = \tan^{-1} (T_y/T_x)$$

$$= -8'$$

$$\epsilon = \sin^{-1} \left[(18\, R_{1R} - 120\, R_{2R})/21.79 \times 10^7\right]$$

$$= 9'$$

$$\theta = \theta_H + \epsilon = -8' + 9' = 1'$$

$$T = T_x / \cos \theta_H$$

$$= 32180 \text{ lb.}$$

To investigate the previous assumption that β_1, β_2, and β_3 are small, these angles are also computed for this example:

$$\delta_1 = 18 \times 10^{-7} R_{1R}$$

$$= .0579 \text{ in.}$$

$$\delta_2 = 120 \times 10^{-7} R_{2R}$$

$$= .000264 \text{ in.}$$

$$\delta_3 = 70 \times 10^{-7} R_{3R}$$

$$= -.000742 \text{ in.}$$

$$\beta_1 = \sin^{-1} \left[(\delta_3 + E_1 \sin \epsilon) / D_1 \right]$$

$$= 4'$$

$$\beta_2 = \sin^{-1} \left[(\delta_3 + E_2 \sin \epsilon) / D_2 \right]$$

$$= 8'$$

$$\beta_3 = \sin^{-1} \left[(\delta_1 + E_3 \sin \epsilon) / D_3 \right]$$

$$= 20'$$

From the example shown, it is seen that some terms in the equation will always be negligible for a normal round. The equations are thus simplified to:

$$T_x = R_{1R} + R_{2R}$$

$$T_y = (R_{1R} + 80)(.349 R_{1R} - 2.32 R_{2R} + 4.38 R_{3R}) 10^{-7} + R_{3R}$$

$$T = T_x$$

$$\epsilon = \sin^{-1}\left[(18\ R_{1R} - 120\ R_{2R})/(21.79 \times 10^{-7})\right]$$

$$\theta_H = \tan^{-1}\ (T_y/T_x)$$

$$\theta = \theta_H + \epsilon$$

R_{1R}, R_{2R}, and R_{3R} are positive in compression and the angular results are positive in the counterclockwise direction.

GLOSSARY

a	=	Distance between R_1 and R_2.
b	=	Distance from nozzle throat to intersection.
$D_{1,2,3}$	=	Distance between pivot centers of the flexures.
$E_{1,2,3}$	=	Distances between mounting point and end of flexure.
F_{RH}	=	Horizontal resistance of flexures in struts 3, 4, 5, 6 to deflection δ_1.
F_{RV}	=	Vertical resistance of flexures in struts 1, 2, 4, 5, and 6 to deflection δ_3.
o	=	Intersection
R_1	=	Main gage.
R_2	=	Horizontal gage.
R_3	=	Vertical gage.
$R_{1R,2R,3R}$	=	Gage readouts.
s	=	Vertical displacement of thrust vector at nozzle throat.
T	=	Thrust magnitude.
$T_{x,y}$	=	Components of the thrust.
α	=	Nozzle cant angle.
$\beta_{1,2,3}$	=	Angles
$\delta_{1,2,3}$	=	Strut deflections.
ϵ	=	Angle
θ	=	Angle which thrust vector makes with the horizontal.

UNCLASSIFIED

Security Classification

DOCUMENT CONTROL DATA - R&D

(Security classification of title, body of abstract and indexing annotation must be entered when the overall report is classified)

1. ORIGINATING ACTIVITY (Corporate author) Frankford Arsenal Philadelphia, Pa. 19137	2a. REPORT SECURITY CLASSIFICATION UNCLASSIFIED 2b. GROUP N/A

3. REPORT TITLE

Development of XM-15 Escape Rocket

4. DESCRIPTIVE NOTES (Type of report and inclusive dates)

Final Technical Report, Jan 1960 - Mar 1963

5. AUTHOR(S) (Last name, first name, initial)

MacDonald, Hugh D., Jr.

6. REPORT DATE	7a. TOTAL NO. OF PAGES	7b. NO. OF REFS
November 1966	159	12

8a. CONTRACT OR GRANT NO.	9a. ORIGINATOR'S REPORT NUMBER(S)
b. PROJECT NO. 1362	R-1817
c. Task No. 136205 AF MIPR Nos. 33(616)60-15; d. 33(616)60-8; and AS-3-238	9b. OTHER REPORT NO(S) (Any other numbers that may be assigned this report) AFFDL-TR-66-162

10. AVAILABILITY/LIMITATION NOTICES

This document is subject to special export controls and each transmittal to foreign governments or foreign nationals may be made only with prior approval of the Air Force Flight Dynamics Laboratory.

11. SUPPLEMENTARY NOTES	12. SPONSORING MILITARY ACTIVITY
N/A	Air Force Flight Dynamics Laboratory RTD, AFSC Wright-Patterson AFB, Ohio 45433

13. ABSTRACT

This report summarizes the design study and testing of the XM-15 Escape Rocket, a device designed to satisfy the ejection propulsion needs for a single place separable nose emergency crew escape capsule. The XM-15 was used in the feasibility testing of the separable nose escape concept, the test capsule being based on the F-104 aircraft configuration.

The XM-15 Escape Rocket is designed to deliver a maximum thrust of 45,000 pounds, decreasing to 27,000 pounds at rocket burnout. The rocket's burn time is 0.50 second. The XM-15 utilizes 12 singly perforated uninhibited grains of HE-N12 propellant and was validated to operate over a temperature range of 70° ± 20° F.

The over-all performance of the XM-15 rocket was satisfactory throughout both static testing of the motor and feasibility testing of the capsule. Performance was demonstrated to be consistent and reproducible.

DD FORM 1 JAN 64 1473

UNCLASSIFIED

Security Classification

UNCLASSIFIED

Security Classification

14. KEY WORDS	LINK A		LINK B		LINK C	
	ROLE	WT	ROLE	WT	ROLE	WT
Escape Systems Escape Rockets Static Testing of Rockets Stress Analysis						

INSTRUCTIONS

1. ORIGINATING ACTIVITY: Enter the name and address of the contractor, subcontractor, grantee, Department of Defense activity or other organization *(corporate author)* issuing the report.

2a. REPORT SECURITY CLASSIFICATION: Enter the overall security classification of the report. Indicate whether "Restricted Data" is included. Marking is to be in accordance with appropriate security regulations.

2b. GROUP: Automatic downgrading is specified in DoD Directive 5200.10 and Armed Forces Industrial Manual. Enter the group number. Also, when applicable, show that optional markings have been used for Group 3 and Group 4 as authorized.

3. REPORT TITLE: Enter the complete report title in all capital letters. Titles in all cases should be unclassified. If a meaningful title cannot be selected without classification, show title classification in all capitals in parenthesis immediately following the title.

4. DESCRIPTIVE NOTES: If appropriate, enter the type of report, e.g., interim, progress, summary, annual, or final. Give the inclusive dates when a specific reporting period is covered.

5. AUTHOR(S): Enter the name(s) of author(s) as shown on or in the report. Enter last name, first name, middle initial. If military, show rank and branch of service. The name of the principal author is an absolute minimum requirement.

6. REPORT DATE: Enter the date of the report as day, month, year; or month, year. If more than one date appears on the report, use date of publication.

7a. TOTAL NUMBER OF PAGES: The total page count should follow normal pagination procedures, i.e., enter the number of pages containing information.

7b. NUMBER OF REFERENCES: Enter the total number of references cited in the report.

8a. CONTRACT OR GRANT NUMBER: If appropriate, enter the applicable number of the contract or grant under which the report was written.

8b, 8c, & 8d. PROJECT NUMBER: Enter the appropriate military department identification, such as project number, subproject number, system numbers, task number, etc.

9a. ORIGINATOR'S REPORT NUMBER(S): Enter the official report number by which the document will be identified and controlled by the originating activity. This number must be unique to this report.

9b. OTHER REPORT NUMBER(S): If the report has been assigned any other report numbers *(either by the originator or by the sponsor)*, also enter this number(s).

10. AVAILABILITY/LIMITATION NOTICES: Enter any limitations on further dissemination of the report, other than those imposed by security classification, using standard statements such as:

(1) "Qualified requesters may obtain copies of this report from DDC."

(2) "Foreign announcement and dissemination of this report by DDC is not authorized."

(3) "U. S. Government agencies may obtain copies of this report directly from DDC. Other qualified DDC users shall request through _____."

(4) "U. S. military agencies may obtain copies of this report directly from DDC. Other qualified users shall request through _____."

(5) "All distribution of this report is controlled. Qualified DDC users shall request through _____."

If the report has been furnished to the Office of Technical Services, Department of Commerce, for sale to the public, indicate this fact and enter the price, if known.

11. SUPPLEMENTARY NOTES: Use for additional explanatory notes.

12. SPONSORING MILITARY ACTIVITY: Enter the name of the departmental project office or laboratory sponsoring *(paying for)* the research and development. Include address.

13. ABSTRACT: Enter an abstract giving a brief and factual summary of the document indicative of the report, even though it may also appear elsewhere in the body of the technical report. If additional space is required, a continuation sheet shall be attached.

It is highly desirable that the abstract of classified reports be unclassified. Each paragraph of the abstract shall end with an indication of the military security classification of the information in the paragraph, represented as *(TS)*, *(S)*, *(C)*, or *(U)*.

There is no limitation on the length of the abstract. However, the suggested length is from 150 to 225 words.

14. KEY WORDS: Key words are technically meaningful terms or short phrases that characterize a report and may be used as index entries for cataloging the report. Key words must be selected so that no security classification is required. Identifiers, such as equipment model designation, trade name, military project code name, geographic location, may be used as key words but will be followed by an indication of technical context. The assignment of links, rules, and weights is optional.

UNCLASSIFIED

Security Classification